FLUID INDUCED DRILLING DYNAMICS

– A MECHANICALLY SCALED

EXPERIMENTAL INVESTIGATION

By

ESHAN KUMER MAITRA

Bachelor of Science in Mechanical Engineering

Ahsanullah University of Science and Technology

Dhaka, Bangladesh

September, 2019

Submitted to the Faculty of the
Graduate College of the
Oklahoma State University
in partial fulfillment of
the requirements for
the Degree of
MASTER OF SCIENCE
May, 2023

FLUID INDUCED DRILLING DYNAMICS

– A MECHANICALLY SCALED

EXPERIMENTAL INVESTIGATION

Thesis Approved:

Dr. Mohammed F. Al Dushaishi

Thesis Adviser

Dr. Geir Hareland

Dr. Hunjoo Lee

ACKNOWLEDGEMENTS

Name: ESHAN KUMER MAITRA

Date of Degree: MAY, 2023

Title of Study: FLUID INDUCED DRILLING DYNAMICS – A MECHANICALLY SCALED EXPERIMENTAL INVESTIGATION

Major Field: PETROLEUM ENGINEERING

Abstract: Drillstring vibration is an unavoidable detrimental dynamic response due to continuous acting external forces and dynamic loading applied during the drilling operations. Drillstring vibration is one of the primary reasons behind downhole equipment malfunctioning and premature fatigue failure. Laboratory scaled experiments gained much popularity to investigate the physics of induced vibrations by replicating the downhole vibrations phenomena, due to their economic design and versatility. The majority of laboratory scaled experiments oftentimes are only scaled geometrically and address isolated phenomena. Thus, most downscaled investigations provide limited insight and cannot relate to the overall dynamics of field conditions. The objective of this work is to design and fabricate a fully functioning mechanically scaled experiment and fulfill the experimental lacking of fluid hydrodynamic effects on drillstring vibrations. The developed experimental setup is equipped with a high-frequency vibration measurement system and the capability to capture the BHA trajectory. The setup was used to investigate the effect of WOB fluctuation on lateral motion and the effect of fluid flow on drillstring stability.

TABLE OF CONTENTS

LIST OF TABLES

LIST OF FIGURES

CHAPTER I

1 INTRODUCTION

Drillstring (DS) vibration is one of the most detrimental issues for drilling inefficiency (Al Dushaishi et al., 2016). Drilling and exploration for the extraction of energy such as hydrocarbons and geothermal energy is a destructive process of cutting through the earth's subsurface, either by chipping the rock formation using drag and polycrystalline diamond compact (PDC) bits or by crushing the rock using roller-cone bits. DS vibrations are the dynamic responses due to continuous acting external forces and dynamic loading applied during the drilling operations. The physical structure of the DS makes it prone to vibrations (Dareing, 1984a; Dykstra et. al., 1996). DSs consist of a bottom hole assembly (BHA) and a slender section of connected drill-pipes that transfer the driving forces from the surface to the drill bit (Figure 1.1).
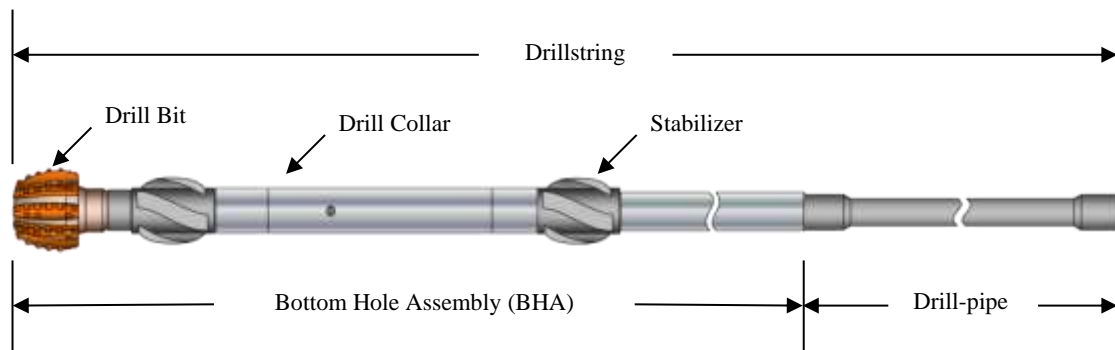
Figure 1.1. General construction of drillstring.

BHA generally consists of drill collars, heavyweight drill-pipes, drill-bit, various mechanical tools, and measurement/logging while drilling (MWD/LWD) tools. The BHA is the most dynamically active portion of the DS and is constantly subjected to various external forces. Including periodic impacts or continuous friction with the wellbore, internal and external damping forces, centrifugal forces, and drilling mud pressure fluctuations (Shyu, 1989; Chen et al., 2017; Li et al., 2019). Drilling vibrations increase the DS to wellbore contact frequency and accelerate DS component wear (Duman et al., 2003). High magnitudes of DS vibrations can interfere with the MWD tools and increase dynamic stress per cycle leading to premature fatigue failure (Heisig and Neubert, 2000; Cobern et al., 2007).

The nature of the vibration ranges from an expected modulation of motion to highly erratic behavior. Vibration can be explained as the instability from its dynamic equilibrium position (Khalil, 2002). Thus, drilling vibrations are often measured in terms of dynamic displacement over time, or as unintentional erratic acceleration. Such occurrence of dynamic disposition can be characterized through flexural studies and spectral analysis, which are used to identify critical operating frequencies. Dong and Chen (2016) and Macpherson et al., (2001) presented a categorized summary of DS vibration frequency ranges for common harmful vibration modes and phenomena. Avoidance of these operational critical frequencies or system eigenvalues of a DS assembly reduces the probability of premature catastrophic failure of the downhole components and enhances the overall drilling performance (Patil and Teodoriu, 2013; Bailey et al., 2016). Decades worth of work have been summarized in several surveys of practical heuristic DS vibration mitigation strategies (Zhu et al., 2014; Ghasemloonia et al., 2015; and Dong and Chen, 2016). Dareing (1984a and 1984b) emphasizes that rather than relying on heuristic processes to find the suitable operational ranges such as rotational velocity, weight on bit (WOB), and rate of penetration (ROP), etc., adjusting the BHA design alone and changing its natural frequency to detune the system, more effectively reduces the probability of severe mechanical vibrations. Vibration

mitigation practices also include specialized downhole tools to reduce vibration severity (Al Dushaishi 2012; Tian et. Al., 2016; Zang et. Al., 2016; Fu et al., 2018; Tang et al., 2021).

The three basic modes of DS vibrations are longitudinal vibration in the axial direction, torsional vibration on the axis of rotation, and bending or transverse vibration in the lateral directions (Shyu, 1989). Axial vibration is the up and down motion that results in repetitive loss of contact between the bit with the rock formation, i.e., bit-bounce (Figure 1.2-a). This is a more common occurrence with roller-cone drill bit operations. Torsional vibration is the result of periodic rotational acceleration and decelerations of the drill bit. In severe cases, the drill bit would stop rotating for an instance or "sticks", and suddenly release or "slips" at a much higher angular velocity than the applied rotation (Figure 1.2-b). The stick-slip phenomenon has been documented to occur at every other rotation during drilling operations (Henneuse, 1992). Lateral vibration, i.e., transverse vibration, bending vibration, or walk of the bit around the wellbore, is widely recognized as the leading cause of DS failures (Vandiver et al., 1990). Whirling is the most dangerous lateral vibration phenomenon for being the major reason behind borehole enlargement and DS damage, where the instantaneous center of rotation moves around the bit face during its rotation (Zhu and Di, 2011; Ghasemloonia et al., 2015). The whirling motion can be a form of rolling, sliding, or a completely random movement (Figure 1.2-c). Whirling is usually categorized as a forward, backward, or chaotic motion (Warren et al., 1990).

While DS vibrations can be classified in individual modes, each vibration conjointly contributes to these hindering phenomena (Spanos et al., 2003). Experimental results have shown that bending and axial vibrations are often coupled and lead to additional axial shortening of the DS (Vandiver et al., 1990; Yigit and Christoforou, 2000). Torque on bit (TOB) and dragging effects are studied as coupled dynamics of axial and torsional vibration (Baumgart 2000; Christoforou and Yigit, 2003). The frictional interaction between the bit and the wellbore, including the key-sitting of the DS, is not well understood due to the coupled nature of torsional and lateral vibrations (Mihajlovic

et al., 2004). For example, increased stick-slip due to frequent wellbore contact during backward

greatly weakens PDC bit cutters since, this phenomenon exploits the PDC bit cutter's low tensile

strength and leads to unexpected failure (Fear et al., 1997). More details regarding the primary area

of tool damage for each vibration phenomenon can be found in the survey done by Dong and Chen

(2016).
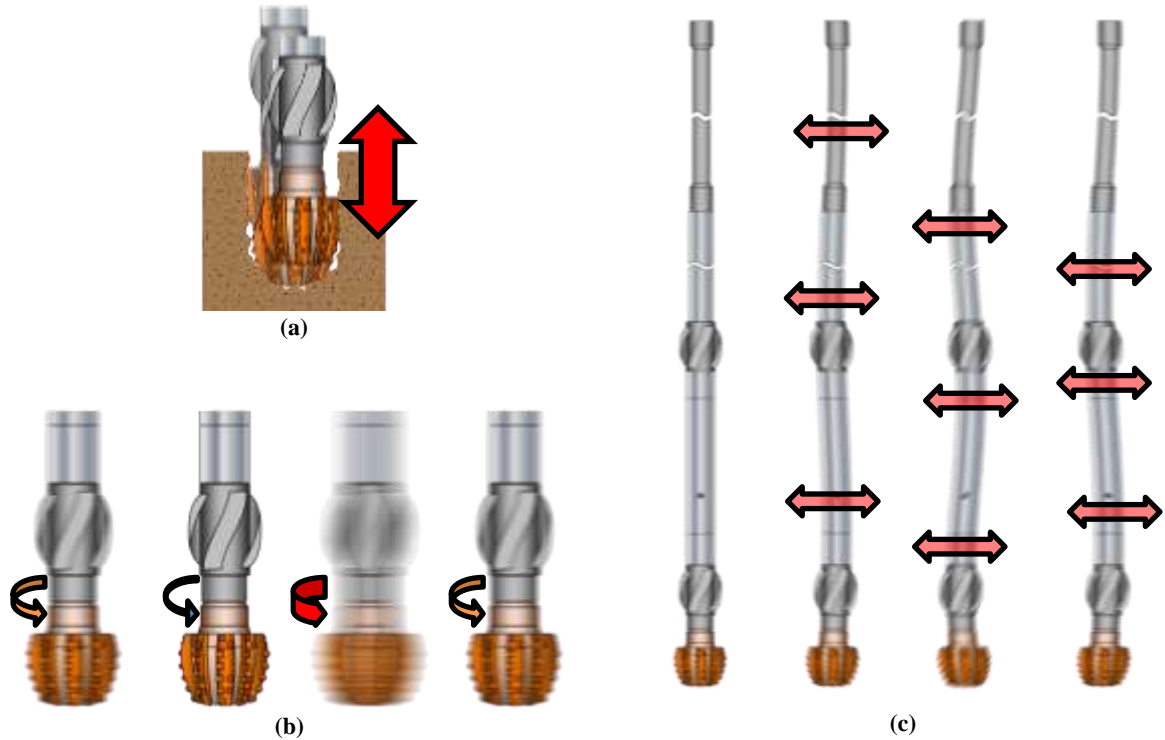
Figure 1.2. Drillstring vibration modes: (a) Bit-Bounce, (b) Stick-Slip, and (c) Bending.

Vibration and dynamic behavior analyses of DS have been performed since the invention of rotary

drilling operations in the 1930s (Stonneger, 1937). Bailey and Finnie (1960) and Finnie and Bailey

(1960) developed the first dynamic model, and the theory was verified with experiments. Most of

the DS vibration literature focuses on theoretical models (Spanos, 1992; Samuel et al., 2006; Al

Dushaishi et al., 2016) but only a few follow up with experimental tests to verify their mathematical

models (Bailey et al., 2008). DS vibrations are analyzed either quantitatively, based on the forced

vibration response of the entire DS using Finite Element Analysis (FEM) (Dykstra, 1996) or Lumped Mass models (Bradbury, 1962), or qualitatively, based on the definition of resonance frequencies, i.e., Spectral Analysis (Deily et. al., 1968). Saldivar et al., (2016) presented an extensive survey on the mathematical models for the propagation of vibrations along the DS, i.e., equations of motion (EOM). They stated that the extreme complexity of the physical phenomena occurring during the drilling operation makes the modeling of drilling vibrations difficult. Hence, models are limited by determined assumptions and simplifications. Meanwhile, multiple dynamic variables are often ignored or lumped into a single constant. The effectiveness of these models is determined by their relatability and accuracy between the assumptions and representation of real-life practices in terms of geometric aspects of the DS configuration, excitation sources, and damping effects including the rock-bit interactions during drilling operations.

The above-mentioned limitations may also carry over to the experimental investigations in the downscaled laboratory experimental design to compensate for experimental facilities and capabilities (Gao and Miska, 2010). Thus, even if the experimental setup is successful in recreating predetermined vibration phenomena, it may not be perfectly relatable to a field example. Therefore, downscaled experimental investigations were often deemed less reliable than full-size field tests for studying drilling dynamics (Arrestad et. al., 1986). However, small-scale experimental approaches have always been favored for easier implementation with less power requirement and resources, within the limited laboratory environment, hence the name "laboratory scaled" experiments.

The design of these scaled experimental setups often resembles a Jeffcott Rotor; where the BHA is dynamically simplified as an unbalanced rotor supported by two bearings (Shyu, 1989). One can also assume the entire DS dynamics as two spatial independent disks, one resembling the laterally free-moving drill-pipe and the other being the BHA constrained within a limited space (Liu et al., 2013). Such models incorporate various components and dynamic aspects with their respective

mechanical interpretation in free bodies and these lumped mass disks are linked through physical conditions that embody different vibration phenomena (Jansen, 1991 and 1993).

The majority of previous laboratory scaled investigations only scaled for the geometric aspects in the design of their experiments as per theoretical presumptions. Such a general way of scaling was acceptable since experimental investigations never aimed to closely verify the overall outcomes of a field-size model. Early experimental investigations were limited to field data and full-scale test-rigs correlations with surface data (Aarrestad et al., 1986; Halsey et al., 1986; Skaugen 1987). Thus, laboratory scaled studies also developed theoretical and mathematical models solely based on surface data (Macpherson et al., 1993). Since real-time downhole dynamic conditions are difficult to quantify with surface measurements, they can often be misleading (Mabile et al., 1996). Most of the DS excitations originate at the drill bit and then propagate upwards through the DS with exponentially reduced amplitude. This is due to the vastly different wavelength propagation velocities of different vibration modes (Shyu 1989). Yet, past experimental studies have proven to be quintessential for the first iterations of understanding vibration mechanisms in a laboratory environment, leading to improving mathematical models and the development of vibration mitigation strategies. Due to the modern advancement of downhole measurement tools, more accurate downhole data of the BHA can be acquired. Thus, experimental verification between such field BHA data and the experimental responses of a laboratory scaled BHA, can help establish more reliable analytical relations, mathematical models and further aid in improving the experimental procedures (Veeningen et al., 2013; Wiktorski et al., 2019). A proper mechanically scaled experimental setup of the DS or BHA most appropriately could fulfill this purpose because, a true mechanically scaled experimental study with well-rounded scaling or similarity analysis, can scale a field assembly into a smaller experimental setup with the ability to recreate downhole conditions more accurately as seen in the field.

The biggest shortcoming of most laboratory scaled experiments is scaling the experimental model without having any proper practical relatability to field-size DS or BHA. Therefore, it loses the credibility of direct comparison with the overall field data. Since a fully mechanically scaled DS and BHA would be constructed and modeled based on direct scaled relations of geometric dimensions, material properties, and all the implied external dynamic conditions of a field assembly, the experiment results can help in developing a more accurate analytical model for future dynamic predictions of field practices. Halsey et al., (1986) constituted that, the lowest torsional frequency is very sensitive to the mechanical properties of the DS. Also, Patil and Teodoriu (2013) suggested that for experiments a rigid drill-pipe is necessary for determining the mechanical characteristics of a drill-bit, but an assembly with relatively flexible material is a better choice for examining all the drilling dynamics. The practical DS slenderness, i.e., length to diameter ratio, requirement reduces to 30:1 from 50:1 if PVC is used instead of steel in scaled experiments (Cayeux et al., 2017). The use of flexible plastic materials makes the experimental prototype design more feasibly implementable to study drilling vibrations in a limited laboratory space. Ambrus et al., (2018) presented an extensive numeric study on drilling vibrations and discussed the effectiveness of designing mechanically scaled experimental BHA, based on the scaling laws by Wu (2007, 2015), with prospective market available soft materials.

Most laboratory scaled experimental studies aim to establish the mathematical relation for the research-specific assembly based on the recreation efficiency of the vibration phenomena under study. However, only geometric, or arbitrary dynamic scaling isolates the study to replicate particular vibration mechanisms that would occur under specific conditions and therefore limits direct correlations with field-size operations. Hence, recreating the vibration phenomenon on a mechanically scaled experiment with the operational parameters scaled from the field-size operations would result in the observation and measurement of more accurate dynamic responses.

Nicholson (1994) investigated the integration of different approaches for preventing drilling vibration severity and documented the utilization and limitations of developed models. According to Nicholson (1994), analytical or numerical models can never account for all drilling dynamics dysfunctions, and heuristic approaches always had a better success rate than analytical approaches in preventing the occurrences of severe DS vibrations. Even after decades of technological advancements, Nicholson's statement still holds. Modern field data-acquisition technologies have not been widely implemented yet due to high costs. Hence, there is a shortage of downhole field data on different operational parameter combinations. While the shortage of downhole data might be addressed with test rigs, the development of such a rig would be equally expensive and requires considerable space and resources (Aldred and Sheppard, 1992; Popp et al., 2018). Therefore, the next step for the small-scaled experimental approaches is to focus on building experimental setups that could mimic the dynamic conditions as seen in the field, under the applied external forces directly scaled from field operational parameters.

The objective of this work is to address shortcomings in drilling vibration laboratories by constructing a mechanically scaled experimental assembly to study Fluid Induced Drilling Dynamics (FIDD). The following chapter summarizes the aiding knowledge to formulate the experimental approach, inspire design improvement, and proper mechanical scaling of laboratory experimental setups for analyzing drilling vibrations. Consecutively, further discussions regarding the philosophy and detailed construction information on the versatile FIDD test assembly have been provided for future replication and improvement.

Two experimental investigations were conducted using the FIDD experiment to give a glimpse into its possible research endeavors. First, characterizing spectral signatures in relation to lateral vibrations and visualizing the trajectory of BHA during WOB fluctuation. Second, investigating the effect of different flow rates on drilling vibrations.

CHAPTER II

2   LITERATURE REVIEW

This chapter discusses the amassed knowledge in recent decades of different laboratory scaled experimental setups used to investigate DS vibration including different approaches, findings, and experiment design details. This chapter summarizes the aiding knowledge to formulate the experimental approach, inspire design improvement, and the proper scaling of laboratory experimental setups for analyzing drilling vibration. At the end of the chapter, a compact set of information was presented to distinguish between the experimental attempts, their developing perspectives, novelty, and the driving goal of individual studies with critical comparison. Experimental design details of previous laboratory scaled DS vibration experiments were outlined, investigation approaches and findings were discussed, and the limitations of the experiments were highlighted. The laboratory scaled experimental setups have been largely categorized into generally scaled and mechanically-scaled experiments.

2.1 Generally Scaled Experiments

Generally scaled experiments are usually designed by scaling the DS geometric aspects only and sometimes considering a limited number of acting dynamics pertaining to the investigation such as major excitation sources, and damping effects including the rock-bit interactions. Theoretical assumptions, limited assembly, and instrumentation difficulties already limit the scope of vibration studies with scaled experimental models (Gao and Miska, 2010). Many practical drilling conditions are often ignored for simplicity and ease of investigation. This is because generally scaled experiments mostly address specific vibration phenomena and their excitation mechanism. The overall geometric scaling is only arbitrarily adapted for sufficient relatability for field-size operations, and dynamic scaling can only relate to very specific normal drilling conditions. Material scaling is fully disregarded in the experimental design and generally scaled experiments never aim to create a scaled prototype relating to a field-size drillstring. Thus, the results of the generally scaled experiments carry less relevance to complex engineering operations and are not practical for direct dynamic predictability for field-size operations. In a wide survey on laboratory scaled experiments, Patil and Teodoriu (2013) labeled such generally scaled experiments as steady state dynamic studies, which are a practical means for cost-effective repetitive DS analysis that can provide some insight into field behavior rather than pure numeric predictions. All the generally scaled experiments are organized in chronological order of their publication in APPENDIX A. GENERALLY SCALED EXPERIMENTS.

For example, Majeed et al., (2013) built a very simplistic experimental setup of a 2 degree of freedom (DOF) Jeffcott rotor model of a DS to validate their proposed self-tuning closed-loop control algorithm for the reduction of torsional vibration and stick-slip (Figure A.4-a). The experimental setup consisted of a 1 m long slender rod with a heavier bottom section theoretically resembling an 8 - 10 km DS. Later, Ullah (2018) improved upon this model by building a larger 4.1 m long setup that allowed the observation of high-frequency torsional oscillation (Figure A.5-

b), which was not observed in the shorter setup of Mazeed et al., (2013). Therefore, experimental setups based on arbitrary scaling may often fall short of recreating all the DS dynamics, where certain field observations would not be apparent or feasibly observable without a large enough or improperly assembled experimental setup.

Yet, multiple large-scale laboratory experiments have been established, which have a satisfactory record of predicting qualitative characteristics and range of vibration behavior for different drilling operations such as the Hard Rock Drilling laboratory test rig at the Sandia National Laboratories (Raymond et al., 2008) (Figure A.2-a). There had been several attempts to automize laboratory drilling rigs to simulate practical drilling operations vibrations as well. For example, Esmaeili et al., (2012) constructed a fully automated laboratory drilling rig with dimensions of 40 mm diameter and 524 mm long (Figure A.4-c). The assembly allows testing of 2 - 3 in (50.8 - 76.2 mm) diameter roller-cone bits on drilling core samples of brick, concrete, and rock with a maximum of 360 RPM and 80 kg WOB. Their results showed the effect of different combinations of WOB and RPM on DS vibration and TOB-ROP behavior. Later, Esmaeili et al., (2013) used the same setup to develop a neural network architecture for formation prediction through specific energy and ROP in combination with higher order vibration frequency for rock formation classification. Experimental data from this setup also allowed Elmgerbi et al., (2021 and 2022) to develop an application of machine learning techniques for real-time ROP optimization.

Many generally scaled experimental investigations have been conducted over the past decades to observe DS/BHA drilling dynamics. Almost all the experiments mention observing drilling vibration to some extent due to its crucial significance during the study of any DS operations or its components. Even if these experimental investigations had provided extensive data on different operational conditions, they did not analyze the vibration data or determine the effects of vibration.

2.1.1 Near Bit Interaction Studies

In recent years, bit manufacturers have also grown a keen interest in the effects of vibration on ROP. Especially due to the current popularity of unconventional drilling practices and often drilling into unprecedently hard rock formations. However, their laboratory experiments are further simplified to only study ROP for specific bit-rock interactions in a very controlled drilling environment. The experimental setup mostly consisted of scaled drill-bits and load-cells or drilling rock samples. Such vertical laboratory scale representation can be found in the work of Franca et. al., (2011) (Figure A.3-b). The authors investigated the drilling action of roller-cone bits and developed a numerical ROP model. Similar work was done by Mostofi et al., (2013), on a slightly larger scale, where a lathe machine was used to drill into rock samples (Figure A.4-b). The issue with these approaches is that they do not bear resemblance to actual DS models. Their methodology only investigates drill-bit performance with respect to ROP.

The few drill-bit focused investigations that investigated the effects of drilling vibration mostly focused on pure axial vibration and recreated the bit-bounce phenomenon. For example, Raymond et al., (2008) broadened the scope of bit interaction research by investigating DS dynamics with different bit-rock combinations using model-based control and mechanical analog system to reproduce specific DS vibrations (Figure A.2-a). The experimental rig was fully instrumented to measure RPM, TOB, WOB, ROP, accelerations, and longitudinal and rotational displacements of the drill-bit. A 3 in (76.2 mm) diameter metal rod resembled the DS that accommodated a 3.25 in (82.55 mm) diameter coring bit operated between 140 - 260 RPM and 5,000 lb (2,268 kg) WOB.

In another study, Cheng et al., (2011) investigated the transmission rate of vibration responses from the drill-bit to the BHA (Figure A.3-c). The authors used a laboratory rig to perform near-bit force measurement and vibration data transmission along their experimental BHA. Four-straight beam strain gauges were used as dynamic force sensors to measure the axial and lateral forces and TOB. The experimental BHA was 6.45 m long, consisting of multiple carbon steel DS segments. The DS

design followed the pattern of lower drill-pipe, first drill-collar, flexible drill-pipe, second drill-collar and upper drill-pipe. The drill-collars were 87 mm diameters and 5 mm long. The flexible drill-pipe was 34 diameters and lower/upper drill-pipe was 38 diameter, and their lengths varied for two different drillstring assemblies in the experiment.. From one end, rotation was provided using a hydraulic device and on the other end, a three-jaw chuck connection resembled fixed bit contact. The experiments were conducted with 180 RPM, an average of 1,984 lb WOB, and at 0 – 90-deg angle deviations.

Many researchers only focused on collecting an extensive amount of data for correlation between operational variables and future extrapolations. Such experimental tests were conducted by Bavadiya et. al., (2015 and 2017) to amass data on the drilling behavior of PDC bit for soft and hard sandstone samples (Figure A.4-d). The authors observed lateral and axial vibration with a Drillbotics Test Rig. A 36 in (0.9 m) long and 0.375 in (9.525 mm) diameter aluminum pipe resembled the experimental DS with stabilizers and a custom-built two cutter 1.125 in (28.575 mm) diameter PDC bit with 0.078 in (1.981 mm) diameter nozzles on each cutter. A swivel was attached at the top of the drill-pipe section to supply drilling fluid through the nozzles with measured pressures and flow rates while drilling between 50 - 900 RPM with 10 - 50 lb (4.5 - 22.7 kg) WOB. The test setup was equipped with displacement sensors to measure lateral vibration, load cells to measure WOB, and other instrumentation means to measure RPM, torque, and axial vibration. Despite explicit design details, there was no discussion on the scaling relation between the experimental setup and any field-size operation.

Among the near-bit investigations that discuss friction induced vibration, Mihajlovic (2005) and Mihajlovic et al., (2006) investigated friction-induced torsional vibration and its coupled nature in the presence of lateral and torsional vibration (Figure A.1-d). The experimental setup used a 2-disc lumped mass connected by a 3 m low-stiffness steel string which created a flexible rotor system resembling a field DS. The top disc rotates at a fixed center by a DC motor and the bottom disc is

free to move in lateral directions. Additional mass could be added to the bottom disc to induce unbalanced rotational conditions leading to producing lateral vibrations observed during drilling action. A brake and a small oil-box with felt stripes were used to induce direct friction on the bottom disc. The experimental results showed that continuous contact with the wellbore and BHA results in downhole friction that induces negative damping and ultimately leads to vibrations. The authors characterized the nature of both torsional and lateral vibrations in terms of friction and damping. Similar studies were inspired based on this work to investigate coupled vibration phenomena, especially the studies on the coupled effect of axial and torsional vibration for stick-slip.

Liao et al., (2011) built a very similar rotor model to Mihajlovic (2005) (Figure A.3-d). However, instead of incorporating a brake system, the bottom disc was rotated within a confined circular perimeter resembling wellbore walls. The authors claimed to have created a 25:1 laboratory scaled experimental setup in terms of rig height and diameter. However, no field scaled relations were provided. They investigated friction coefficients leading to vibration instability and developed a 5-DOF lumped mass model, by incorporating two previous works on a 2-DOF model on bending-torsional motions (Leine et al., 2002) and a 4-DOF model that addresses the effect of friction (Melakhessou et al., 2003).

Mitigation strategies of stick-slip oscillation through control mechanisms have been heavily investigated. Such experiments rely on a heuristic approach and build control algorithms to tune the operational parameters, i.e., WOB and RPM. For instance, the Oscillation Killer (OSKIL) mechanism (Canudas-de-Wit et al., 1995) is based on heuristic control of the applied RPM during drilling to mitigate torsional oscillations. Canudas-de-Wit et al., (2008) improved the control algorithm to incorporate WOB from surface data in a closed loop control system (D-OSKIL Control Mechanism). Lu et al., (2009) experimentally validated the control algorithm for suppressing DS stick-slip oscillations (Figure A.2-c). The BHA of their experiment was a short series of connected tubes, two lumped mass discs, and helical drill-bit drilling into a woodblock.

Pehlivantürk et al., (2017) showed that control algorithms can perform much better if downhole data can be incorporated along with surface data (Figure A.5-a). The authors built an experimental DS model with 35 precision inertial coupled masses (35 DOF), driven by a precision servo motor and equipped with Vicon motion tracking system. They developed a mathematical model for the closed-loop automated feedback controller where both surface data, including rotational and torque data, and downhole data with bit velocity and trajectory data were fed into the control algorithm.

2.1.2   Lateral Vibration Studies

Isolated torsional vibration studies have significantly progressed in recent decades and conjointly insight into coupled near-bit interaction further helped to explore how coupled vibration modes excite lateral vibrations. For deeper insights, many have attempted to conduct studies on isolated lateral vibration phenomena, i.e., buckling and whirling. Lubinski et al., (1950) first proposed the coupled mathematical model for helical buckling. Later, others extended the model to establish relations between analytical and numerical methods to include the effects of friction, contact force, and material strength capacity (Mitchell, 1982, 2007; Dawson, 1984; Deli et al., 1998; Duman et al., 2003; Gao and Miska, 2009; Wang et al., 2012). However, only a few experimental attempts were made, and even fewer approaches incorporated a DS experimental model due to experiment design and instrumentation difficulty. In one of the rare cases, Popp et al., (2018) investigated backward whirl with an in-house field-size BHA section in continuous and discontinuous borehole profiles. The majority of the experimental investigations for lateral vibration focused on the study of BHA dynamics, as it is generally the source of critical lateral vibration and whirl development (Stroud et al., 2011).

For example, Gao and Miska (2010) analyzed the dynamic behavior of rotating pipes under critical static-dynamic buckling load and interpreted the nature of two different snaking motions based on

the applied static and dynamic WOB (Figure A.2-b). Their horizontal DS consisted of a steel pipe under axial compressive load. It was designed to be in constant contact with a transparent plastic outer tube to resemble deviated drilling. The authors recreated all the major phenomena of lateral vibrations including snaking, irregular, and whirling motions. The experimental setup was simplified to neglect stick-slip, TOB, viscous damping, and wellbore tortuosity.

Forster et al., (2010) designed a vertical vibration test rig to investigate both lateral and torsional vibrations separately to test the vibration mitigation effectiveness of a BHA tool (Figure A.3-a). A slender 5 mm diameter and 2 m long steel rod resembled the DS. Bending limits were observed for lower modes of lateral vibration for 1 - 3.5 kg compressive WOB. Later, Forster (2011) investigated the effect of axial loads on stick-slip vibration mitigation. The rig was modified to only a 1 mm diameter and 1,250 mm long slender steel rod. While valuable insights into DS lateral and torsional vibrations were obtained from these experiments, the reasoning behind the scaling relations was not properly described.

Rather than studying individual isolated phenomena with individual experiments, Wiercigroch (2010) begin developing a BHA experiment to gradually improve the means of studying all modes of drilling vibration with a single experimental setup (Figure A.5-c). Kapitaniak et al., (2015) presented the modified setup that investigated the coupling between axial-torsional-lateral vibrations with emphasis on torsional oscillation during buckling. The experiment investigated bit-rock interaction with scaled bits and rock samples, and the effect of WOB and RPM on vibration stability. The experimental DS comprised both slender-rigid and flexible-wounded wire sections. The lower section of the DS could hold different numbers of discs to both resemble the heavier BHA section and apply 2.06 - 2.71 kN WOB. The experimental rig was modified from a small pillar-drilling machine that operated at a maximum of 1,032 RPM. Loose bearing at the BHA section acted as a stabilizer. Commercial drill-bits and 150x150x150 mm blocks of sandstone, granite, and limestone rock samples were used in the study. The structure was instrumented with

rotary encoders at both ends to measure RPM, eddy-current probes fitted into the loose bearing measured DS displacement, and an LVDT fitted near the drill-bit measure ROP. A special 4-component dynamometer setup was used to measure WOB, TOB, axial force, transversal loads, and resistive torque below the rock samples. Kapitaniak et al., (2016) further studied the torsional vibration nature of second-degree helical buckling and successfully recreated the phenomenon. DS trajectory during stick-slip was analyzed to develop a numerical finite element analysis. In their recent iteration of work, they investigated isolated phenomena of both backward and forward whirling and characterized parametric ranges for chaotic and periodic whirling (Kapitaniak et al. 2018).

Each of the previously mentioned experimental investigations provides crucial insights into designing experimental setups for studying BHA and DS vibrations. They all emphasize the need for designing experiments with better relatability to overall DS vibration observed in the field. In every iteration of an individual experiment, they recognized the shortcomings of their design and perfected the experimental response relatability for additional investigations. Yet, these experimental setups are limited due to their inherent design philosophy and lack of scaling.

2.1.3   Integration of Hydrodynamics

Drilling operations are performed under submerged hydrodynamic conditions to maintain wellbore structural stability and mechanical integrity of downhole drilling equipment. Fluid properties and hydrodynamic pressure variation along the wellbore due to continuous circulation during the drilling operation, however, little attention has been given to studying its effect on DS vibration. Theoretically, fluid-induced vibrations of DS have been addressed in multiple forms (Chen et al., 1976; Campbell 1980, Paidoussis 1983 and 1998; Merlo et al., 1995; Paidoussis et al., 2008; Ritto et al., 2009; Jafari et al., 2012; Khulief et al., 2014a; Al Dushaishi et al., 2016).

Due to the difficulty of experimental implementation, and instrumentation, the presence of fluid is often ignored in the experimental investigations of drilling vibrations. Also, in the mathematical modeling for drilling vibrations, the fluid effect is highly simplified to overlook its dynamic relations and defined with lumped terms as viscous damping. Sengupta (1993) considered the drilling mud to be an incompressible Newtonian viscous fluid and addressed that, the damping ratio depends only on the dominant frequency of vibration. Studying the change in frequency responses due to the presence of different fluids during the drilling operation is a practical approach for quantifying the viscous damping for a particular operation. Therefore, most of the past experimental investigations that are relatable to DS vibration conducted flexural analysis for confined rotor dynamics under partially or fully fluid submersion; following the theory of hydrodynamic mass effects on dynamic bodies originally proposed by Stokes (1843).

For example, Fritz and Kiss (1966) presented a 1-DOF theoretical model for unbalanced mass and fluids damping, and to validate this model, Fritz (1970) formulated an experimental vibration study of a flexible supported rotor with a small degree of unbalance, surrounded by a thin layer of fluid (Figure A.1-a). The experiment included a 1.125 in (28.575 mm) diameter and 6 in (152.4 mm) long vertical aluminum rotor representing the DS within a larger steel container acting as the wellbore, with a radial clearance of about 0.2 in (5.08 mm). A 1-HP DC motor was used as the top-drive, and a wooden mallet was used to create sharp impulse shocks to the rotor. Fluid damping effects for air, water, oil, and water-glycerol mixture were investigated. The radial deflection, rotational vibration amplitude, and natural frequencies of the system were measured and compared, with and without rotation.

In 1992, Antunes et al. used a large experimental setup of a rotor to investigate the lateral vibration dynamics including different whirling, under submerged conditions and qualitatively validated their mathematical model in Axisa and Antunes (1992) (Figure A.1-b). A vertical rotor shaft of 1 m could be partially or fully submerged in fluids within clear cylindrical confinement. Struts were

used for rotor stabilization, and a shaker was used to apply lateral excitation from the top. They investigated the damped vibration response due to added mass of the fluid, fluid viscosity, and fluid friction, for different submersion levels of fluid. The result showed a parabolic relation between the critical velocity and the fluid level.

One of the first laboratory scaled experiments of DS vibrations under submerged conditions was conducted by Berlioz et al., (1996) (Figure A.1-c). They experimented with two different DS assemblies, one fully vertical and one deviated. A slender 3 mm diameter steel rod, with 1,485 mm straight length and 1,880 mm curved section with stabilizers, represented the experimental DS. Water-tight removable plexiglass pipes of different diameters could be installed around the DS to mimic the wellbore with different annulus clearances. The rig was remodeled from a small vertical drill-machine that operated within $0 - 200$ N axial force, $0 - 10$ Nm torque, and 150 RPM. A shaker was used to simulate the bit rock interaction from the bottom end to induce lateral instability. The results showed that increasing fluid density and viscosity decrease the lateral frequency and reduce the vibration levels through dissipation as previously discussed by Iwatsubo et al., (1973). This experimental investigation validated several other previous assumptions, such as the increase of lateral natural frequencies with tension force and decrease with a compression force (Willems and Holzer, 1967). The experimental investigation also bridged previous mathematical models of dynamic instability (Hsu, 1963), theoretical rotor dynamic (Wehrli, 1963; Ziegler, 1977; Unger and Brull, 1981), and experimental rotor dynamic (Eshleman and Eubanks, 1970; Iwatsubo et al., 1973; Dufour et al., 1985). Melakhessou et. al. (2003) further modified the experimental setup of Berlioz et. al., (1996) to develop a 4-DOF mathematical model for all modes of vibrations. This time, a magnetic brake was used at the bottom end before the shaker, to simulate contact friction and stick-slip.

Khulief and Sulaiman (2009) incorporated the drilling fluid effect on DS axial, torsional, and lateral vibration modes using fluid elastodynamic and fluid interaction models (Blevins, 1974;

Dimarogonas and Paipetis,1983; Paidoussis, 1983) and verified their model with spectral analysis (Figure A.2-d). The experiment consisted of a uniform steel rod of 6 mm diameter with an effective length of 1,440 mm resembling a vertical BHA. A magnetic tension brake and electromagnetic shakers were used to simulate the bit rock interaction in the torsional and axial directions. The DS rod ran through a plexiglass tube resembling a wellbore filled with air, turpentine oil, or water. Water-tight eddy current proximity probe stations were placed at equal distances onto the plexiglass to measure the vibratory deflection. They recognized that the fluid friction depends on the oscillation frequency of the vibrating elastic structure and decreases with the frequency of the axial load throughout the DS as a tethering effect. Khulief et al., (2014b) used a similar approach to model the fluid effect on DS vibration and verified their fluid-induced vibration model in an experimental test with heat exchangers.

Although all these investigations provided more practical insight into the effects of different quality fluids on DS vibrations and how the presence of fluid affects some operational conditions, they neglected the effect of fluid circulation and hydrodynamic pressure variance in the annulus.

2.1.4   Limitation of General Scaling

Generally-scaled laboratory experiments are adequate in recreating vibration phenomena and destructive drilling conditions to observe drilling vibration mechanisms at a closer distance to formulate vibration mitigation strategies. However, only with geometric scaling, the experimental results would always lack the design and scaling qualities to directly quantify the vibration reproduction parameters or to directly interpret the dynamic responses expected in a practical field-size operation. Generally-scaled approaches for experimental investigations have proven to be a reliable base to improve the mathematical models through isolated studies. However, these setups would always be limited from representing an actual rig due to the inherent characteristics of having

too many simplified geometric or dynamic assumptions and lumped parametric conditions of the operating variables. Even if precise geometric scaling rules were followed, claiming to relate the acquired data for a similar field-size rig based on the geometric ratios, would be just arbitrary.

Vibration data from a well-rounded mechanically scaled experimental setup would be directly comparable to overall downhole data with the scaling relations. Mechanically scaled experiments are scaled, designed, and constructed based on a real field-size rig, where such an approach would be more beneficial for both the numeric development and have more practical relevancy to predict the operational behavior of an actual rig. Yet, attempting to build a true scaled setup can be a rigorous task not only for dealing with too many mechanical similarity aspects of the design but also for technical limitations of data acquisition hardware. The most effective and successful outcomes from the novel experimental studies on drilling vibrations were the result of a decade's worth of experimental endeavor and improving modifications to the same experimental design.

2.2 Mechanically Scaled Experiments

Mechanically scaled experiments account for all the geometric aspects, mechanical material properties, and operating parameters during downscaling and designing. The scaling factors to construct ideal mechanically scaled experiments are to be always derived from a field-size DS.

From the initial designing phase, all the geometric aspects, mechanical material properties, and operating parameters of the field-size operation are scaled based on the available space for experimentation, market available suitable materials, power capabilities, and adequate hardware to record the responses. It is very important to scale within an acceptable range so that the amplitude of all drilling dynamic responses stays within the range of available instrumentation capability and that, there are available materials that fit the description for the scaled material properties. The success of a fully mechanical scaled experiment does not only rely on the reproducibility of specific

21

vibration phenomena under certain conditions but also on providing overall information on drilling dynamics that are directly relatable to practical field operation.

Shyu (1989) presented the first comprehensive dimensional analysis for an experimental setup of DS lateral vibration in the light of mechanical scaling that incorporated relations between the scaling of geometry, material properties, and internal and external forces. The experimental responses were correlated with the field data and compared the effectiveness of the proposed experimental method to the full-scale tests based on the works of Baird et al., (1984, 1985), Aarrestad et al., (1986), and Burgess et al., (1987).

Shyu's (1989) scaling approach represented the BHA by simplified drill collars, where the Buckingham Pi Theorem was constructed for the drill collars using ten parameters affecting the DS lateral vibration (Equation 1).

$$s = f(l, d, D, E, \rho, \rho_m, T, g, \phi, \Omega) \tag{1}$$

Where s denotes the lateral displacement of the drill collar, l is the characteristics length of the drill collar, d is the drill collar outside diameter, D is the diameter of the borehole, E is the drill collar's Young's modulus, T is the weight on bit, g is the acceleration due to gravity, ϕ is the borehole slant angle, Ω is the collar's rotational speed, ρ and ρ_m are the drill collar and mud density respectively.

Using three independent parameters namely, l with a dimension of L length, ρ with dimensions of $M.L^{-3}$, and E with dimensions of $M.S^{-2}.L^{-1}$ where S denotes time, the Buckingham-π was used to establish non-dimensional relationships as seen in Equation 2.

$$\frac{s}{l} = f^*(\theta_1, \theta_2, \theta_3, \theta_4, \theta_5, \theta_6) \tag{2}$$

Where $\theta_1 = d.l^{-1}$, $\theta_2 = D.l^{-1}$, $\theta_3 = T.l^{-2}.E$, $\theta_4 = E.g^{-1}.l^{-1}.(\rho - \rho m)$, $\theta_5 = l.\Omega.\left((\rho - \rho m).E^{-1}\right)^{\frac{1}{2}}$, and $\theta_6 = \phi$.

In terms of the independent variables, scaling ratios and operational parameters similarity relating the laboratory prototype to the real model are derived and summarized in Equation 3, where "P" and "M" subscripts denote the prototype and model respectively.

$$\frac{d_M}{d_P} = \lambda_1 \qquad\qquad \frac{D_M}{D_P} = \lambda_1 \qquad (3)$$

$$\frac{T_M}{T_P} = \frac{(l^2E)_M}{(l^2E)_P} = \lambda_1^2 \lambda_3 \qquad\qquad \frac{(\rho - \rho_m)_M}{(\rho - \rho_m)_P} = \frac{E_M l_P}{E_P l_M} = \frac{\lambda_3}{\lambda_1}$$

$$\frac{\phi_M}{\phi_P} = 1 \qquad\qquad \frac{\Omega_M}{\Omega_P} = \frac{\left[l\left(\frac{\rho - \rho_m}{E}\right)^{\frac{1}{2}}\right]_P}{\left[l\left(\frac{\rho - \rho_m}{E}\right)^{\frac{1}{2}}\right]_M} = \left(\frac{\lambda_3}{\lambda_2 \lambda_1^2}\right)^{\frac{1}{2}}$$

Where the notation ratios are defined as $\lambda_1 = \frac{l_M}{l_P}$, $\lambda_2 = \frac{(\rho - \rho_m)_M}{(\rho - \rho_m)_P}$, and $\lambda_3 = \frac{E_M}{E_P}$. Several researchers presented methods of mechanical and dynamic scaling of unbalanced rotor bodies, however, very few bridged the relation for DS operations.

One of the notable numeric modeling studies had been conducted by Wu et al., (2002) and Wu (2007, 2015), discussing the predictability of vibration characteristics by the scaled models relating to full-scale rotor-bearing and rotor-shift systems for lateral and torsional vibrations respectively. For the numeric formulation the description of similarity relation and dimensional analysis for practical scaling by Bridgman (1992) and Baker et al., (1973), lateral vibration studies on lumped rotor dynamic by Nelson et al., (1980) and Bathe (1982), and torsional vibration motion prediction by Clough and Penzien (1993), were adapted. Shyu also referred to similitude studies of marine structures by Vassalos (1999), and vibration response studies of scaled down experimental models by Rezaeepazhand (1996).

2.2.1 Experimental Attempts

Shyu (1989) presented a detailed mechanically scaled experiment to investigate DS lateral vibrations (Figure B.1-a). The experimental setup resembled a 60 ft (18.29 m) drill collar BHA with a density of 490 lb/ft3 (7,849.05 kg/m3) and a Young's Modulus of 30×106 psi (206.84 GPa), operating with 8.8 lb/gal (1.05 g/ml) drilling mud. Meanwhile, the vertical BHA prototype consisted of an Acrylic 0.25 in (6.35 mm) diameter and 1 m long rod having a density of 80 lb/ft3 (1,281.48 kg/m3) and 380×103 psi (2.62 GPa) young's modulus. The BHA was connected to a DC motor with a slip ring connection, and axial excitation was induced with a shaker. Lateral vibration stability, including forward and backward whirls, and the influence of coupled axial excitation and rotational speed were investigated using spectral analysis.

Westermann et al., (2015) used the principle of mechanical similarity and derived proportionality factors described in Grote and Feldhusen's (2011) DS vibration experiment addressing lateral vibrations (Figure B.1-b). The experimental design was based on an 870 m long DS that consisted of a 160 m long BHA, where they identified a 20 m BHA section with a 165 mm outside diameter for investigation. A geometrical scaling ratio of near 1:4 was maintained, where the DS was represented by a horizontally pinned 5.4 m long shaft with 44.5 mm outside diameter and 19.5 mm inside diameter supported by two bearings. A drive motor and axial force modules were used at one end supplying rotational speed and axial force. In the middle of the shaft, a contact module was set to act as the borehole wall of 60 mm inside diameter that housed force sensors and displacement sensors to measure contact forces and map the trajectory of the shaft. The scaling description in Grote and Feldhusen (2011) categorized similarity ratio notations into four categories – geometric, temporal, dynamic, and thermal. The constant geometric scaling ratio between the experimental prototype versus the real model was taken, $\varphi l =\sim 1:4$, and sixteen other dynamic and mechanical material property parameters were scaled for different power magnitudes of φl.

Most DS experimental attempts lack proper documentation and details behind the scaling principle. For example, Ren et al., (2017) investigated BHA vibrations using a horizontal experimental setup with a continuous shaft, where the shaft was placed inside a jacket of circulating fluid (Figure B.1-c). They used the similitude principle presented by Shao et al., (2013) to scale the applied WOB and RPM to the experimental setup under field conditions. However, similarity ratios between the experimental to field conditions were given only for RPM and WOB, where their work lacked sufficient descriptions of the experimental setup, and the effect of fluid presence was not discussed. They categorized the nature of bending vibrations to rotational speed and stated that rotational speed does not affect the critical axial load for buckling.

An investigation of all DS vibration modes was presented experimentally by Lin et el., (2018) (Figure B.1-c) using the similarity principle presented by Fan et al., (2013). A scaling ratio of 1:8 was used for six geometric parameters for the wellbore and DS, and eight dynamic parameter scaling ratios were calculated in terms of different power magnitudes of the proposed scale. The scaling ratio of the DS mechanical material properties to the experiment was kept constant, i.e., 1:1. Their experiment consisted of a horizontal 25 m long connection of multiple steel tubes with 12 mm outside diameter and 1.5 mm thickness, within three discontinuous tubes of glass wellbore with 20 mm inside diameter. The electromotor was housed on a separate axially movable block to provide axial force and isolate mechanical vibration. Their results showed that whirling can be observed for different imposed rotational speeds, however, no stable whirling could be observed in the experiment, and a variable rate of stick-slip was always present.

Wang et al. (2018) conducted an experimental investigation focused on lateral vibration of horizontal deviated wells using a mechanically scaled design, without providing details of similarity derivation and scaling ratios analysis (Figure B.1-a). Four similarity ratio relations based on geometric length, density, elasticity modulus, axial force, and inclination angle were considered for similarity analysis based on Shao (2013). The BHA was represented by a 10 m long ABS

engineering plastic rod of 18 mm OD and 5.8 mm ID, with material properties of 1.05 g/cm^3 density and 2.3 GPa elasticity, which was placed inside a clear Lucite-e tube resembling a 25 mm wellbore. The setup was mounted in adjustable rails providing a wellbore inclination of 11° from the horizontal plane. The results provided limited observations of DS dynamics, where it showed that RPM has more effect on BHA lateral displacement than WOB or inclination and suggested using higher RPM for drilling practice with the real model to experience less lateral vibration.

A review of past laboratory-scale experiments was performed by Srivastava and Teodoriu (2019) to address the novelty of downscaling laboratory test rigs, summarized downscaled factors, and discussed experimental component selection. They also constructed a test rig with 1:30 geometric scaling (Figure B.2-b) following the approach of similarity analysis presented in Westermann et al. (2015). The experimental setup consisted of a tall 15 m PVC pipe with a 4 mm diameter representing the drill-pipe. The top drive assembly is mounted on a fixed structure, while the bottom end of the pipe was connected to a computer precision-controlled hexapod capable of providing axial and lateral vibrations and a brake system to simulate stick-slip vibrations.

In a recent experimental study of BHA vibration, Li et al., (2020) investigated lateral vibration modes for highly deviated wells (Figure B.2-c) based on the similarity principle (Shi et al.,2006; Butterfield, 1999; Shao, 2013). Scaling ratios of 4:1 and 1:130,000 were used for rotational speed and WOB, respectively. From a geometric point of view, 1:43, 1:70, and 2:13 scaling ratios were used for the length and elasticity, and material density of their proposed experiment. For similarity analysis, six scalable key parameters affecting the lateral vibration of DS were identified. Meanwhile, length, density, and elasticity were selected as their independent variables. The friction coefficient and inclination angle were considered key parameters affecting lateral vibration but, these were dimensionless parameters and needed no scaling. The experimental BHA setup consisted of a 2 m long with 5 mm outside diameter soft material pipe, a near-bit stabilizer of 7 mm diameter, and an 8 mm diameter drill-bit at the end. The drill collar material had 1200 kg/m^3 density

and 3 GPa elasticity modulus, where the BHA was housed in an 8 mm inside diameter wellbore. The BHA was rotated from the top end with a servo motor and had a loading screw at the bottom end to apply WOB, where the entire structure was mounted on an adjustable horizontal bench creating 0, 30°, 45°, 60°, 75°, and 90° BHA deviation. They investigated the effect of friction by using different materials for the wellbore, and the effect of WOB, rotational speed, and wellbore inclination in the whirling motion of the DS. Their experimental results showed that lower RPM and larger WOB result in stable drilling in highly deviated wells, and higher ROP increases the contact friction to the wellbore, which leads to more violent lateral vibrations.

2.3   Critical Discussion

An overall summary of the generally scaled laboratory experiments addressing BHA and DS vibrations is outlined in Table 2.1. Several studies used the same experimental setups to investigate different phenomena so, those were listed together in the first column (Esmaeili et al., 2012 and 2013; Elmgerbi et al., 2021 and 2022). Oftentimes the experimental setup was gradually modified and improved to better correlate with field operations and recreate different vibration phenomena (Wiercigroch, 2010; Kapitaniak et al., 2016; Wiercigroch et al., 2017). The far-right column, i.e., DS Angle, represents the angle of the experimental setups with respect to the ground or the horizontal plane where 0° represents a fully horizontal setup (Gao and Miska, 2010), and 90° represents vertical experimentation (Lu et al., 2009). Some experimental investigations included the ability to vary the DS experiment to different angles or even deviated DS (Cheng et al., 2011; Berlioz et al., 1996). The column adjacent to the last column, i.e., Recreated Phenomena, addresses the intended phenomena of investigation. Even though all the listed generally scaled experimental investigations provided insight into drilling vibrations to some degree, not all of them focused on recreating any specific vibration phenomena in their investigation (Mostofi et al., 2013). Some

investigations aimed to study different modes of vibrations, yet the experimentations could not

recreate stable vibration phenomena for analysis (Cheng et al., 2011).

Table 2.1. Summary of Bit-Rock Interaction Models.

| Paper | Investigation | | | |
	Objectives	Approach	Recreated Phenomena	DS Angle
Fritz (1970)	Observing vibration damping effect of different fluids on a rotor system submerged in thin fluid.	Creating sharp impulses/velocity-shock to observe radial vibratory responses and system eigenvalues.	-	90°
Antunes et al. (1992)	Studying dynamic vibration of a rotor system in different fluids, for different levels of immersion.	Proposing fluid friction constants and damping ratios for different rotational speeds based on frequency responses	Whirling	90°
Berlioz et. al. (1996) and Melakhessou et. al. (2003)	Evaluating lateral vibration dissipation by dense viscous fluid. Mathematical modeling for all modes of vibrations.	Correlating flexural responses with fluid viscosity and density, and empirically validating literary presumptions.	Stick-slip, Whirling	90° and 90° to 0° (Deviated Well)
Mihajlovic (2005)	Proving continuous BHA-wellbore contact causes downhole friction that induces negative damping and ultimately leads to vibrations	Formulating mathematical model in correlation with extensive number of experimental data	Stick-slip, Whirling	90°
Raymond et al. (2008)	Formulating for vibration mitigation strategy and operational severity management	Conducting extensive number of experimental studies for different bit-rock operational combinations	Bit-Bounce	90°
Gao and Miska (2010)	Interpreting the nature of two different snaking motion based on the nature of downward amplitude	Analyzing dynamic behavior of rotating pipe under critical static-dynamic buckling load	Whirling, Snaking	0°
Lu et al. (2009)	Validating control method model for the suppression stick-slip oscillations, D-OSKIL Control Mechanism.	Correlating drilling data on a woodblock for different WOB	Stick-slip	90°
Khulief and Sulaiman (2009)	Developing fluid-elastodynamic model.	Correlating with traditional fluid friction models by observing oscillation frequencies	Stick-slip	90°
Forster et al. (2010) and Forster (2011)	Developing strategy, asymmetric vibration damping tool and predictive software for vibration mitigation	Testing various BHA tools and axial loading effectiveness to observe stick–slip and bending vibration. Utilizing of numeric simulation.	Stick-slip	60°, 90°
Franca et. al. (2011)	Investigating drilling response of roller-cone bits and simplifying characteristic model	Lumping the effect of the bit geometry into a few parameters and averaging operating parameters	-	90°
Cheng et al., (2011)	Measuring near-bit forces and observing vibration data transmission of BHA	Utilizing a dynamic force sensor device comprising of four-straight beam strain gauges with a developed laboratory rig	-	0°, 30°, 60°, 90°
Liao et al., (2011)	Establishing relation between DS RPM and wellbore friction. Formulating a 5-DOF numeric model including Axial loading.	Determining preferred DS centralizing friction coefficient	Stick-slip	90°

Mazeed et al., (2013)	Verifying self-tuning closed loop control algorithm	Testing bit-whirl and bit-rotation stabilization for operations at different RPM	Stick-slip, Bit-Whirl	90°
Mostofi et al. (2013)	Investigating drilling response of impregnated diamond bits for a given status of wear	Establishing relation with rotational speed and ROP	-	0°
Esmaeili et al. (2012, 2013) and Elmgerbi et al. (2021, 2022)	Developing a fully automated test-rig and a neural network architecture for real time hydraulic and ROP optimization.	Implementing real-time experimental instrumentation and combining past field data for machine learning.	-	90°
Bavadiya et al., (2015, 2017)	Validating TOB response model with a Drillbotic Test-Rig	Collecting 105 test data of a PDC bit performance on soft and hard sandstone samples, at variable WOB and RPM.	-	90°
Pehlivantürk et al., (2017)	Building a 35 DOF testbed to develop a closed-loop vibration control system	Testing against traditional open-loop system for rotation stabilization and developing numeric model	Stick-slip	90°
Ullah (2018)	Improving self-tuning closed loop control algorithm for high-frequency torsional oscillation	Following up with a larger experimental setup for high-frequency oscillation detection	Stick-slip, HF torsional oscillation	90°
Wiercigroch (2010), Kapitaniak et al. (2015, 2016. 2018) and Wiercigroch et al. (2017)	Developing the best experimental method for studying torsional vibration and consequently developing an experimental setup for recreating all vibration modes.	Analyzing multiple bit-rock combination interactions in relation to various WOB, RPM and different vibration phenomena.	Stick-slip, Buckling, Whirling	90°

Table 2.2 provides more comparable experimental design info on the implementable drilling dynamics and interactive features of the same generally scaled experiments listed in Table 1. The last column in Table 2.2 "Analyzed Vibration Modes" addresses the modes of vibrations being studied in each investigation, i.e., "A" for Axial, "T" for Torsional, and "L" for Lateral. The fully coupled vibration modes investigations were categorized under "All", and the "N/A" category was used for the investigation those had no specific aim for investigating any vibration mode. Several generally scaled experimental investigations briefly discussed drilling vibration and its effect on the outcomes, however, vibration data were not analyzed since that was not their primary focus (Franca et al., 2011). Many experimental investigations were carried out for different purposes rather than pure vibration study and analyzed different modes of vibrations only as a means of

validating control systems (Mazeed et al., 2013), testing tools (Mostofi et al., 2013), or developing new downhole equipment (Forster et al., 2010).

The rest of the columns of Table 2.2 under the "Dynamic Simulation" addresses whether a certain common drilling dynamic condition was simulated or investigated. The first column of this set "Axial Loading" categorizes different mechanisms of applying axial loading or WOB: Constant Loading (CL), Variable Loading (VL), Periodic loading (PL), loading with Bit Interaction (BI), and loading with actual Bit Rock Interaction (BRI). Each investigation had its own rationale to achieve the resemblance of field operations within the limited laboratory confinement. Since it is generally assumed that the DS experimental setup would be under a mechanical compression state, studies investigating only the rotational behavior, often only had the setup in compression between fixed supports without applying any additional loading, i.e., Constant Loading (CL) (Liao et al., 2011; Pehlivantürk et al., 2017). Several investigations incorporated control systems with their mechanism to vary the axial loading magnitude with time, where these types of loading systems were termed Variable Loading (VL) (Lu et al., 2009; Raymond et al., 2008). Few experiments used a shaker to simulate periodic drilling motion, i.e., applying Periodic Loading (PL) (Berlioz et al., 1996; Khulief and Sulaiman, 2009). Some experimental investigations had to observe Bit Interaction (BI) and utilized various methods to reproduce such conditions regardless of the direction of the loading: using an actual bit, a scaled or modified field bit (Bavadiya et al., 2017), a helical bit (Lu et al., 2009), or even only implementing a system that resembles the operation of a bit (Ullah, 2018). But some studies tested the bit response using an actual rock sample to study the effect of bit-rock interaction (BRI).

The "Torsional Impediment" column indicates whether an experimental setup had facilities to directly obstruct the rotational movement of their modeled BHA or DS. Some utilized sort of braking mechanisms or direct impediments to the rotation (Mihajlovic, 2005), and others implemented continuous wellbore interaction with the DS (Liao et al., 2011). It is to be mentioned

that several experiments investigated the effect of wellbore interactions, for example, Liao et al. (2011) used a ring wall that only surrounded the lumped disc representing the BHA portion of the DS in their experiment. Other studies constituted full enclosure whether it was straight or deviated wellbore (Berlioz et al., 1996).

Experimental studies that implemented Bit Interaction (BI) or Wellbore-Interaction, often investigate the effect of friction as well. Since it is very difficult to quantify, often a neutral or simplified condition is adopted (Forster et al., 2010). Few experimental investigations analyzed the effect of friction and further formulated the methods to measure the frictional property before testing with identified frictional values, to correlate with the vibratory responses (Mihajlovic, 2005; Liao et al., 2011). This is addressed in the "Measured Friction" column.

The majority of the experimental investigations were unable to implement fluid interaction into their experimental setups. However, studies almost always emphasize the crucial necessity for the consideration of fluid interactions or viscous damping for the DS system (Gao and Miska, 2010; Forster et al., 2010). Therefore, the studies regarding drilling vibrations that lack experimental data on the effect of hydraulic interaction, often incorporate or correlate the practical understanding of the effect of hydraulic interactions from other experimental investigations or field data (Elmgerbi et al., 2021 and 2022). Hence, the "Fluid Interaction" only addresses the experiments that considered stationary fluid, i.e., submerged DS.

The "Additional Excitation" column indicates whether any external random vibrations and lateral excitation were exerted onto the drilling setups. This additional excitation is a dynamic that is not spontaneously generated through rotation or axial loading. For example, applying direct impact to induce random vibration (Fritz and Kiss, 1966) or inducing directional excitation using a shaker to create lateral excitation (Antunes et al., 1992).

Table 2.2. Dynamic simulations of generally scaled DS vibration experiments.

Paper	Dynamic Simulation						Analyzed Vibration Modes**
	Axial Loading*	Torsional Impediment	Additional Excitation	Measured Friction	Wellbore Interaction	Fluid Interaction	
Fritz (1970)			✓			✓	T
Antunes et al. (1992)			✓			✓	T
Berlioz et. al. (1996) and Melakhessou et. al. (2003)	PL, BI	✓			✓	✓	T, L
Mihajlovic (2005)		✓		✓			T, L
Raymond et al. (2008)	VL, BRI						A, T
Gao and Miska (2010)	CL				✓		L
Lu et al. (2009)	VL, BRI						T
Khulief and Sulaiman (2009)	PL, BI	✓			✓	✓	T
Forster et al. (2010) and Forster (2011)	CL						T, L
Franca et. al. (2011)	CL, BRI						N/A
Cheng et al. (2011)	CL						All
Liao et al. (2011)	CL		✓		✓		T
Mazeed et al. (2013)	CL, BI				✓		T, L
Mostofi et al. (2013)	CL, BRI						N/A
Esmaeili et al., (2012, 2013) and Elmgerbi et al. (2021, 2022)	CL, BRI						All
Bavadiya et. al. (2017)	CL, BRI						All
Pehlivantürk et al. (2017)							T
Ullah (2018)	CL, BI						T
Wiercigroch (2010), and Kapitaniak et al. (2015, 2016. 2018)	CL, BRI						All

* CL = Constant Loading, PL = Periodic Loading, VL = Variable Loading, BI = Bit Interaction, BRI = Bit-Rock Interaction
** A = Axial Vibration, T = Torsional Vibration; L = Lateral Vibration, All = All Vibration

The different investigations of mechanically scaled DS vibration experiments and their dynamic simulations are summarized in Table 2.3. On the mechanically scaled experiment side, all investigations shared a common purpose of developing a fully mechanically scaled experimental assembly following an existing field-size rig (Li et al., 2020; Westermann et al., 2015), or maintaining the scaling ratios within the realizable practical range of field operations (Lin et al., 2018; Wang et al., 2018). The approach of these experiments was to follow a similarity principle and scale down the geometric, material properties, and dynamics of field-size operation for a laboratory-size setup. Some studies provided practical suggestions for safe operational practices and qualitative judgment for field operations based on the data produced from experiments (Lin et al., 2018; Wang et al., 2018).

Table 2.3. Investigations and dynamic simulation of mechanically scaled DS vibration experiments.

Paper	Investigation		Dynamic Simulation						Analyzed Vibration Modes **
	Recreated Phenomena*	DS Angle	Axial Loading	Torsional Impediment	Additional Excitation	Measured Friction	Wellbore Interaction	Fluid Interaction	
Shyu (1989)	Bending, Stick-Slip	90°	PL, BI						All
Westermann et al., (2015) and Gorelik and Höhn (2015)	Whirling, Snaking	0°	CL	✓			✓		T, L
Ren et al., (2017)	Buckling	0°	PL				✓	✓	A, L
Lin et el., (2018)	Stick-Slip	0°	CL				✓		All
Wang et al., (2018)		0°, 11°	CL				✓		T, L
Srivastava and Teodoriu (2019)		90° to 0°	CL, PL	✓	✓				
Li et al., (2020)	Whirling	0°, 30°, 45°, 60°, 75°, 90°	CL			✓	✓		T, L
* CL = Constant Loading, PL = Periodic Loading, VL = Variable Loading, BI = Bit Interaction, BRI = Bit-Rock Interaction									
** A = Axial Vibration, T = Torsional Vibration; L = Lateral Vibration, All = All Vibration									

A summary of the analyzed parameters for similarity principles can be found in Table 2.4 for the mechanically scaled experiments. Mechanically scaled models are specific about scaling all the major downscaling factors including geometric dimensions, mechanical material properties, and simulated dynamic forces acting on the BHA. Most of the mechanically scaled investigations provided very detailed information regarding these scaled parameters. For instance, Lian et al., (2015) developed a mechanically scaled experimental setup to verify the theoretical model. Westermann et al., (2015) built their setup based on a partial portion of the BHA, where the setup was validated with the mathematical model proposed by Gorelik and Höhn (2015). Several investigations lack the necessary details regarding the similarity analysis (Ren et al., 2017).

Table 2.4. Mechanically scaled DS vibration experiments downscaling parameters.

Paper	Downscaled Parameters								
	Geometric			*Material*		*Simulative External Forces*			
	Wellbore Dia	BHA Dia	Characteristic Length	Elasticity	Density or Mass	Axial Load	Rotary Speed	Torque	Gravity or Weight
Shyu (1989)	✓	✓	✓	✓	✓	✓	✓		✓
Westermann et al., (2015) and Gorelik and Höhn (2015)		✓	✓	✓	✓	✓	✓	✓	✓
Ren et al., (2017)		✓	✓	✓	✓	✓	✓		✓
Lin et el., (2018)	✓	✓	✓	✓	✓	✓	✓	✓	✓
Wang et al., (2018)		✓	✓	✓	✓	✓	✓		
Srivastava and Teodoriu (2019)		✓	✓	✓	✓		✓	✓	
Li et al., (2020)	✓	✓	✓	✓	✓	✓	✓	✓	

Generally-scaled DS experiments have proven to be the most feasible experimental study. Even though, these experimental models were inherently limited in adapting all the physical and dynamic parameters that affect drilling vibration. The experimental approaches have become more

innovative and sophisticated due to technological advancements in instrumentation and higher computing resources. The development over the last few decades is observable in Table 2.1 and Table 2.2.

The advancement in material engineering and drill-bit design has greatly reduced the detrimental effects of axial vibrations. But axial vibration itself is not being deeply studied to directly mitigate its causation. The studies on axial vibrations are not broadly discussed in drilling vibration investigations and are only reported without analyzing the effects of vibrations in most bit ROP performance studies. Especially, a recent surge in the availability of reliable bottomhole data can only mean the boon for further development of previously established mathematical models and understanding of vibration mechanisms more effectively by relating the field data to experimental data.

A properly mechanically scaled experiment model would directly relate to a field operation and the acquired data can directly be translated to describe a BHA in field conditions. Only if the experimental setup is downscaled considering all the external and internal forces affecting a BHA. Maintaining this practice of adhering to the governing similarity parameters and discovering more of such affecting scalable parameters, can also establish a rigorous standard for drilling vibration study and more effectively relate to field operations. Such experiments, those listed in Table 2.3 and Table 2.4 are also more relatable to one another regarding their design strategy, and sometimes general instrumentation. These types of experiments have shown that all the essential simulative dynamics and the wide range of drilling operations can be scaled and feasibly implemented based on their similarity analysis. The survey of the mechanically scaled experiments also indicates that implementation of fluid interaction is rare and must be difficult to implement and instrument. Ren et al., (2017) implemented fluid interaction in their design however, they pumped fluid down the annulus section of their experimental BHA from top to bottom, and it was passed to a separated section walled from the initial wellbore section where the experimental BHA operated.

Nonetheless, all these notable attempts had the common purpose to study different modes of drilling vibration in a manner that can be directly related to field operation and their approach was to build a proper mechanically scaled laboratory experiment.

CHAPTER III

3 METHODOLOGY

3.1 Experimental Setup

The core principle of the experimental design was to construct a mechanically scaled versatile, easily implementable and reproducible, and modifiable experiment. The extent of the laboratory space, dynamic capabilities of feasibly attainable power system, market availability of the material, and visually observable vibration phenomena, all were taken into consideration during the mechanical scaling, i.e., geometric, material, and dynamic scaling. Mechanical scaling was chosen over general scaling for its versatility of experimental freedom and field relatability. Because mechanically scaled systems are expected to behave similarly to their field counterpart in modes of vibrations. Detailed downscaling relations were established using the similitude analysis presented by Shyu (1989) while designing the experimental setup. Full details regarding the respective BHA scaling can be found in front of the experimental investigations in the next chapter, in Table 4.1 and Table 4.2. The initial overall schematic design of the experiment is provided in Figure 3.1, while a full view of the experiment is shown in Figure 3.2. Details regarding the structure and individual experimental components are presented in the following subsections and a full structural fabrication blueprint is provided in APPENDIX C. FABRICATION BLUEPRINT OF THE STRUCTURE.
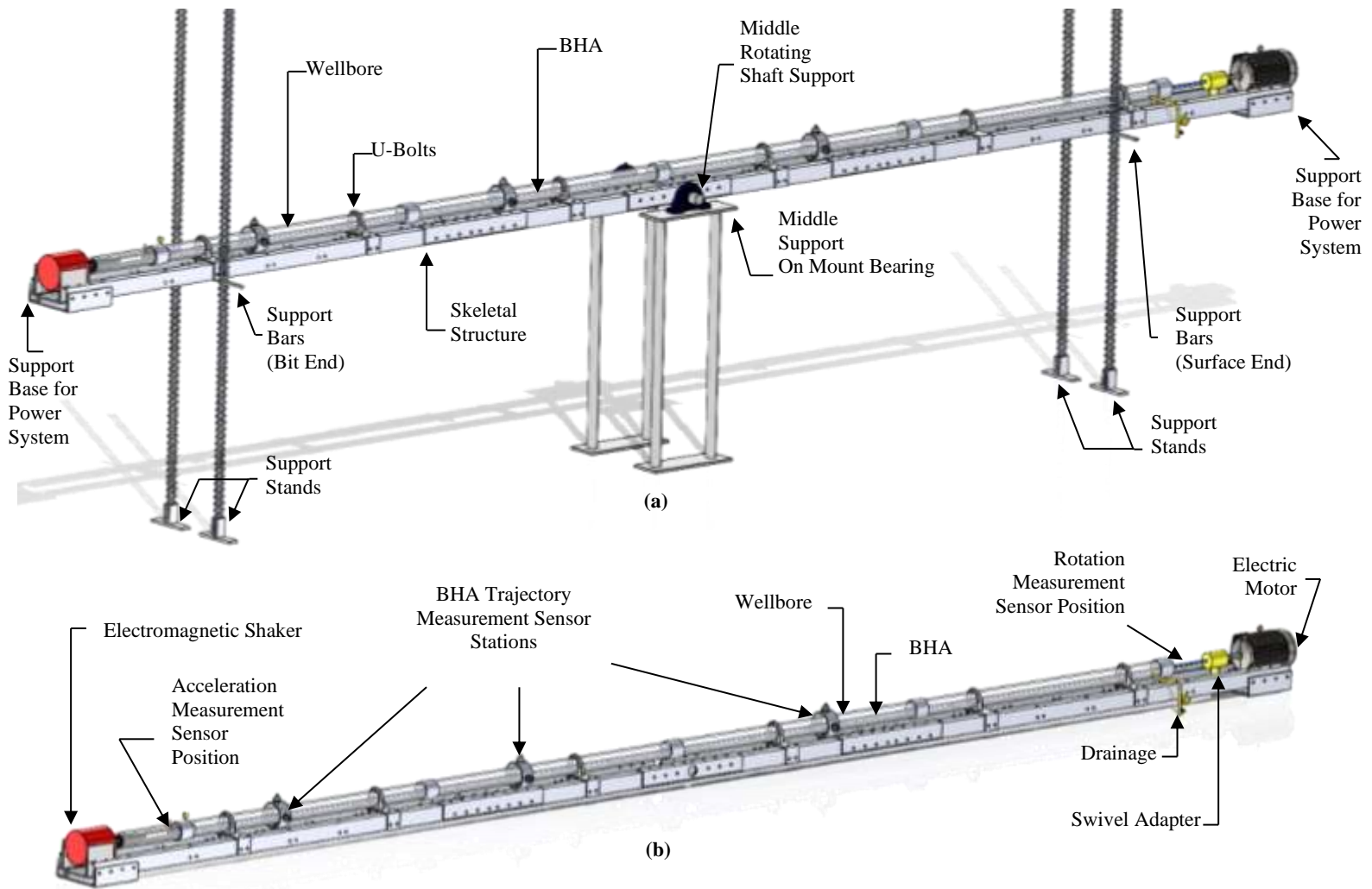
Figure 3.1. Schematic design of the experimental setup: (a) the support structures, (b) the power system, sensor positions, and fluid transportation passages.
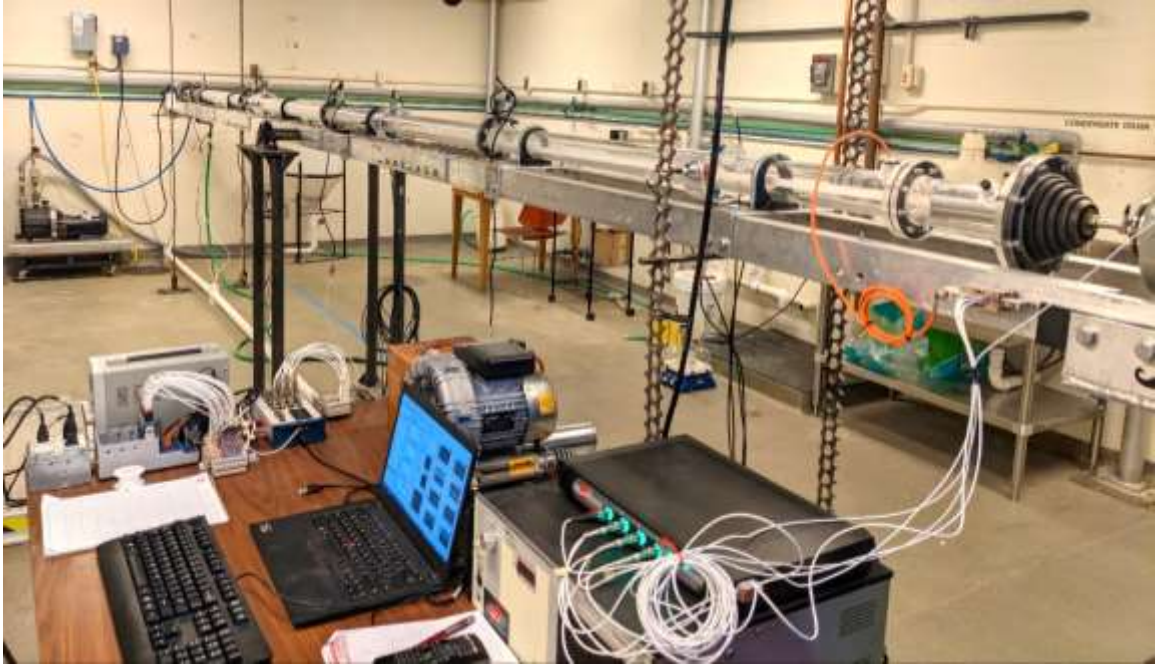
(a)
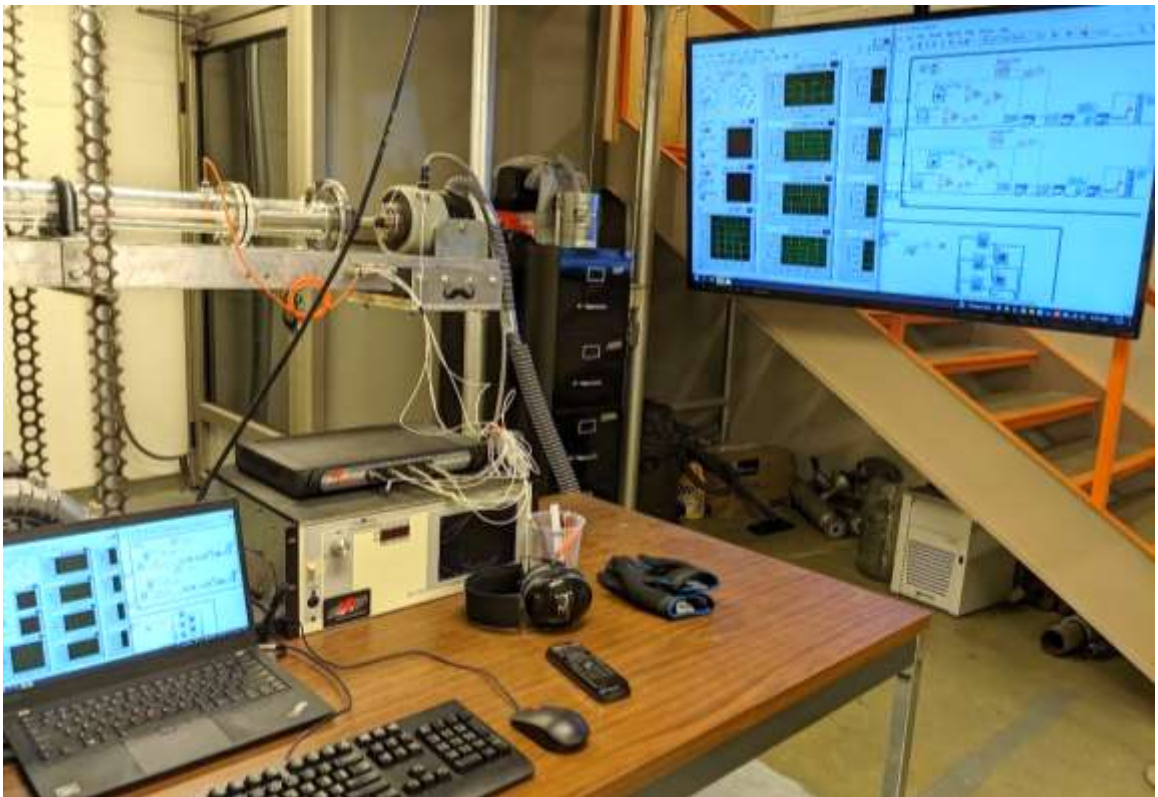
(b)

Figure 3.2. Full view of the experimental setup: (a) structure, (b) workstation.

In brief, a PEX-A tube represents the rotating experimental BHA of the experiment. The BHA is encased within a set of connected clear acrylic cylinders that represent the wellbore. Rotation is provided by an electric motor and fluid is pumped through the swivel adapter into the BHA from the surface end of the experimental setup. Meanwhile, an electromagnetic shaker provides axial bit excitation to the BHA from the bi end. The experiment was equipped with 22 sensors, 3 communication-feedback systems, and 2 sets of terminals paired with 2 data acquisition (DAQ) devices, for well-rounded experimental control and instrumentation. The system is fixated and supported by the skeletal structure made of assembled aluminum angles and u-shaped plates referred to as tables in the blueprint. The skeletal aluminum structure is supported in the middle on a supporting and rotating shaft while two support bars at both ends keep it balanced. Support bars are inserted through the slots on the pair of support stands and can be moved up/down to create wellbore deviation.

3.1.1   Base Structure

A lighter partitioned and compartmentalized design was adapted to be easily implementable and economically viable. The design of the parts was kept symmetric and interchangeable for easy reproducibility with the wider scope of future modification.

Multiple materials with specific purposes were used in the construction of the overall structure - aluminum, mild-steel, wood, and rubber. Only widely market-available premade shapes were used with symmetric design to ensure reproducibility and extension of the structure. The majority of the skeletal structure in direct contact with the power inducing system and the wellbore support has been fabricated using 6061-T6 aluminum (Figure 3.3).

Figure 3.3. Skeletal structure housing the experimental wellbore and BHA, the power system.

This is a lightweight and corrosion-resistant metal that provides great structural strength. This was chosen over other alternatives such as stainless steel since lighter material is more effective in dissipating vibration energy and is more economic. Holes were drilled on aluminum angles symmetrically for multipurpose support, fixation, and interlocking joints. Chamfered and smoothed-edged angles were used for safer handling.

Finite Element Analysis was conducted for maximum loading for a single 25 ft long aluminum angle to ensure the post fabrication integrity. Figure 3.4-a represent the total deformation of the static structure of a 25 ft aluminum angle with edge support and twice as much distributed load as the anticipated load for the experimental setup. The color bar depicts a bending deformation range of 0 – 8.5 mm or 0 – 0.31 in. The stress analysis results showed an average bending of 6 mm or 0.24 in for the overall structure and maximum bending of 8.5 mm or 0.31 in bending at the top middle edges, where the deformation is very low compared to the structure. In order to identify the relative location of the deformation and to perceive the deformation angles better, the figure of the deformation analysis was scaled 10 times larger than its true scale in Figure 3.4-b. The aluminum structure proved to be sufficiently strong for the experiment. Additionally, in the final design, a 24 ft long skeletal structure was constructed with a maximum of 8 ft long aluminum angle segments, and multiple mechanical angle joints were used to strengthen the overall structure and to ensure higher bending resistance.

(a)

(b)
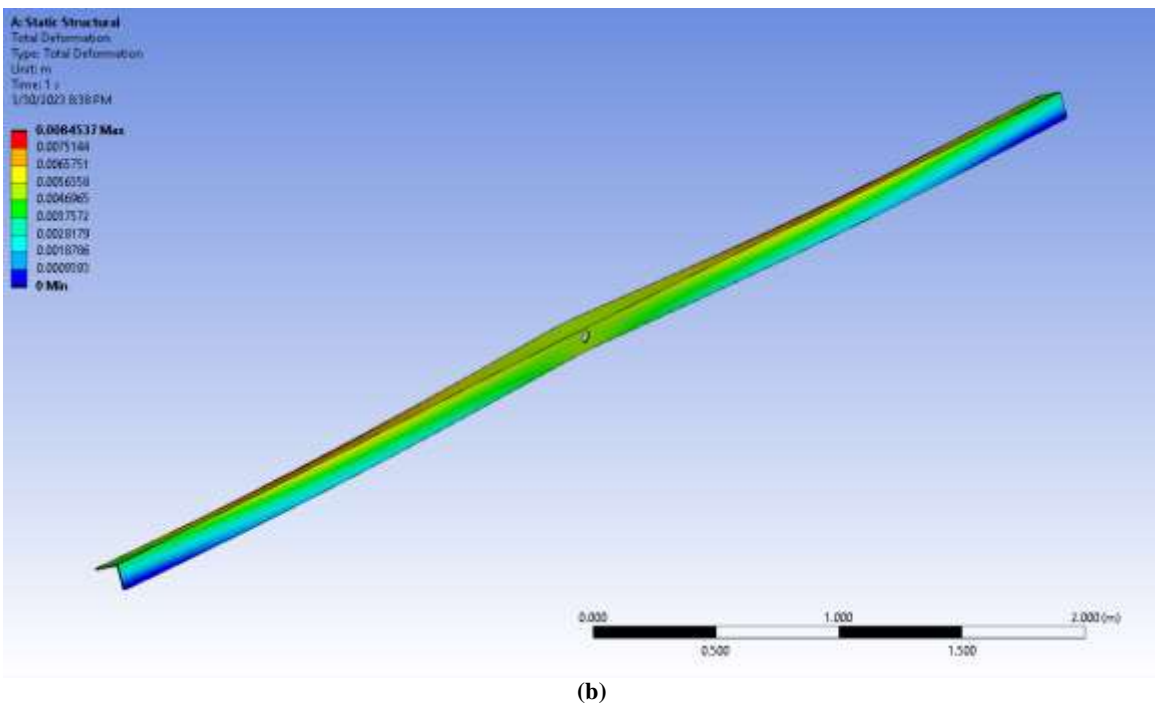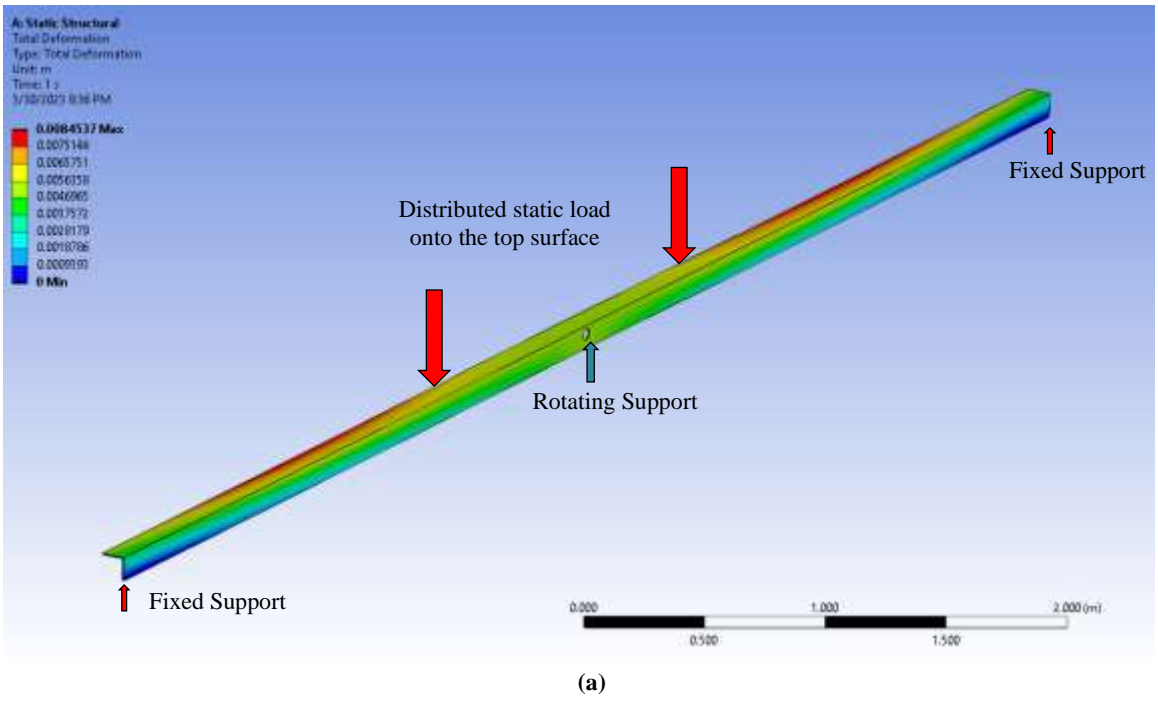
Figure 3.4. Structural load capacity test result: (a) True scale and (b) 10 times the true scale.

The full extent of all the connected parts of the skeletal structure is 24 ft horizontally. Vibration-isolating sandwich support bases consisting of wood and 50-duro Sorbothane rubber were laid under the power system devices housed on the structure to dampen and dissipate vibration during their operation (Figure 3.5). Sorbothane rubber was also put between the contact surfaces of the base carrying supporting bodies and similar rubber bushings were used on the fixating bolts.

| (a) | (b) |
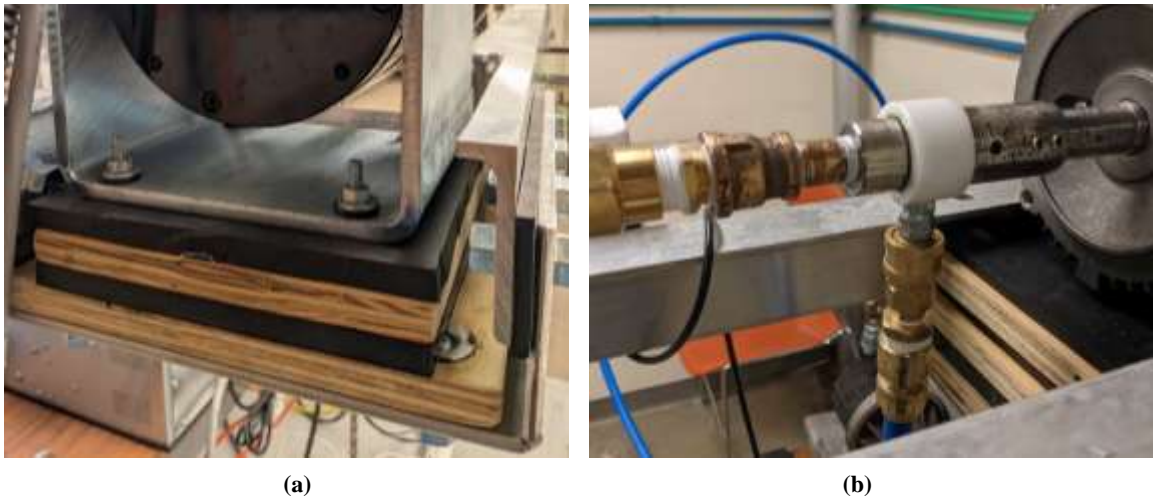
Figure 3.5. Vibration damping support base made of wood and 50-duro Sorbothane rubber sandwich under the dynamic bases of the experiment: (a) Shaker base, (b) Motor base.

Hot rolled A36 mild steel was used to fabricate the strong base support structures to hold the skeletal structure. The horizontal skeletal structure is supported on a high-carbon shaft, like a seesaw, on the middle base support (Figure 3.6-a). Both ends are held on half-circle support bars which can be moved to different slots on the perforated support stands to create a 22°+ deviation from either end (Figure 3.6-b). Half-circle bars were used for circular slots to ensure free rotational adjustments. These support structures hold the skeletal structure 4 ft above the ground level at 0° deviation.
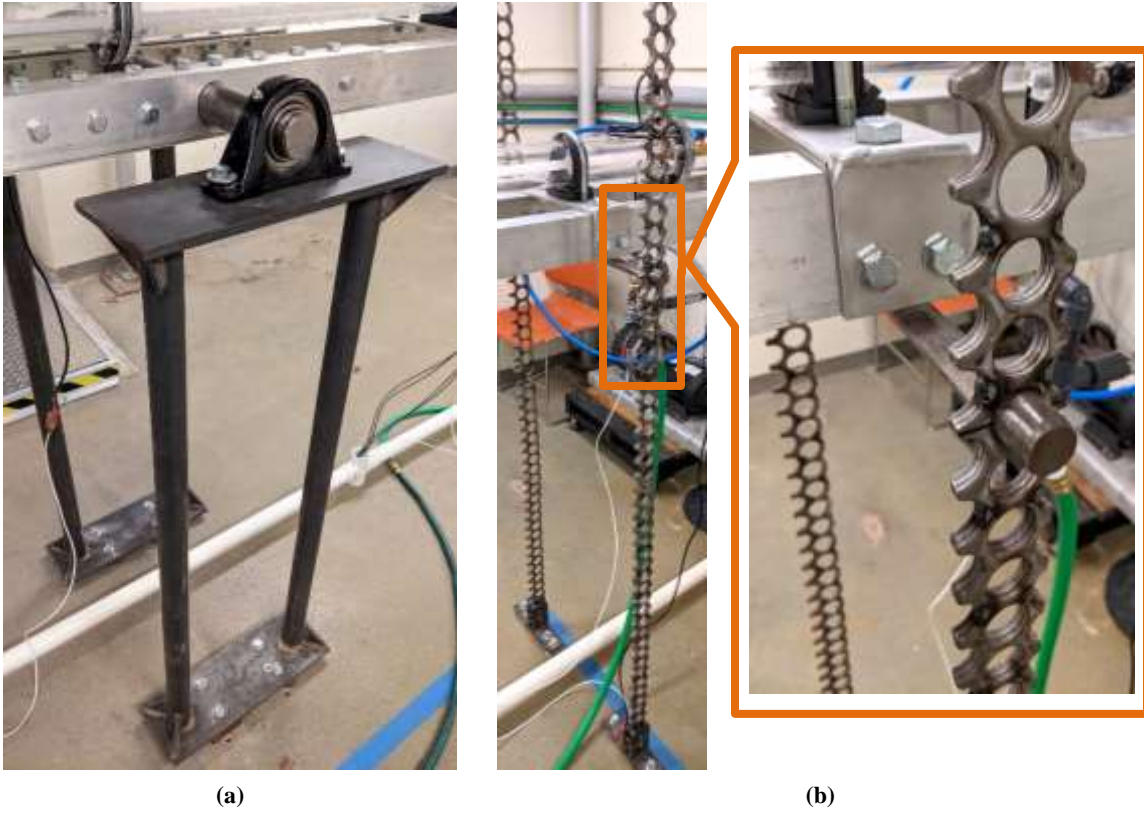
Figure 3.6. (a) Middle support base, (b) Surface-end end-support, and support bar.

3.1.2 Power System

An electromagnetic shaker VR5500 was used to induce axial bit excitation and WOB fluctuations with a maximum capacity of 75 lbf. It has been tested for inducing 0.005 – 1 in reciprocal motion at 20 – 250 Hz while staying within the 18g limit (Figure 3.7-a). The electronic magnetic shaker requires an amplifier and power distributor, an air blower for cooling, a control unit connected to the computer, and a 220 volts power supply to operate. A breaker box has been installed for safety.

An electric 3-phase 1 HP 60 Hz 1150 RPM AC motor was used to provide rotation to the DS (Figure 3.7-b). The motor is operated with an input power of 110 volts, via a variable frequency drive (VFD), FRENIC-Mini FRN0005C2S-6U, which is connected to the computer to input drive commands via an ethernet cable to its ethernet communication port. A breaker box with a 150%

maximum current load capacity than the motor's maximum current load capacity is connected in series to the VFD and the motor to regulate safe power flow.
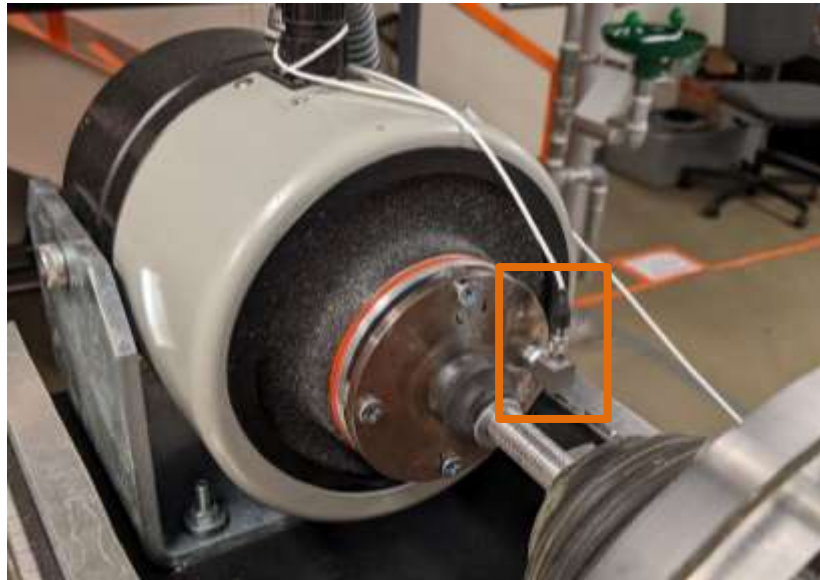
(a)

(b)

Figure 3.7. Power system: (a) Electromagnetic shaker, orange-box marks input feedback sensor for the shaker, (b) Electric AC motor and its operating VFD mounted on the wall alongside its breaker box.

A 1 HP 52 ft max-head (23 psi) 53 GPM (at 10 ft) max-flow centrifugal magnetic drive pump was used to supply water through the experimental BHA. The pump and its VFD are seated on an elevated lockable cart for safety from flooding and easy movement if needed. The pump is operated using another similar 3-phase electric motor and thus a similar VFD setup has been used as the electric motor with another individual VFD (Figure 3.8-a). The same breaker box regulates power to this VFD. On the suction end of the pump, a metal coil reinforced suction pump is connected from a reservoir tank (Figure 3.8-b) to ensure uninterrupted flow. The reservoir tank is equipped with a valved backchannel for drainage. A PEX-B tube is connected at the outlet to supply high velocity flow through quick-connect onto the three-way swivel adapter (Figure 3.8-c). The swivel adapter allows free rotation while water is supplied into the inline connection to the experimental BHA.

| (a) | (b) | (c) |
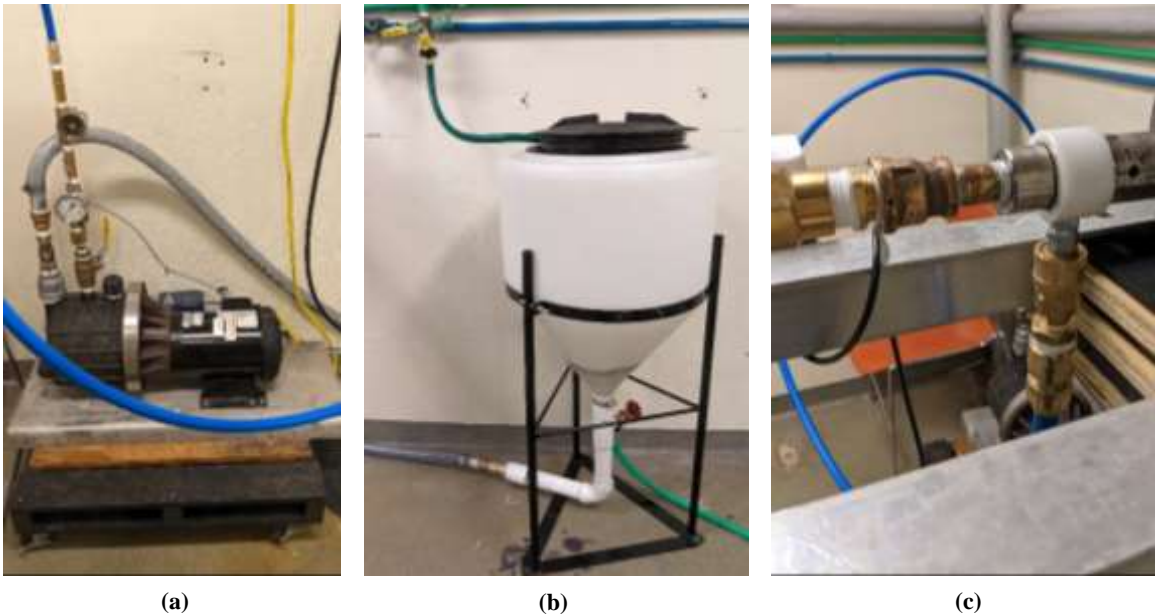
Figure 3.8. Fluid supply system: (a) Centrifugal Pump, (b) Reservoir tank, (c) Swivel adapter.

3.1.3   BHA and Wellbore

PEX-A type flexible tube was used as the experimental downscaled BHA. This is a flexible tube with the desired material property for downscaling because downscaled dynamic properties of the experiment stay within feasible and implementable range. For example, if a PEX-A tube with 0.375 in nominal diameter and 20 ft length represents a mechanically downscaled steel BHA of 5.375 in nominal diameter and 328.1 ft length, only 0.46 lbf experimentally induced WOB on that downscaled prototype would be equivalent to 56,000 lbf in the field following its dynamic scaling ratios. Similarly, the experimental 700 RPM rotation field equivalent would be over 314 RPM. The PEX-A tube has been fitted with brass fittings and couplings transfer rotational torque from the electrical AC motor. A three-way swivel adapter is used in line with these fittings to transfer fluid through the tube. The best practice has been found to have the fittings fixated on the bearing for the best sealing of the wellbore and have the PEX-A fixed to the fitting inside the wellbore (Figure 3.9-b).

On the other end of the experimental BHA, an in-house two-piece fabrication attachment made of stainless steel connects and supplies reciprocating motion from the electromagnetic shaker to the experimental BHA's bit. It was named Power Arm in the design of this experimental assembly (Figure 3.9-a). The power arm has a disc-shaped end that attaches to the shaker and a long hollow shaft extension has a water-resistant bearing to hold the bit-end of the PEX-A tube to let it freely rotate. The tube is passed through the bearing and fixated using metal crimp rings. The fixation on the bearing on the power arm from the shaker and the threaded joint to the brass fittings from the motor mechanically defines two fixed modal points of vibration modes for the PEX-A tube, and the length in-between is considered as the total experimental BHA length. The figures in this section represent the latest design, where the total experimental BHA length is 17.75 ft. Also, three stabilizer bodies of 1.5 in outside diameter are fixed on the tube at 2 ft, 8 ft, and 14 ft away from the bit section.

Figure 3.9. BHA fixtures: (a) Power arm at the bit-end, (b) Brass fittings at the surface-end.

Figure 3.10 shows one of the stabilizers along with a BHA trajectory measuring station. Ultra-weather-resistant EPDM foam strip with adhesive side was wrapped around the tube and 2 in long stainless-steel cylinders sleeves with 1.5 in outside diameter, were pushed over the foam. The foam stays tightly squeezed between the stainless-steel sleeves and the tube and keeps the whole

stabilizer assembly fixed. For protection for the acrylic wellbore inside from the metallic edges of the stabilizer, a thin layer of plastic tape was added on the surface of the stainless-steel sleeves and for additional water resistance, a light coat of polyurethane glue was applied on the side of the stabilizer bodies. The weight ratio of the 2 in long stainless-steel stabilizer and 1 ft of the PEX-A was kept at approximately 4:1.

Figure 3.10. Proximity-sensor stations over the metallic stabilizer of the BHA.

The wellbore is assembled of multiple interchangeable 5 ft long clear acrylic cylinders of 3 in outside diameter and 2.25 in inside diameter (Figure 3.11). Such a design would allow the possibility of future extending the wellbore from the middle. This light material was chosen for lasting clear see-through walls and a practical pressure rating of 100 psi. The acrylic cylinders have

0.25 in NPT connections at each end of the bodies, to install sensors and to run wires for other measurement devices within the wellbore. The connected acrylic cylinders representing the wellbore are fixed to the base-structure via vibration damping U-bolts (Figure 3.11 - marked with an orange box). Vibration damping Sorbothane rubber pieces are also put in between the U-bolts and the base structure skeletal structure to isolate structural noises from the wellbore. It has already been mentioned that the brass fittings run through the wellbore enclosure (Figure 3.9-b) on the electric AC motor end. The long wellbore cylinder part on this closure end has one additional 0.25 in diameter NPT connection at the bottom to drain the wellbore with a valve to control pressure. The wellbore enclosure on the electromagnetic-shaker end is made of flexible rubber material to allow reciprocal motion of the power arm (Figure 3.11 - marked with a blue box). A shorter wellbore cylinder part was used on this end for easy removal and future implementations. More information regarding these data measurement devices and instrumentation can be found in the following sub-section.
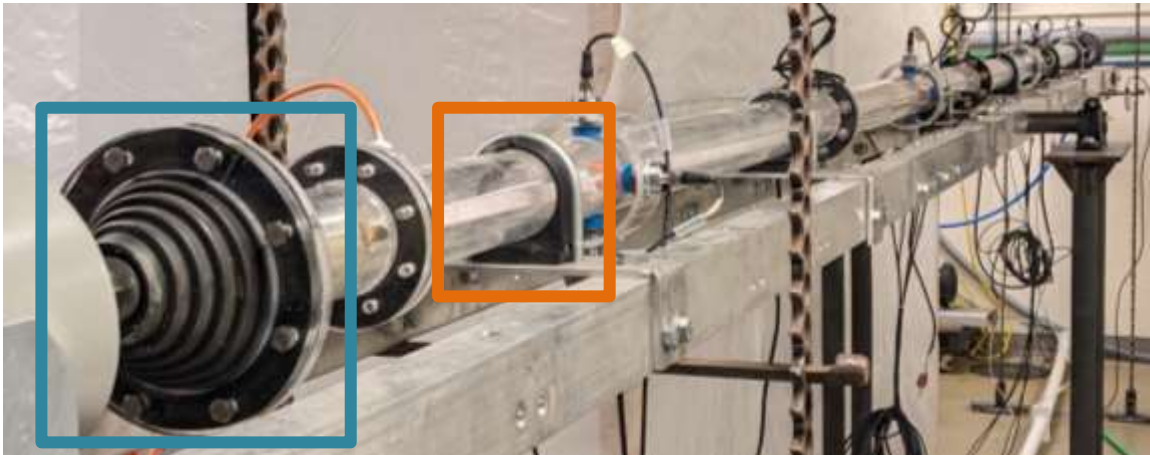
Figure 3.11. Wellbore – the U-Bolt fixture is marked with the orange box and the plunger end-encasing with the blue-box.

3.1.4 Instrumentation

A total of 5 types of sensors were installed in this experimental setup to measure fluid flow rate, pressure profile along the wellbore, rotational speed, the lateral trajectory mapping of the BHA, and lateral acceleration in all three directions at the bit end section. This section discusses the technical purpose, physical placement, wiring, and working principle of the sensors used for these data measurements. Details regarding the control and data measurement can be found in the following sub-section. The data flow from the experimental setup or the full data acquisition (DAQ) system is shown in Figure 3.12.
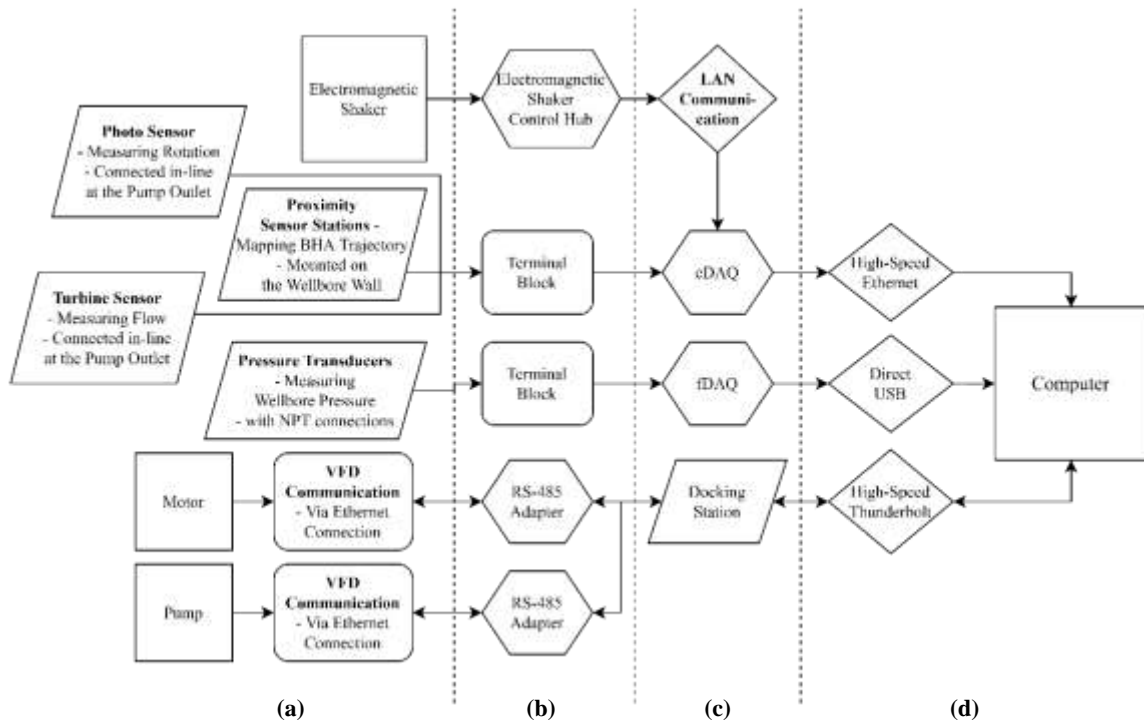
Figure 3.12. Data flow chart of the experiment: (a) Experimental Zone, (b) Data termination and communication processing zone, (c) DAQ modules, and (d) Data storage and communication control.

A turbine flow sensor was connected from the outlet of the pump (Figure 3.13-a). The turbine flow sensor was chosen since these are reliable, easily implementable, additional calibration is not necessary for hysteresis signal or noise, does not require calibration for measurement, and provides

long-lasting accuracy. The sensor has three wire configurations – two for power and one for pulse/switching output signal. The negative/ground wire of the sensor meets at a three-point junction at a splitter connection where one was connected to the negative end of the power supply unit (PSU) and the other acts as the negative differential connection to the DAQ module. Without any flow, the electrical-current signal from the sensor lays flat. During fluid flow, the turbine within the flow sensor rotates, which can visibly be observed through the clear casing of the sensor, and the blades pass an inductive sensor that triggers the generation of electrical current. Hence, the signal jumps to maximum whenever the turbine is rotating. The frequency of the signal jumps can be counted and converted to flow rates in gallons-per-minute (GPM) as per the manufacturer's instructions. Such signal producing mechanism makes these sensors robust and does not require complicated data filtration or adjustments for signal noise or discrepancies. It is to be noted that, if the fluid flow velocity is lower than the flow-sensor's calibrated configuration, the rotor within the sensor would not rotate. A flow sensor with a smaller diameter or adapter needs to be used to restrict flow to have a higher velocity to make the rotor rotate for higher flow rates. But that would also change the conversion relation between the signal frequency and the actual flow rate.

A photoelectric sensor was used to measure the applied rotational speed. The dark-operate signal-wire of the sensor was used (Figure 3.13-b). The photoelectric sensor is also another switching type sensor with a similar wiring configuration as the flow sensor used for this experimental setup. The signal wire supplies a maximum electric current signal whenever the emitted laser from the photoelectric sensor is absorbed by a black surface. The photoelectric sensor laser is pointed at a comparatively bright surface created by wrapping white Teflon tape over the brass fitting that has a tiny dark surface marked by black insulating tape. During the rotation of the fitting, every time the dark surface passes the pointed laser, a peak in signal is acquired and a single revolution can be counted. Thus, the frequency of passing of the dark surface per second can be counted as revolution per second and converted to revolution per minute (RPM). The photosensor could not be

52

implemented to collect rotational data of the BHA from a section that is inside the wellbore since the laser refracts by the acrylic wall or if fluid is passing through the experimental wellbore.
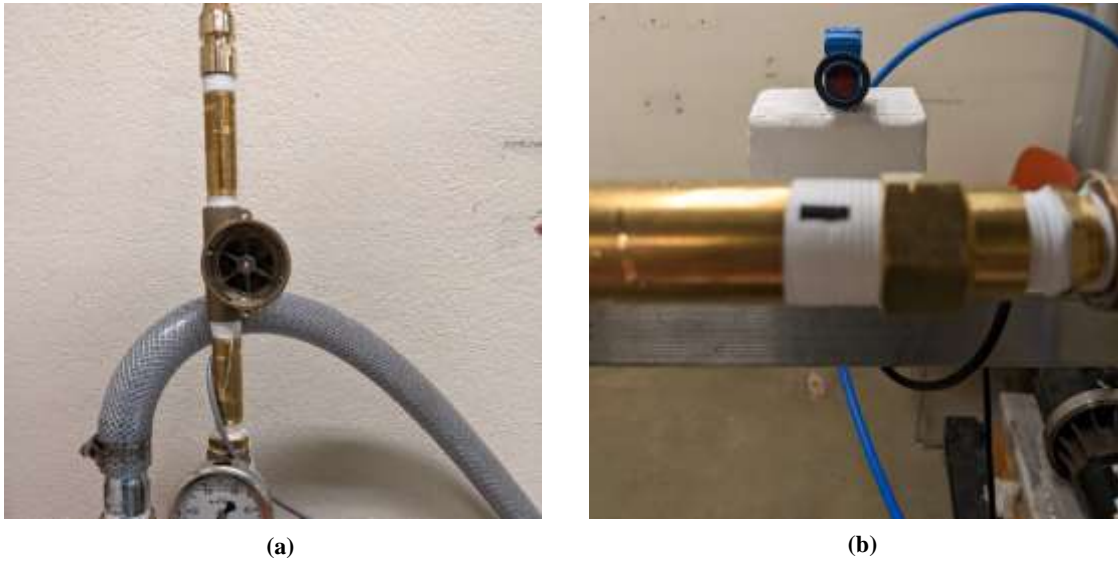

Figure 3.13. (a) Turbine Flow Sensor, (b) Photoelectric Sensor.

Four general-purpose stainless-steel pressure transducers with 0-100 psi rating were installed onto the wellbore's 0.25 in NPT connections at 5 ft intervals and 1 pressure transducer at the drainage connection (Figure 3.14). The pressure transducers have the same wiring configuration as the flow sensors, however, the signal output is analog instead of digital. Voltage output pressure transducers were used for calibration to give an output of 0-10 volts in linear relation to pressure rating and only require calibration for the DAQ module's additional voltage gain and minimum noise filtration.

<center>(a)   (b)</center>
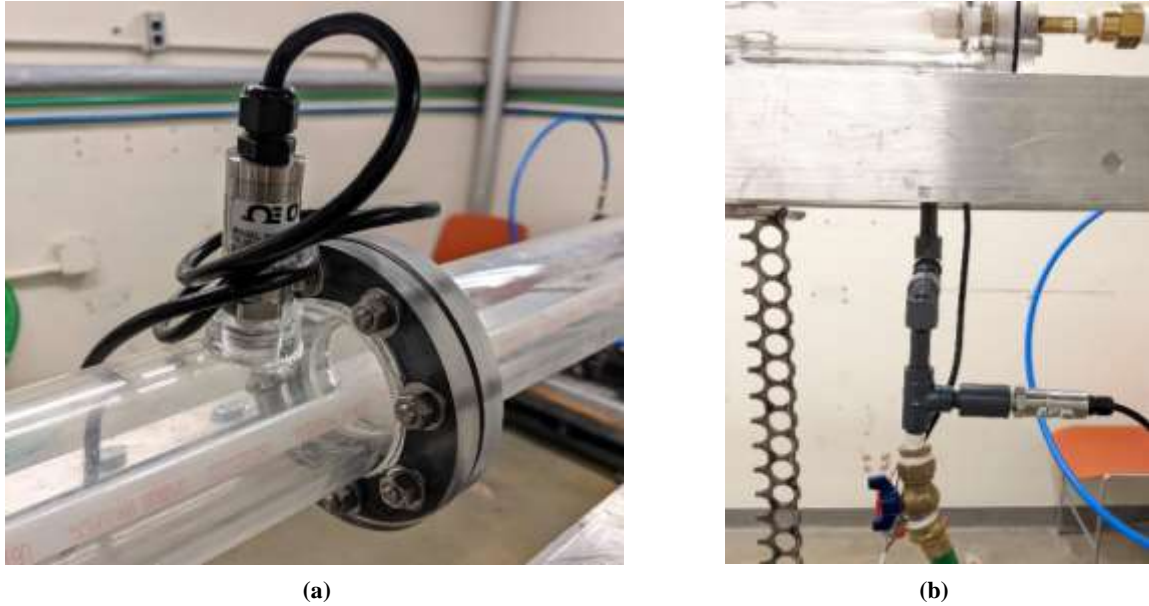
Figure 3.14. Pressure Transducers: (a) on the wellbore wall, (b) at the drainage.

Three inductive analog proximity sensor stations were installed on the outside wellbore wall to measure the lateral displacement of the BHA. Each station consists of two pairs of proximity sensors and each pair conjointly measures the two-dimensional position of the center of the experimental BHA. Acrylic detachable 4 in diameter collars were fabricated with 2 pairs of holes and each pair aligned exactly vertically and horizontally to pass and fixate the proximity sensor (Figure 3.10). Additional fixtures were not necessary as tightly screwed sensors onto the collar balance and hold themselves onto the wellbore outside wall. The proximity sensors have a 4-wire configuration, 2 for power and 2 for differential analog voltage output signal of 0-10 volts. The inductive proximity sensors can only detect ferromagnetic objects and the signal output voltage is greater the closer the ferromagnetic object is to the sensor. Thus, the output signal can be calibrated to measure the distance of the object from the sensor. Also, the signal output magnitude greatly changes depending on the ferromagnetism of the object, i.e., for the same distances from the sensing surface, the voltage output magnitude in the presence of a stainless-steel object is much greater than an aluminum object. Each sensor has a minimum limit to measure objects that are 0.25 in away

<center>54</center>

from the sensing surface and can easily measure the maximum desired 0.75 in distance between the wellbore outside wall to the outer surface of the stabilizer individually. However, when the output signal is too weak at a further distance, i.e., in the case of using aluminum objects, the signal might not be strong enough to overcome the inductive-field-crowding error. Since 4 inductive sensors must be installed in close proximity for accurate 2-dimensional mapping, the inductive fields of the sensors are intersecting, and influence each other's voltage gain. Thus, the same voltage reading could be observed for different distances in the case of weaker ferromagnetic objects. Therefore, after testing aluminum foil, aluminum foil and mild-steel dust sandwich, and aluminum sleeve stabilizer prototypes, stainless-steel sleeves were used to create the stabilizers for the experimental BHA. The sensor responses from the wellbore wall to the stabilizer wall, for 1.5 in outside diameter aluminum and stainless-steel cylinder sleeves with respectively 0.045 in and 0.035 in wall thickness, are presented side by side in Figure 3.15. The figures were created to establish a calibration relationship between the distance of the stabilizer from the sensor (y-axis of the figure) and voltage gains by the sensor (x-axis of the figure). Figure 3.15 shows that the response for aluminum is exponential in terms of voltage and the discerning difference is very low, i.e., only 1 volt difference between 0.6-0.8 in distance, hence a very weak voltage response. Meanwhile, the Stainless-Sleeve response is almost linear, and the voltage gain is more than double for a similar distance reading. Instead of linear, a polynomial function was used to establish the distance-conversion trendline for better accuracy with the calibrating responses. The manufacturer's data also shows polynomial relations for these inductive proximity sensors.
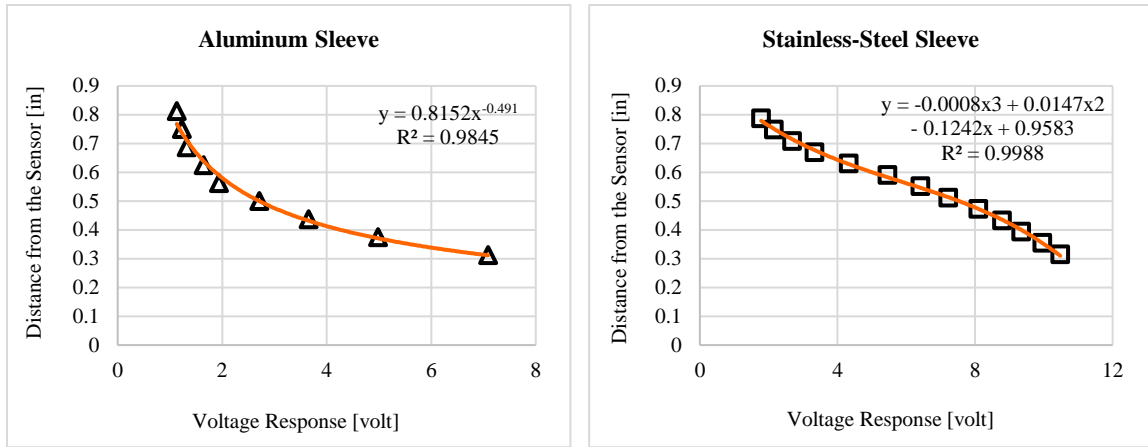
Figure 3.15. Proximity sensor responses of the stabilizer sleeves for different material.

A single-axis accelerometer is attached to the shaker to have a feedback loop to ensure desired axial movement is given by the shaker (Figure 3.7-a – marked by orange-box). This also measures the input acceleration in the axial direction to the BHA bit section. Meanwhile, a tri-axial submersible accelerometer is attached at the end of the power-arm to measure the acceleration response of the BHA at the bit section for all 3 directions (Figure 3.9-a – marked by orange-box). Both accelerometers are connected with 2-wire configuration BNC connectors to the control unit of the shaker for both powering and data acquisition (Figure 3.16-a).

All the sensor's wiring ran through a PVC conduit for wire management and safe encasing in case of liquid spillage (Figure 3.16-b). Additional wiring is left wrapped near all the sensors for free deviation and height change.
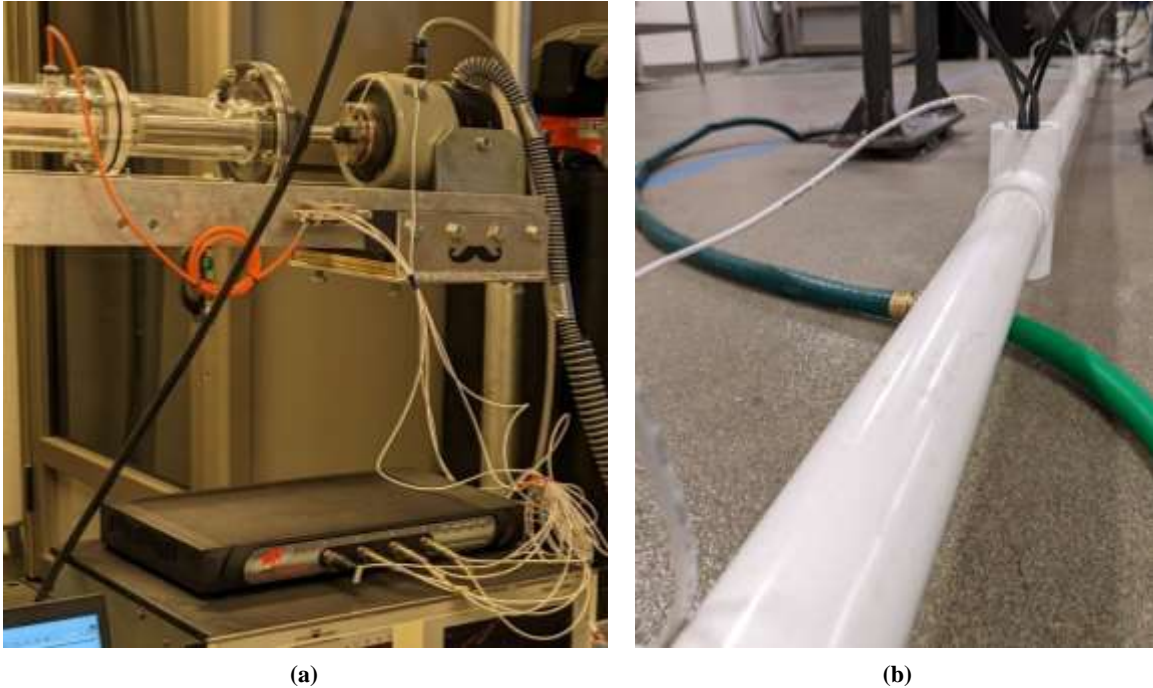
Figure 3.16. (a) Accelerometer wiring of the electromagnetic shaker's control unit, (b) Wire conduit.

3.1.5 Control and Data Measurement

Except for the accelerometers and the electromagnetic shaker, simultaneous data visualization and acquisition from the rest of the sensors, and full operational control is conducted from a single user interface window, created using LabView (Figure 3.18).

The VFDs for the motors are connected to the computer's docking-station using an RS–485 to USB adapter. These adapters convert the communication between the ethernet port on the VFD and USB connection on the computer's dock-station. Detailed block diagrams for both motors are presented in Figure 3.17.
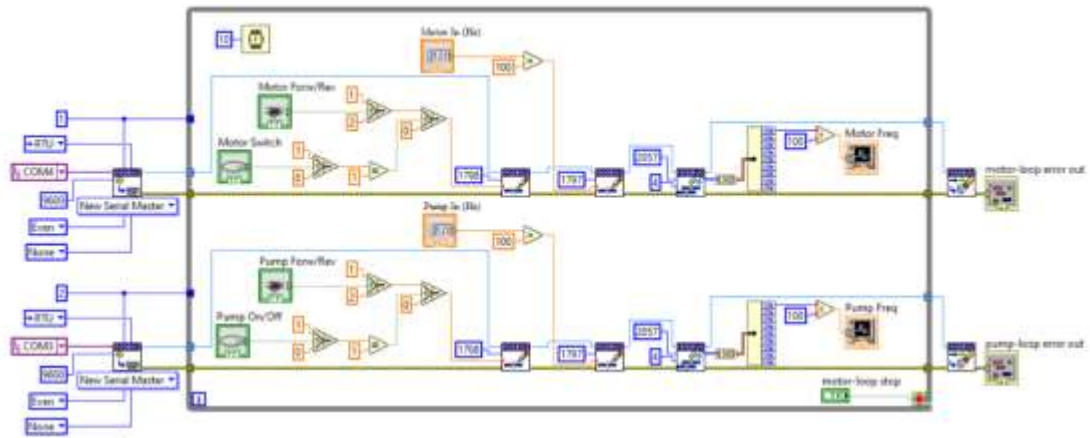
Figure 3.17. LabView block diagram for the motor control via VFD.
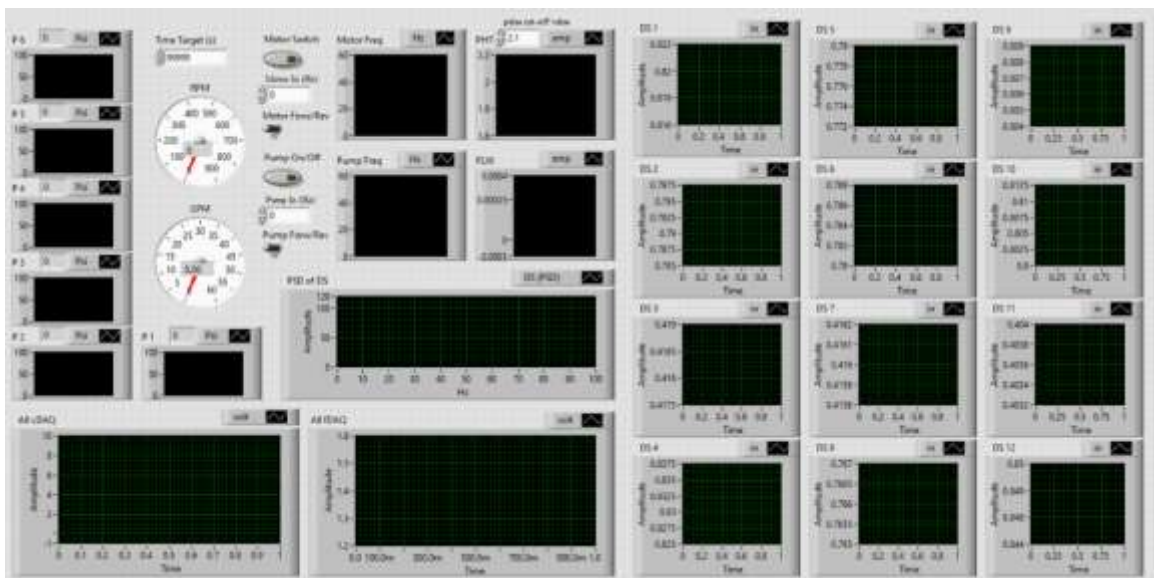
Figure 3.18. Graphical User Interface (GUI) for experimental control and data recording.

A detailed LabView block diagram for data filtration, conversion, and recording of all the sensors is shown in Figure 3.19.
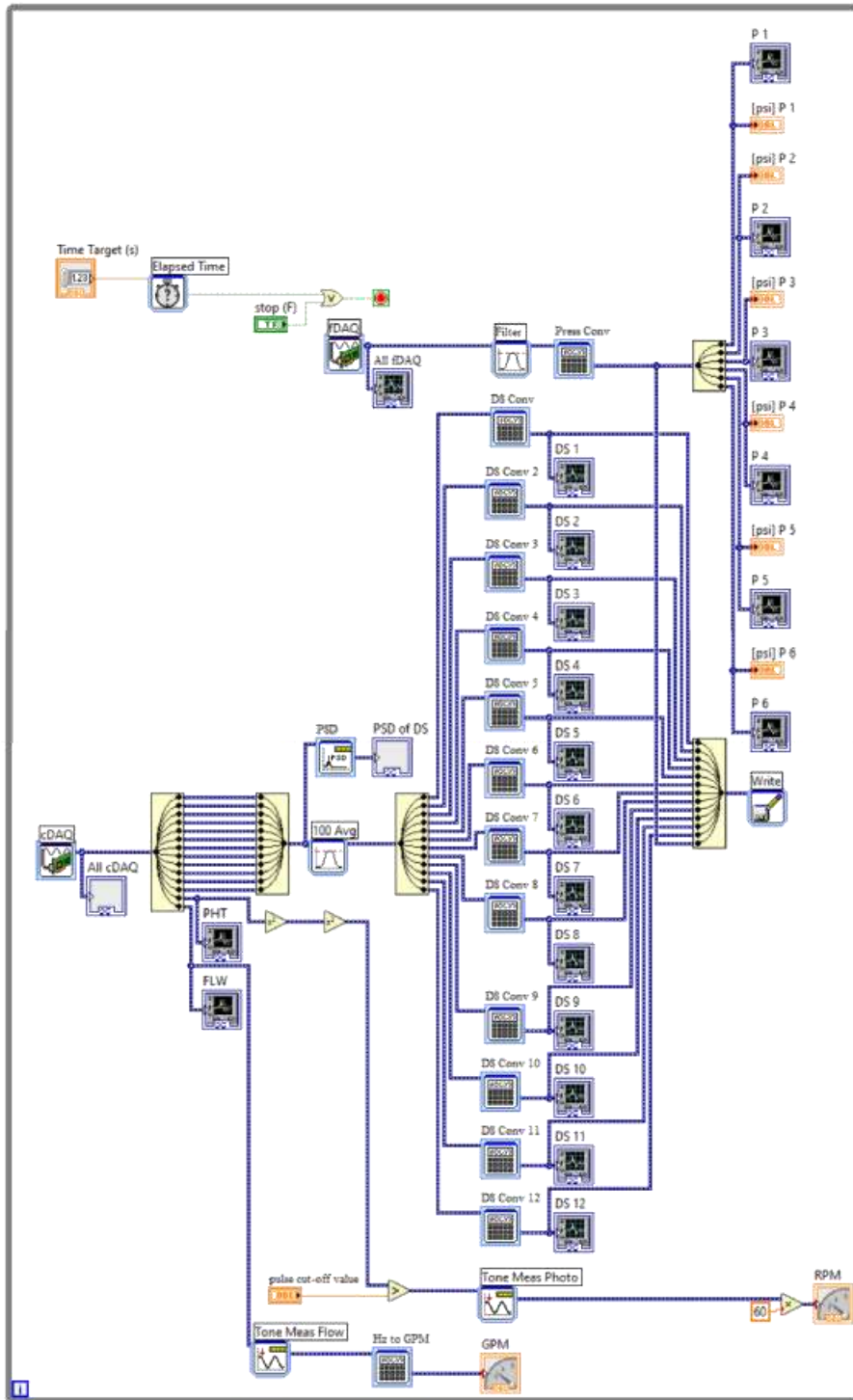
Figure 3.19. Full LabView block diagram for all the sensor data conversion and data storing.

The pressure transducers are connected via a terminal setup for power-supply and the differential voltage data is fed into a field DAQ module BNC-USB-6218 that directly connects to the computer via a USB cable (Figure 3.20). The sampling rate for the pressure transducers is set at 1 kHz and display data is averaged per second. The offset reading was adjusted, and the manufacturer's calibration was tested to ensure data accuracy. The pressure transducers have a linear relation between 0-10 volt output for 0-100 psi.
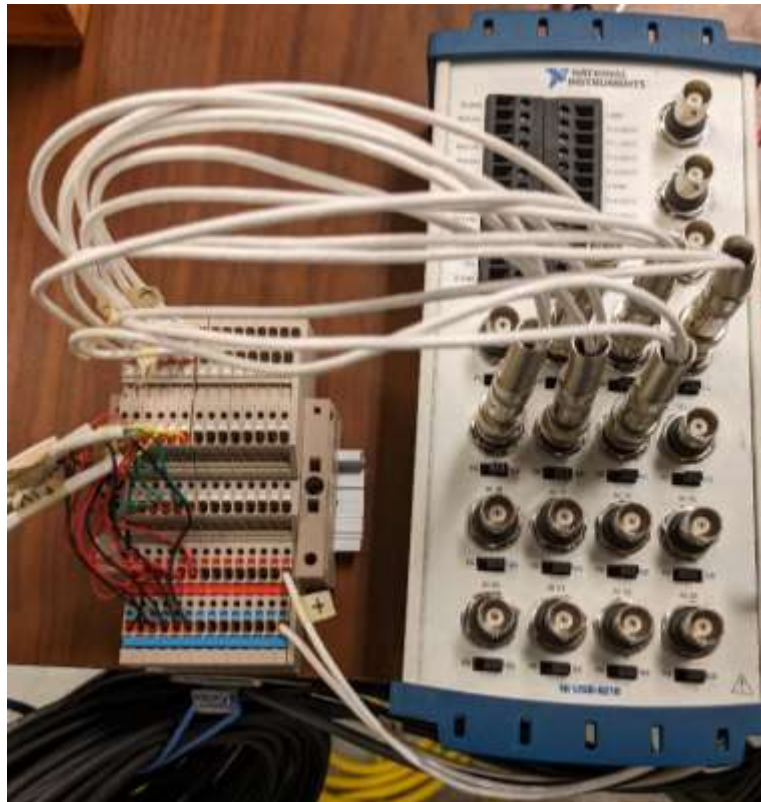
Figure 3.20. Field DAQ (fDAQ) and its terminal block.

Meanwhile, the flow sensor, the photoelectric sensor, and the proximity sensors are connected to another terminal for power-supply and their signal is fed into a simultaneous sampling voltage module NI-9202 at a sampling rate of 10 kHz, and it is housed in the chassis cDAQ-9185 (Figure 3.21). The chassis connects to the computer through a high-speed ethernet connection. Each sensor was individually tested and calibrated. The flow sensor pulse outputs magnitude varied by 100-fold

hence, the frequency detection was easier due to the distinct differentiating nature. Linear Hertz to gallon per minute relation could be followed as instructed by the manufacturer. But the photoelectric sensor has a low pick-up resolution, and the pulse magnitude output is lower. The pulse output responses were squared twice and had a cut-off comparison block to generate digital pulses which are more discernable through a tone-measuring block for frequency counting. Proximity sensor data is set to sample at a high frequency sampling rate to capture vibratory motion. For clearer trajectory mapping, the overall data is filtered as a moving average. Each proximity sensor data is fed through different conversion factors as per their individual response relations, which was on average between 1.78-10.33 volts for 0.78-0.31 in distance away from the sensing surface of the proximity sensor. Since these sensors are very sensitive and the DAQ also had separate offset responses for each input connection, all the proximity sensors needed to be individually and carefully calibrated.

Figure 3.21. Simultaneous communication DAQ (cDAQ) and its terminal block.

The electromagnetic shaker can only be operated using the manufacturer's proprietary software VibrationView and it required a single-axis accelerometer for operation. Thus, the tri-axial accelerometer is also connected to the control unit of the shaker to acquire simultaneous data from both of these accelerometers. The commands for the axial induction nature of the electromagnetic shaker are controlled and set using the software. For example, to run a sine-sweep test, a new test needs to be created with detailed information on sweep frequency range, sweep rate, and other necessary limiting precautions such as acceleration force limit. The sampling rate of the accelerometers can be changed in the advanced test editing option, and the sampling rates were set at 10 kHz and 100 kHz for two different experiments as discussed in the next chapter.

Both interfaces are set to collect, display and store real-time data from the initiation of a test. Except for the accelerometers, all the sensors are powered by a PSU with 14 volts at their respective terminals.

3.2   Experimental Procedure

Two experimental investigations were conducted with the FIDD test assembly to determine its effectiveness, areas of improvement, and future research possibilities. The first experimental investigation was conducted without any fluid to investigate the Effect of WOB Fluctuation on BHA Trajectory (Section 4.1). The second experimental investigation was conducted with submerged BHA in the wellbore with circulating fluid to investigate the Effect of Flow on Drilling Vibrations (Section 4.2). The first experiment aimed to establish the relation between spectral signature relations to the BHA trajectory for different operating conditions, and the other investigation showcases the effect of flow on the vibration responses. Both experiments explore and investigate lateral vibration responses in the presence of induced WOB fluctuation or axial excitement at the bit and with fixed rotational speed. Axial excitement was provided by the

electromagnetic shaker in a reciprocating sine-wave motion of different peak-to-peak displacement, starting the reciprocating movement at a maximum frequency rate and gradually decreasing the frequency of the motion by a single Hz every 5 seconds or at the rate of 12 Hz/min to nearly 1 Hz hence, providing a maximum to minimum sine-sweep at the bit section. Meanwhile, different fixed rotational speeds varying for different cases of the experiments were provided by the electric motor. For the experiment investigating the effect of fluid flow, the pump supplied water at a fixed flow rate of 0.75 GP and 1.15 GPM. The wellbore pressure profile was kept constant to ensure constant flow and the level of BHA submersion in the wellbore. Further details regarding each investigation are provided in the following chapter with mechanical scaling information, descriptions of the test matrix, data observation, and concluding findings.

3.3   Data Repeatability

The FIDD test assembly is equipped with a versatile set of sensors for experimental monitoring and data collection. Each sensor has not only been both individually tested and calibrated but also has been coordinated as parts of the whole system, to ensure robust reliability and repeatability. All the sensors have been connected from their individual location to two terminal junctions, and shielded wiring was used in these terminals to finally transfer data to the DAQ modules. This allows easy removal and troubleshooting of individual sensors without touching the sensitive connections to the DAQ modules. The terminals have been fixated onto the workstation table surface and additionally DAQ modules are seated over vibration absorbing surface to avoid any sort of movements of the module connections.

High frequency vibration measurement system was established with the proximity sensors and the accelerometers. To test their coordinated reliability, a data-sensitivity or repeatability test has been conducted during one of the investigations conducted by this experimental setup. The original

investigation aimed to observe a relation between dynamic acceleration responses and the physical trajectory of the BHA. More details regarding this investigation are presented in the first section of the next chapter. This sensitivity test highlights multiple runs of only one of the cases of the whole investigation. For this case in the investigation, axial excitement was provided by the electromagnetic shaker in a reciprocating sine-wave motion of peak-to-peak 0.1 in displacement distance, starting the reciprocating movement at the maximum rate of 120 Hz and gradually decreasing the frequency of the motion by a rate of 12 Hz/min to near 1 Hz hence. Meanwhile, a constant 302 RPM rotational speed was provided. The same test was conducted for three repetitions, at different dates and times, and collected data is compared to judge the repeatability of the experimental setup and the repeatability of the instrumented measurement acquisition devices.

Figure 3.22 represents input-output acceleration responses in all directions and the BHA trajectory side by side for each run. Each row or set of a# and b# subfigures represents a different run. Figures in the left column show axial induced excitation or the axial input, and output responses at the bit section in the *x, y,* and *z* directions, over time. Meanwhile, the figures in the right column show the 2D position of the BHA center within the wellbore, and this trajectory is represented over time with the changing range of color. The acceleration responses (Figure 3.22-a1-3) show a very similar response for all directions and high-amplitude excitement is observed between the 180-260 sec mark when the frequency of axial excitation was in the range of 69-85 Hz. The BHA trajectory for all the runs (Figure 3.22-b1-3) shows that the BHA mostly stayed at the low-side of the wellbore. The BHA tries to move up the wall in the opposite rotational direction of its rotating direction, i.e., as the BHA is rotating clockwise, the opposing frictional force moves it counterclockwise.
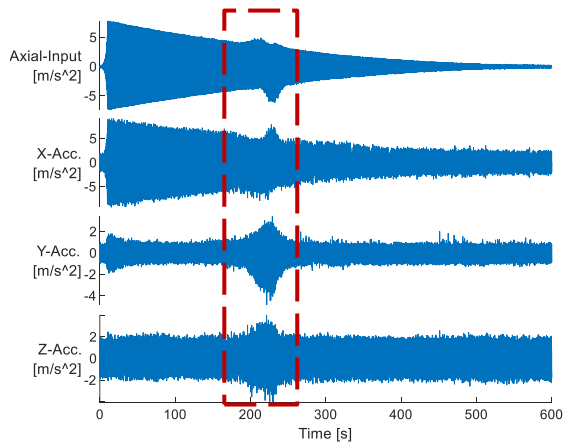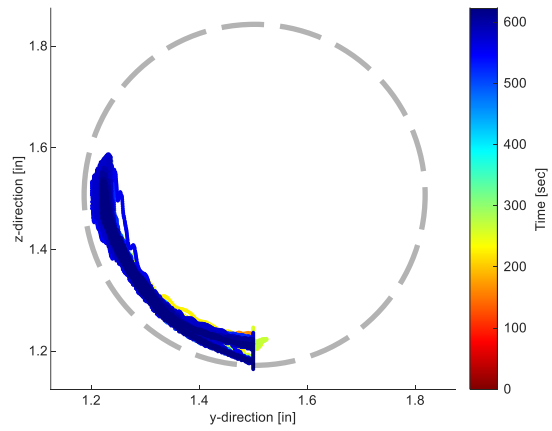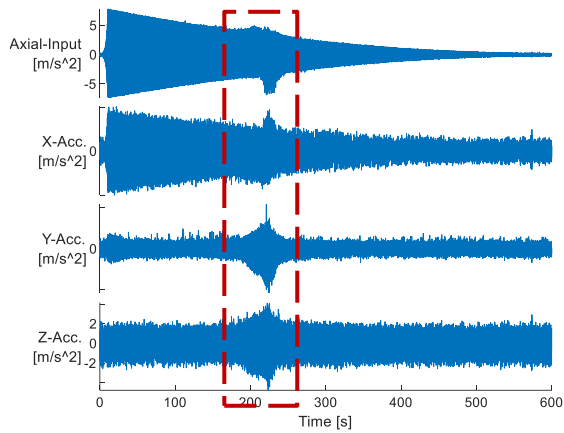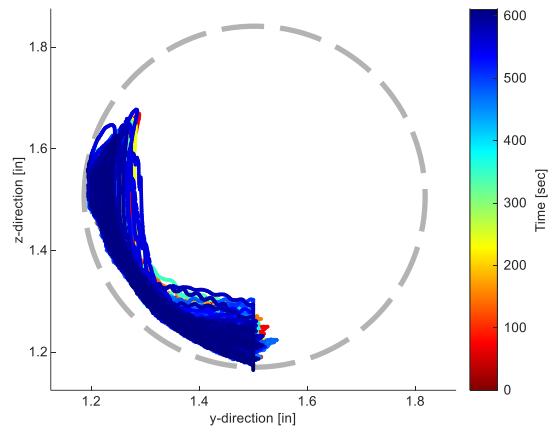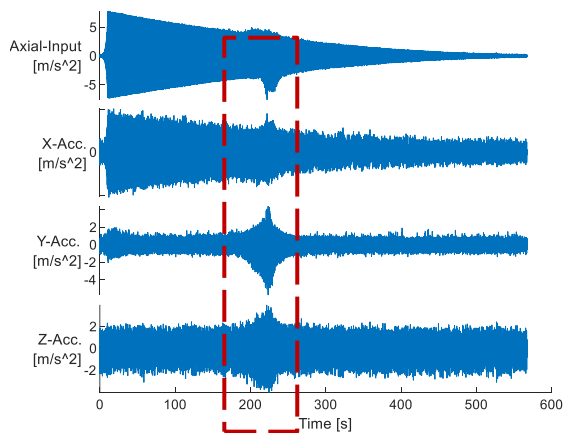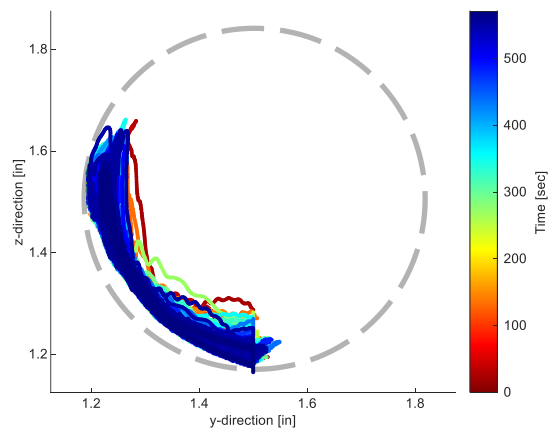
Figure 3.22. Acceleration Responses of axial-input, x, y & z output directions at the bit section, and near bit BHA trajectory of 3 runs of the same repeatability-test-case.
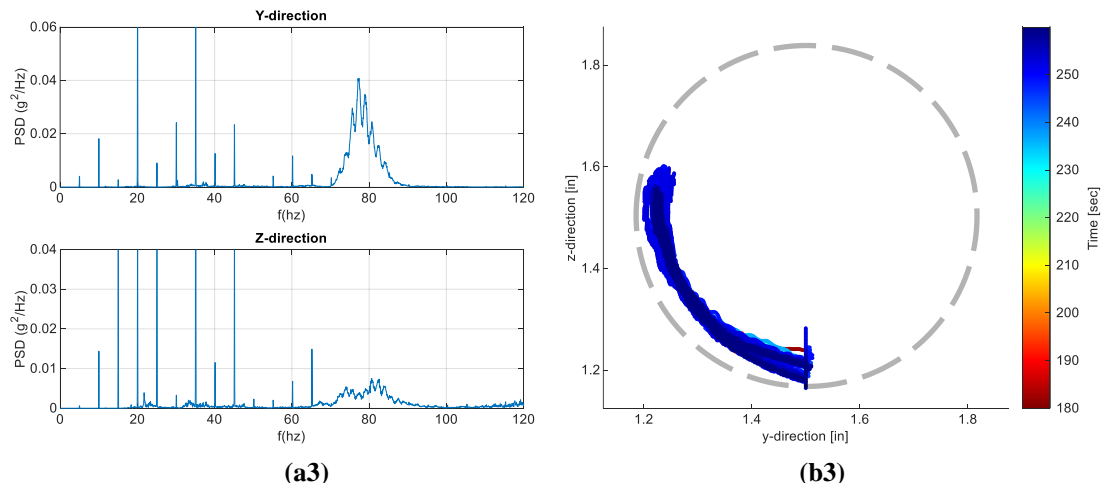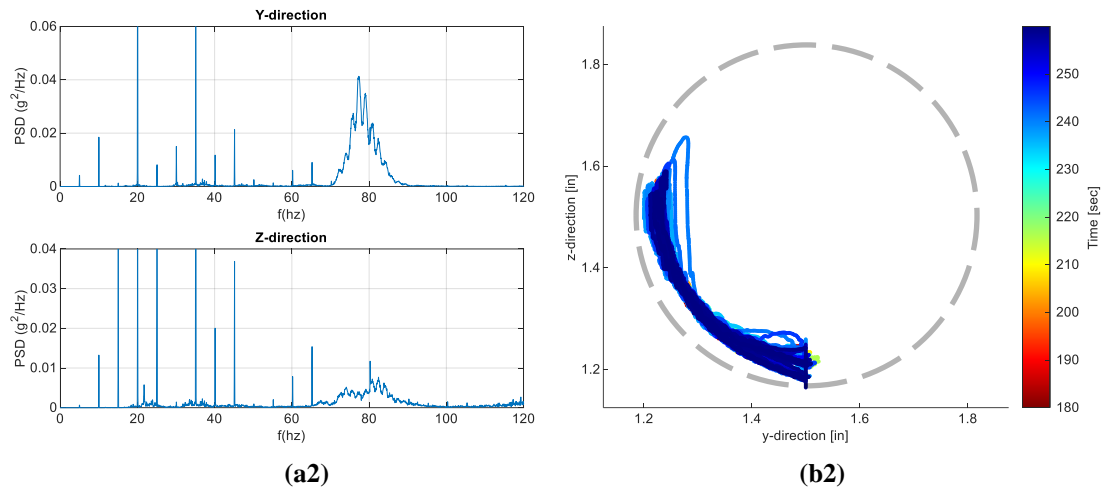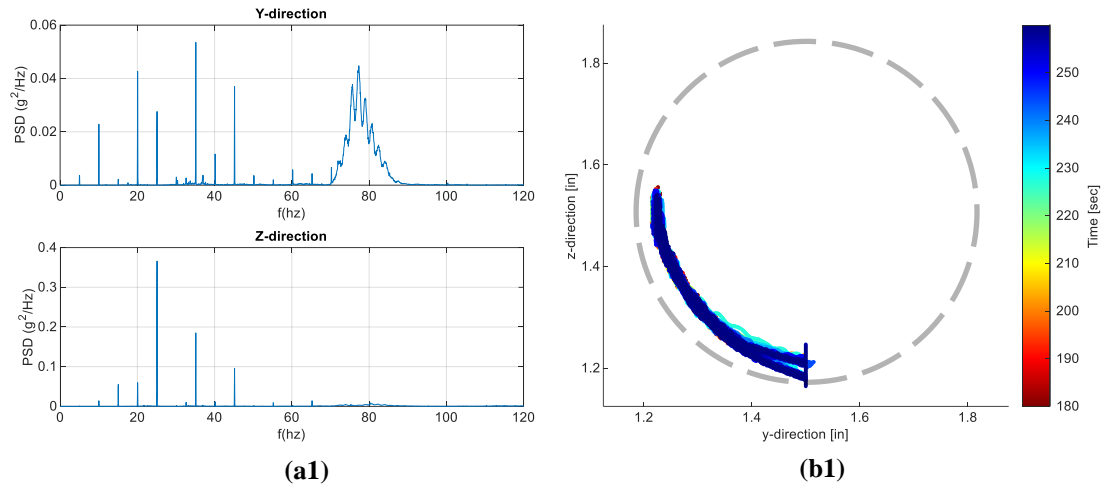
Figure 3.23. PSD of Acceleration Responses in the y & z direction at the bit section, and near bit BHA Trajectory of 3 runs of the same repeatability-test-case between 180-260 sec, at 85-69 Hz sweep.

The high-amplitude excitement in the 180-260 sec period of the experiment was separately observed in the PSD response shown in Figure 3.23. All 3 runs are represented in the same sequential structure as in Figure 3.22. For a better look at the spectral condition, Figure 3.23 a1-a3 represents the power spectral density (PSD) of the acceleration responses in the y and z directions. The acceleration responses for all the runs in both y and z directions show peaks of responses with 5 Hz offsets from 20 and 40 Hz, and lasting dominant response near 80 Hz. It is to be mentioned that the offset of 5 Hz from the multiples of dominant frequency was due to the rotation of BHA, rotating at the frequency of 5 Hz or 302 RPM. Meanwhile, the BHA trajectory shows harmonic motion in the same set of paths for all runs with minimum noise.
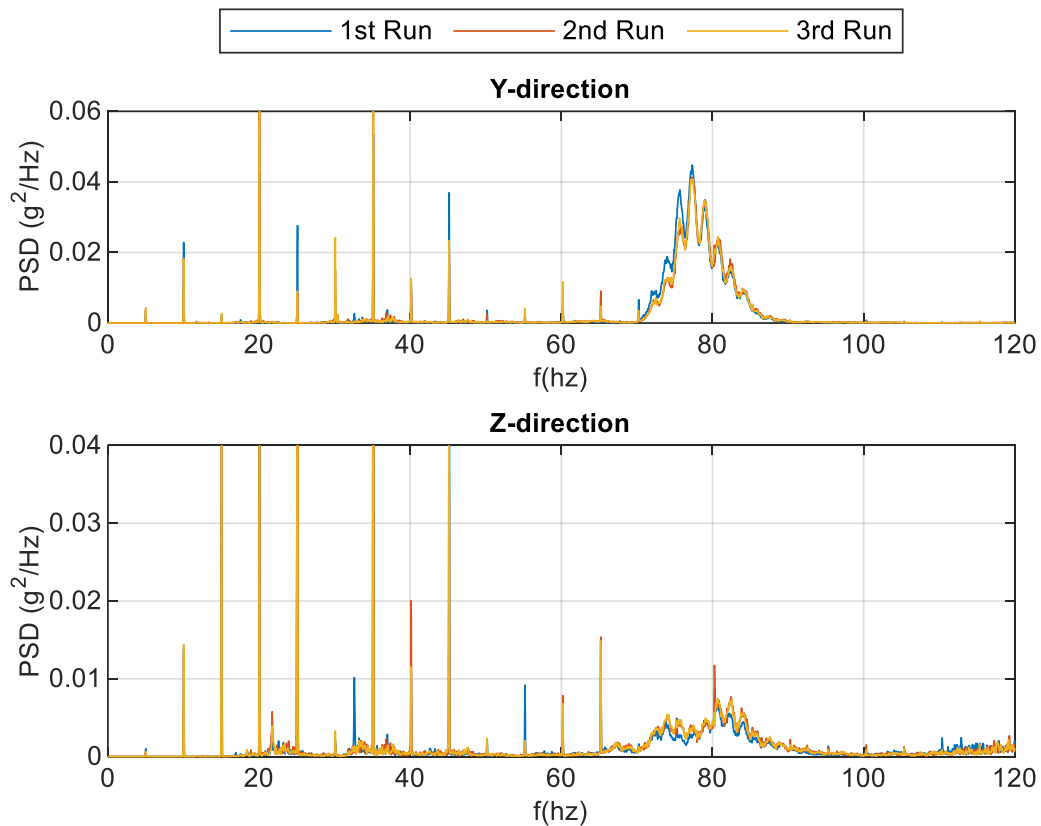
Figure 3.24. PSD of Acceleration Responses in the y & z direction at the bit section of all 3 runs of the same repeatability-test-case between 180-260 sec, at 85-69 Hz sweep.

Thus, both acceleration responses over time (Figure 3.22) and PSD responses in the frequency domain (Figure 3.23) individually prove the repeatability of the test data. The only differences were caused by outside experimental conditions and were most likely to be loosened joints due to continuous testing. Figure 3.24 overlaps all the PSD responses in Figure 3.23 a1-a3 in a single figure for closer comparison and it clearly shows that the responses very closely match, and the irregular noises occur at the same frequencies with a similar level of magnitude.

CHAPTER IV

4   RESULTS AND DISCUSSION

4.1   Effect of WOB Fluctuation on BHA Trajectory

The objective of this investigation is to visualize the downhole condition and trajectory of the BHA during WOB fluctuation and characterize spectral signatures in relation to lateral vibrations for different operating conditions. The aim is to bridge the gap between drilling dynamic data and the lateral motion of the BHA.

The overall details and mechanical scaling relations of the experiment are summarized in Table 4.1, which represents all the mechanical scaling relations of the experimental setup to its field equivalent. The BHA scaling factors on the first rows were derived from both the geometric and material relations, to determine the dynamic conditions. Using these scaling relations, a 328 ft long BHA was scaled down to a 17.75 ft experimental BHA, and providing 68-120 RPM to this experiment is equivalent to 170-302 RPM in the field. The very last column of Table 4.1 shows the rounded ratio between the field-equivalent to the experiment.

The experimental procedure presented in Section 3.2 was followed. All the experimental test cases are organized in Table 4.2.

BHA Scaling Factors			λ_1	λ_2	λ_3
			0.061	0.119	0.002
		Unit	**Field Equivalent**	**Experiment**	**Field/Exp *Ratio**
Geometric	Outside Diameter	*in*	6.75	0.625	11:1
	Inside Diameter	*in*	4	0.5	8:1
	Length	*ft*	328.1	17.75	19:1
Material	Density	*lb.ft^{-3}*	490	58.7	
	Elasticity	*psi*	3.00E+07	6.70E+04	
Dynamic	Rotation	*RPM*	68	170	1:3
		RPM	120	302	1:3

Table 4.2. Effect of WOB Fluctuation on BHA Trajectory experiment - Testing Matrix.

	Bit Displacement [in]	**Rotation [RPM]**	**Max Sweep Frequency [Hz]**
Case# 1		0	
Case# 2	0.01	170	120
Case# 3		302	
Case# 4	0.1	302	60

The acceleration responses of the axial-input and bit responses in all *x*, *y*, and *z* directions over time for a full sine-sweep are shown in Figure 4.1-a, for Case 1 with 0.01 bit displacement, 0 RPM, and 120 Hz maximum sweep frequency. The high lateral vibration time windows were marked in red boxes, and the number of their respective sub-figures are shown in Figure 4.1-c-f. Expectedly, the response in the *x* direction is very similar to the axial-input. Thus, for further vibration studies only vibration responses of *y* and *z* directions were analyzed. Figure 4.1-b represents the BHA trajectory over the full experimental time. The *x* and *y* axis, respectively, depict the position of the center of the BHA in the *y* and *z* direction, i.e., the 2-dimensional surface perpendicular to the wellbore. The color bar represents time relation to the BHA's position. Without any rotation, the stabilizers were very successful in suppressing erratic BHA movement.
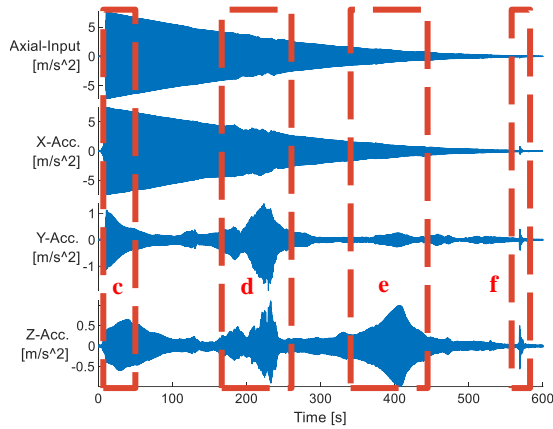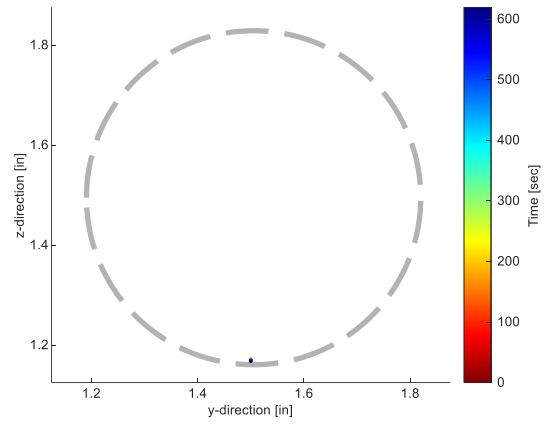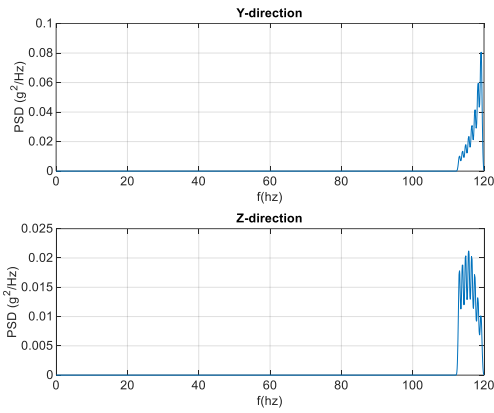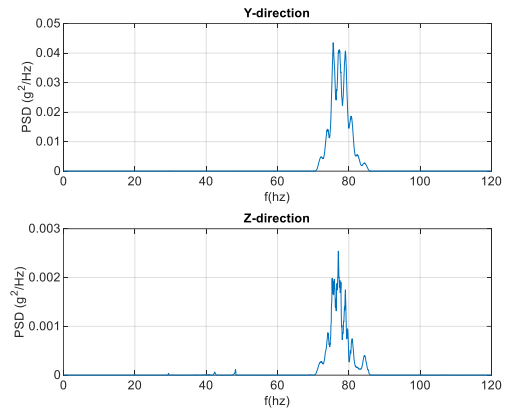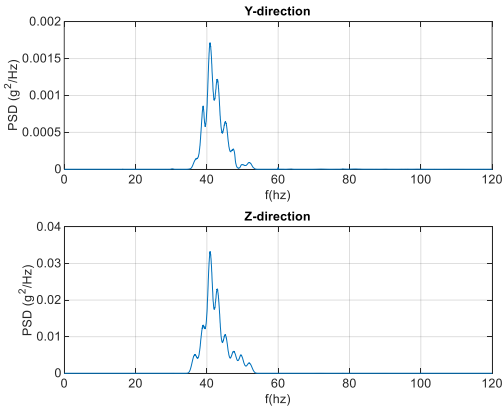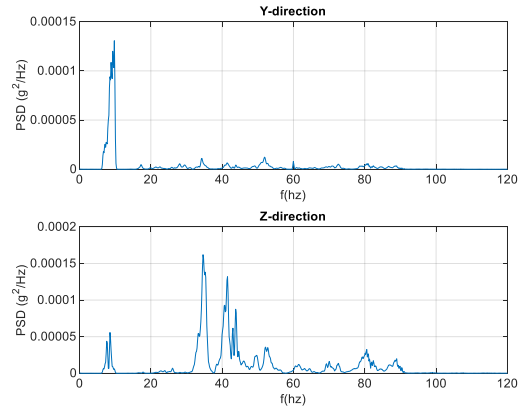
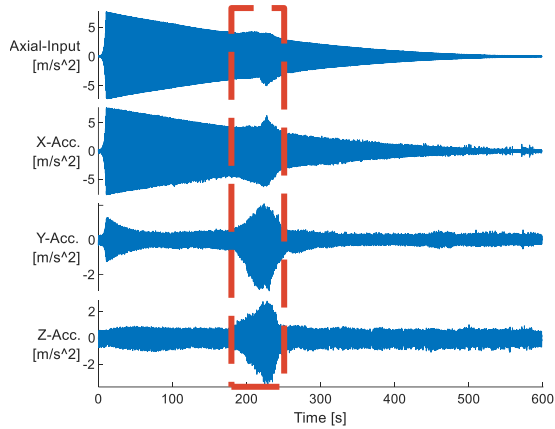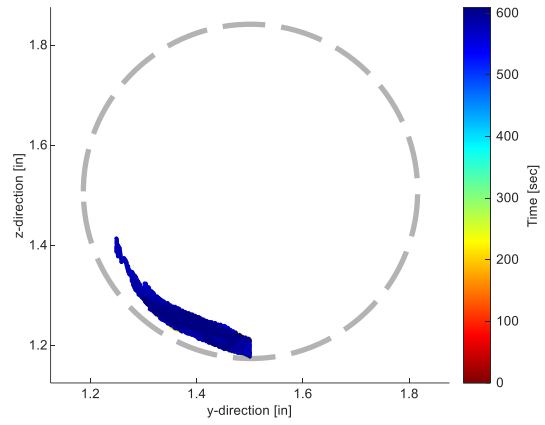*Figure 4.1. Case 1 - 0.01 bit displacement, 0 RPM, and 120 Hz max sweep frequency: (a) acceleration response over full test time with windows of high lateral vibrations marked in red boxes, (b) BHA trajectory, (c)-(f) PSD responses at the high lateral vibration windows.*

For a better look at the nature of lateral vibration and their spectral relations, Figure 4.1-c-f show the power spectral density or PSD of the vibration responses of only the *y* and *z* directions, for the time windows marked in Figure 4.1-a. Vibration amplitude seemed to be the highest close to the range of the frequency of induced excitation in Figure 4.1-c for the *z* direction near 119-111 Hz in the 10-50 sec window and in the *y* direction response near 5-9 Hz (Figure 4.1-f). The majority of lateral vibration excitation peaks were observed at a narrow range of frequencies and near 80 Hz and 40 Hz, as observed in Figure 4.1-d-e. Thus, it is perceived that 40 Hz and 80 Hz are the dominant frequencies of the operational condition of this experimental case. This understanding gets solidified while looking at the PSD responses of the highest lateral vibration peaks in Figure 4.2-c and Figure 4.3-c when rotation is introduced in Case 2 and Case 3. The induced WOB fluctuation or the axial bit-displacement excitation remained the same for both Case 2 and Case 3, only rotation was applied respectively at 170 and 302 RPM.

Figure 4.2-b and Figure 4.3-b show the BHA movement under applied rotation for Case 2 and Case 3. At lower rotational speed, as for Case 2 (Figure 4.2-b&d), the BHA tends to stay at the low-side of the wellbore. The movement becomes harmonic at the high lateral vibration, between 180-260 sec, near the dominant frequency of 80 Hz (Figure 4.2-d). This matches the BHA behavior seen in the field during horizontal drilling as key sitting. At higher rotational speed, as for Case 3 (Figure 4.3-b), the BHA overcomes the wellbore friction and tends to move backward opposite to the applied rotational direction at the dominant frequency of 80 Hz. High RPM also results in more irregular motion in the range of frequencies but, the BHA trajectory follows a similar path at the dominant lateral vibration (Figure 4.2-d).
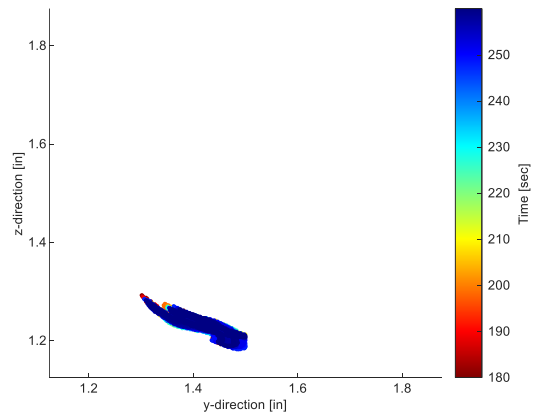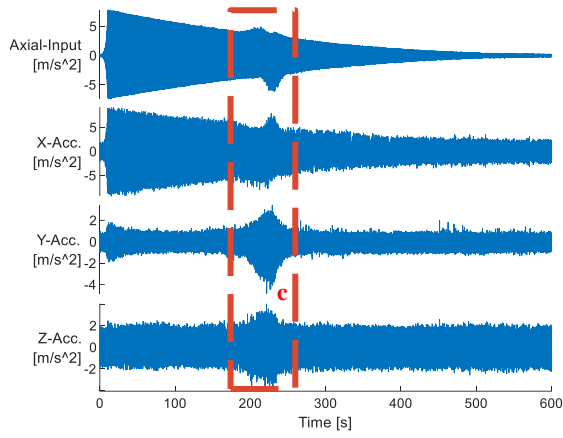
(a)

(b)
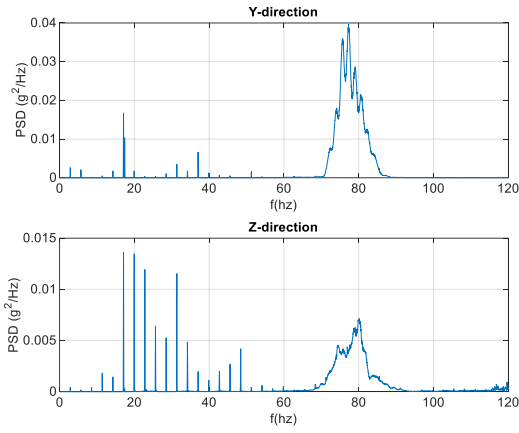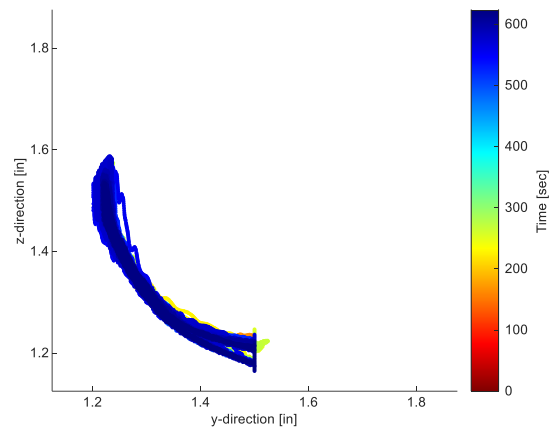
(c) @180-260 sec, 85-69 Hz
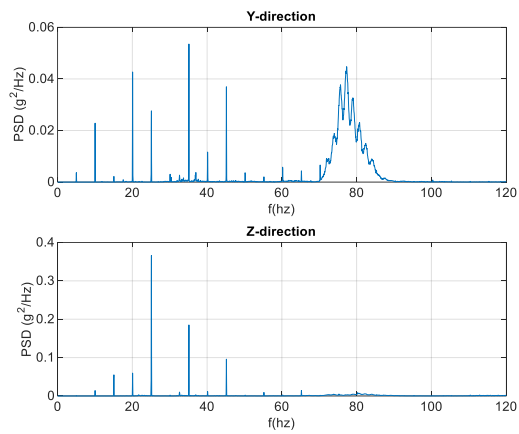
(d) @180-260 sec, 85-69 Hz

Figure 4.2. Case 2 - 0.01 bit displacement, 170 RPM and 120 Hz maximum sweep frequency: (a) acceleration response over full test time with windows of high lateral vibrations marked in the red box, (b) BHA trajectory, (c)-(d) PSD response and BHA trajectory at the high lateral vibration window.
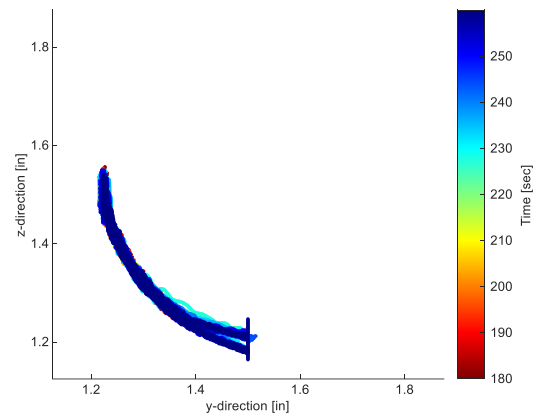
(a)

(b)

(c) @180-260 sec, 85-69 Hz

(d) @180-260 sec, 85-69 Hz

Figure 4.3. Case 3 - 0.01 bit displacement, 302 RPM and 120 Hz max sweep frequency - (a) acceleration response over full test time with windows of high lateral vibrations marked in the red box, (b) BHA trajectory, (c)-(d) PSD response and BHA trajectory at the high lateral vibration time window.

The experiment was conducted with the behavior of PDC bits in mind since most current-day drilling operations are done with PDC bits. Also, PDC bit hardly experiences higher lift-off than 0.01 in except in severe vibration conditions. Thus, in the majority of the investigated cases, the induced bit lift-off for the induced WOB fluctuation was 0.01 in. Thus, to observe critical and amplified vibration conditions, WOB fluctuation with higher drill-bit displacement was induced in Case 4, where backward whirl could be observed (Figure 4.4). The induced drill-bit lift-off was 0.1 in, with a high rotational speed of 302 RPM. At such high WOB fluctuation, the BHA trajectory became very chaotic (Figure 4.4-b). The whirling behavior could be better observed in the time narrowed zones when the lateral vibrations were maximum (Figure 4.4-d-f). The high RPM allowed the BHA to make a full rotation around the wellbore. At a lower dominant frequency zone, chaotic behavior is reduced, and the BHA shows clearer backward whirling movement (Figure 4.4-f). Thus, proving that, at high WOB fluctuation and rotational speed, backward whirling may still occur at lower dominant frequencies.

In Case 4, the dominant frequencies were observed in the form of double-bands, i.e., in the double-band of approximately 25 and 30 Hz in the 10-50 sec time window for both y and z directions (Figure 4.4-c). The difference between these double bands was the frequency of the applied rotation, approximately 5 Hz. A similar observation could also be deducted for Case 3 in Figure 4.3-c.
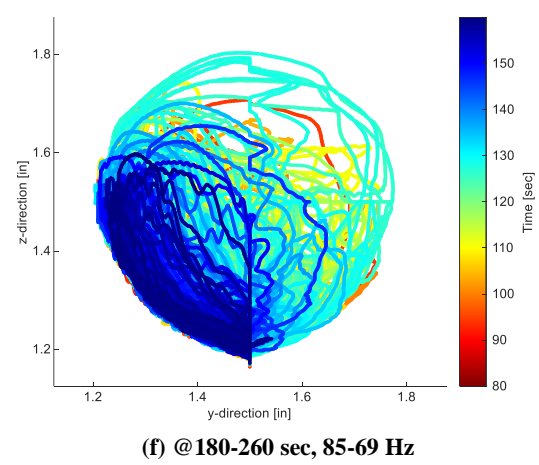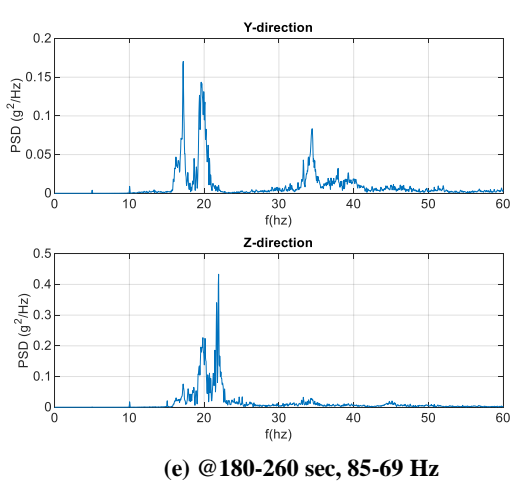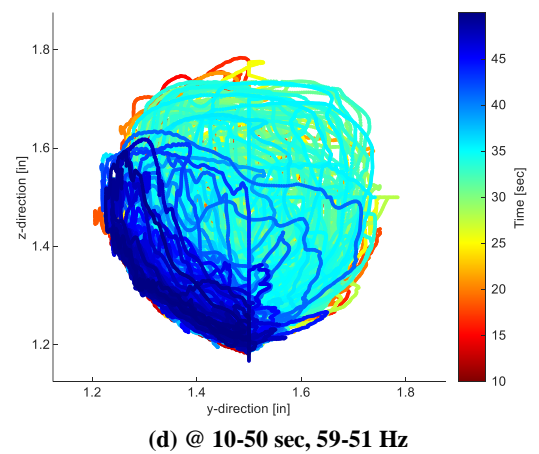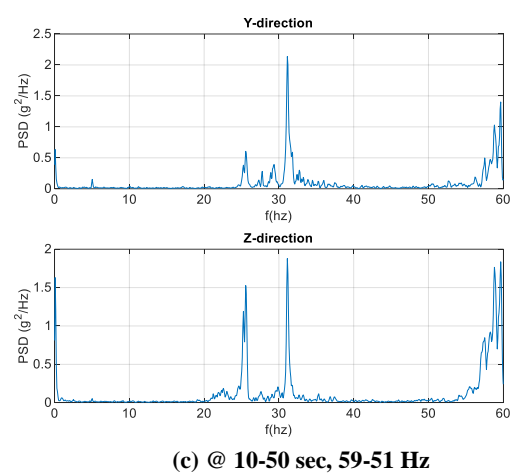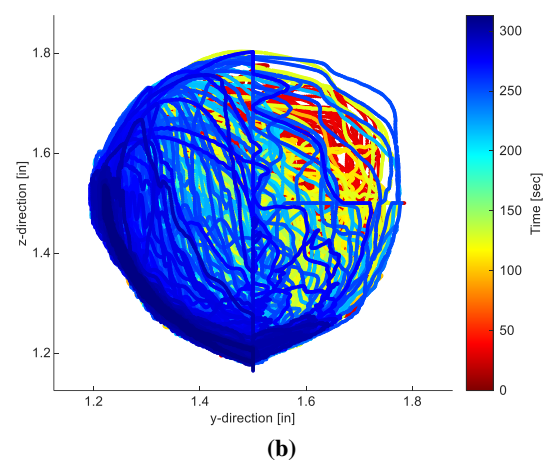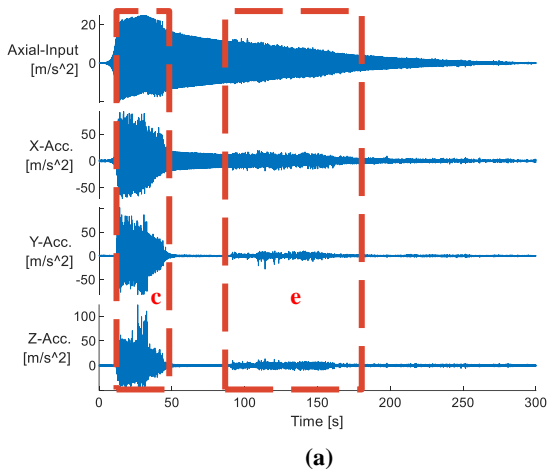
Figure 4.4. Case 4 - 0.1 bit displacement, 302 RPM and 60 Hz max sweep frequency - (a) acceleration response over full test time with windows of high lateral vibrations marked in red boxes, (b) BHA trajectory, (c)-(f) PSD response and BHA trajectory at the high lateral vibration time windows.

4.2 Effect of Flow on Drilling Vibrations

The objective of this experiment is to investigate the effect of flow on drilling vibrations under fully circulating flow. The overall details and mechanical scaling relations regarding the experiment are summarized in Table 4.3. The very last column of Table 4.3 shows the rounded ratio between the field-equivalent to the experiment. All the experimental test cases are organized in Table 4.4.

Table 4.3. Effect of Flow on Lateral Vibrations experiment - Mechanical Scaling.

BHA Scaling Factors			λ_1		λ_2		λ_3
			0.061		0.119		0.002
		Unit	**Field Equivalent**		**Experiment**		**Field/Exp *Ratio**
Geometric	Outside Diameter	*in*	6.75		0.625		11:1
	Inside Diameter	*in*	4		0.5		8:1
	Length	*ft*	328.1		20		16:1
Material	Density	*lb.ft^{-3}*	490		58.7		
	Elasticity	*psi*	3.00E+07		6.70E+04		
Dynamic	Rotation	*RPM*	157		350		1:2
		RPM	314		700		1:2

Table 4.4. Effect of Flow on Lateral Vibrations experiment - Test Matrix.

Flow Rates [GPM]	0	0.75	1.15
	Bit Lift-off [in]	**Rotation [RPM]**	**Max Sweep Frequency [Hz]**
Case# 1	0.2	0	30
Case# 2		350	
Case# 3		700	
Case# 4	0.075	0	60
Case# 5		350	
Case# 6		700	
Case# 7	0.05	0	
Case# 8		350	
Case# 9		700	
Case# 10	0.025	0	120
Case# 11		350	
Case# 12		700	

Four different peak-to-peak bit displacement distances were used, and each was run without rotation, 350 and 700 RPM. Each case was run without flow at 0 gallons per minute (GPM), 0.75 GPM, and 1.15 GPM hence, totaling up to 36 experimental tests. The average wellbore pressures were 13 psi and 15 psi respectively for 0.75 GPM and 1.15 GPM. Only water was used for this experiment.

Figure 4.5 shows the applied acceleration and the BHA acceleration responses in the x, y, and z directions over time for a full sine-sweep of Case 5 and Case 8 – for 60 Hz max sweep frequency and at 350 RPM. The bit-displacements of the WOB fluctuation were respectively 0.075 in and 0.05 in for Case 5 and Case 8. For both cases, the BHA response in the x-direction is similar to the induced axial vibration, besides a few random noises and possible high-frequency coupled vibration responses. From the flow rate effect point of view, it can be seen that the acceleration amplitude for 0 GPM is higher than 0.75 and 1.15 GPM for both cases. For the BHA response in the y-direction, Case 5 (Figure 4.5-a) shows lower vibration amplitude compared to the x-direction, while the flow rate effect shows different behavior for the high and low-frequency excitations. For instance, at high excitation frequency, the vibration amplitude of 0.75 GPM is higher than the other cases, while at low vibration amplitude, the 0 GPM test shows the highest vibration amplitude. A similar trend can be seen for Case 8 (Figure 4.5-b), however, the vibration amplitude for the 1.75 GPM was the highest in the high excitation frequency range. The BHA response in the z-direction for Case 5 (Figure 4.5-a) shows the same behavior seen in the y-direction vibration amplitude. However, Case 8 (Figure 4.5-b) shows the vibration amplitude in the y-direction for the 0 GPM test being the highest across the excitation frequency spectrum.
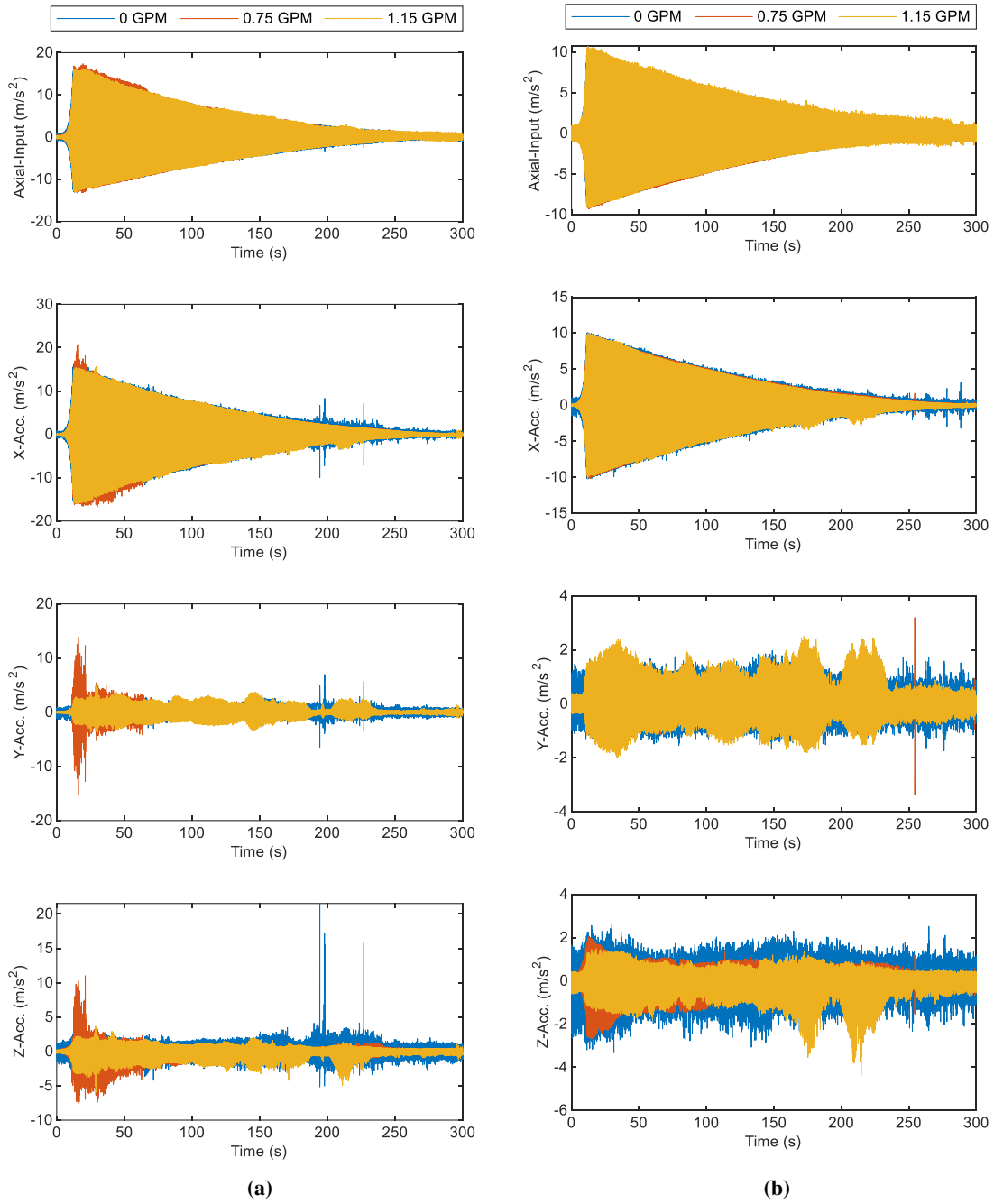
Figure 4.5. Acceleration magnitude of induced axial input motion and recorded acceleration response at the bit section for all the coordinates, respectively from top to bottom - (a) Case 5, (b) Case8

It is to be noted that, due to the general design of the horizontal wellbore, the experimental BHA mostly lays on the wellbore low side and comes in contact with the wellbore more often in the z-direction, which matches filed case observations. Therefore, compared to the *x* or *y*-direction

79

responses, the *z*-direction acceleration responses are not fully symmetric for both Case 5 (Figure 4.5-a) and Case 8 (Figure 4.5-b).

For more insights into the BHA dynamics, the tri-axial vibration response data was processed using the Power Spectral Density (PSD) to investigate the effect of flow on the frequency response spectrums. Figure 4.6 shows the PSD spectrum of Case 5 in the *x*, *y*, and *z* directions for the different flow rates. In the axial direction, Figure 4.6-a1-a3, the flow rate shows a minimum effect, i.e. no change in dominant frequency, on the PSD spectrum at the low and high-frequency range. At the low range, Figure 4.6-a2, a damping effect due to fluid flow can be seen at approximately 12 Hz. In the high-frequency range, increasing the flow rate causes an increase in the spectral energy at approximately 50 Hz (Figure 4.6-a3). In the lateral directions, i.e., the *y* and *z*, due to symmetry, the PSD spectrums of both directions are similar (Figure 4.6-b-c). The fluid flow shows an increase in the spectral energy in the low range of frequency below 15 Hz as seen in Figure 4.6-b2&c2. At the higher frequency range, the fluid flow shows a damping effect (Figure 4.6-b3&c3).

The PSD response of the BHA for Case 8 is shown in Figure 8 for the different flow rates. In the x-direction, similar behavior to Case 5 (Figure 4.6) can be seen at the lower frequency range with an increase in the spectral energy below 15 Hz (Figure 4.7-a2). At the high frequency range, the fluid flow shows a damping effect with lower PSD response, however, the change in flow rate from 0.75 to 1.15 GPM shows a minimal change in damping ratio (Figure 4.7-a3). In the lateral directions, i.e., *x* and *y* response, the PSD spectrum shows similar behavior seen in Case 5, where the fluid flow caused an increase in the energy spectrum at the low frequency range (Figure 4.7-b2&c2) and a damping effect with a small shift in dominate frequency at the high frequency range (Figure 4.7-b3&c3).
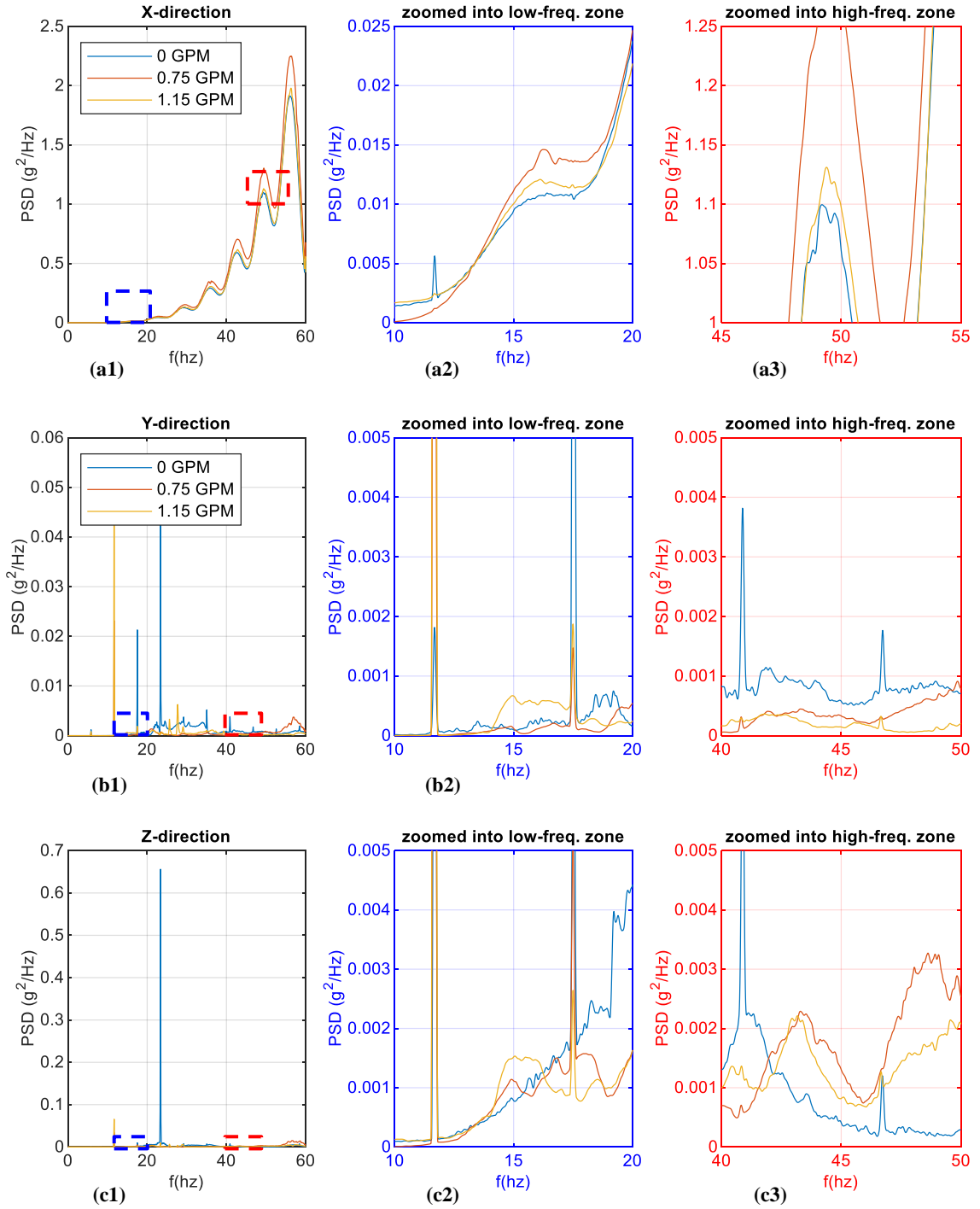
Figure 4.6. Case 5 – Power Spectral Density (PSD) of the axial excitation, x, y, and z responses at the bit.
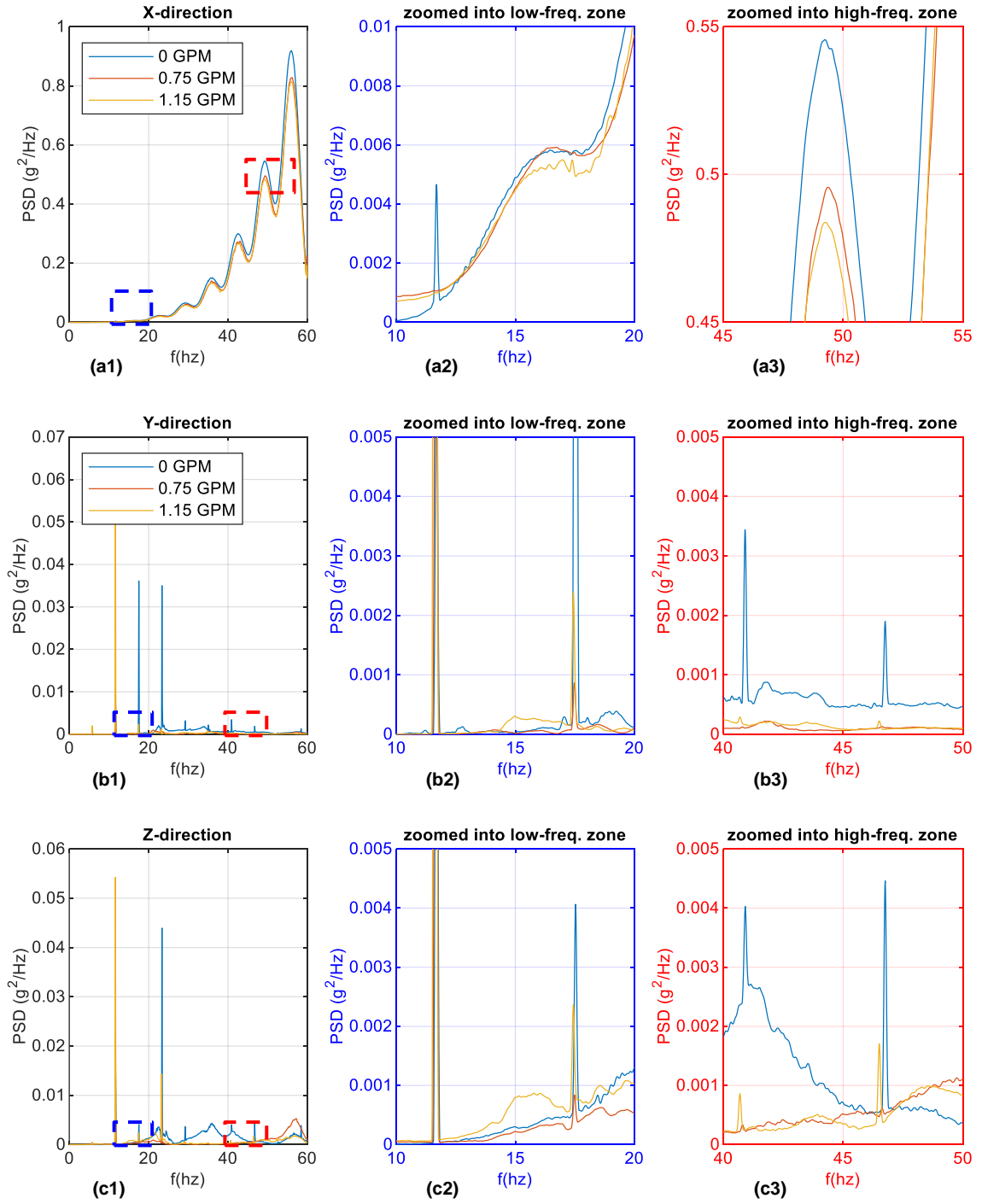
Figure 4.7. Case 8 – Power Spectral Density (PSD) of the axial excitation, x, y, and z responses at the bit.

The axial excitations displacements of Case 5 and Case 8 were 0.075 in and 0.05 in, respectively. Comparing the y-direction responses of Case 5 (Figure 4.6-b3) and Case 8 (Figure 4.7-b3), it can be seen that both flow conditions were more effective in damping the vibration for Case 8 with lower axial excitation levels. This is more evident while comparing the z-direction responses of Case 5 (Figure 4.6-c3) and Case 8 (Figure 4.7-c3).

The effect of flow was investigated at different excitation levels and rotational speeds. Figure 4.8 to Figure 4.19 shows the PSD response of the lateral acceleration in the y and z directions only, for Case 1 through Case 12. A summary of the vibration response observations seen for each case is presented in Table 4.5.

Table 4.5. Observation of the lateral accelerations PSD responses in the y and z directions of all cases of - Effect of Flow on Lateral Vibrations experiment.

Case	Bit Lift-off (in)	RPM	Vibration Response Observations
Case 1 **Figure 4.8**	0.2	0	Flow rate increases vibration amplitude at low frequency (Figure 4.8-a2&b2) and flow dampens vibration in high frequency zones, with low flow rate being more effective (Figure 4.8-a3&b3). Higher flow rate shift frequency of peak responses further to the lower range (Figure 4.8-a1,a3,b1&b3).
Case 2 **Figure 4.9**		350	Excitation amplification at low frequency at 12-13 Hz (Figure 4.9-a2&b2). Vibration dampening and frequency shift due to flow is observed for peak responses at higher frequency zone (Figure 4.9-a1,a3,b1&b3).
Case 3 **Figure 4.10**		700	Similar to Case 1 and Case 2. But peak vibration amplitudes are larger everywhere at higher RPM. Similarly, fluid flow exhibits higher vibration damping effectiveness.
Case 4 **Figure 4.11**	0.075	0	Frequency shift can be observed (Figure 4.11-a2&b2). Overall, higher flow rate is more effective in vibration damping in high frequency range but, high vibration amplitudes are observed between 55-60 Hz (Figure 4.11-a1&b1).
Case 5 **Figure 4.12**		350	Similar to Case 4. Flow is more consistent in damping overall vibration except between 55-60 Hz (Figure 4.12-a1&b1). Vibration amplitudes peak for rotation around 12 & 17 Hz (Figure 4.12-a2&b2).
Case 6 **Figure 4.13**		700	Similar acceleration peak response as Case 5, along with additional erratic peaks (Figure 4.13-a2&b2). More effective damping was observed in the *y*-direction.

Case			
Case 7 **Figure 4.14**	0.05	0	Similar frequency observation window as Case 4 (Figure 4.11) and shows similar nature in low frequency zone (Figure 4.14-a2&b2). But exhibits no large acceleration peaks due to flow (Figure 15-a1&b1). Flow is more effective in reducing overall vibration in this low axial excitation case (Figure 4.14-a3&b3). Except for one irregular jump for 0.75 GPM in the *z*-direction (Figure 4.14-b1).
Case 8 **Figure 4.15**		350	Similar vibration responses as Case 5 (Figure 4.12) but, flow exhibits comparatively more effectiveness in overall damping in this case of lower axial excitation (Figure 4.15).
Case 9 **Figure 4.16**		700	Similar comparison can be stated between Case 6 (Figure 4.13) and Case 9 (Figure 4.16), as seen between Case 5 (Case 5 Figure 4.12) and Case 8 (Figure 4.15). But the irregular *z*-direction vibration amplification is absent in Case 9 (Figure 4.16-b3) compared to Case 6 (Figure 4.13-b3).
Case 10 **Figure 4.17**	0.025	0	Vibration dampening and frequency shift due to flow are more evident. 0.75 GPM is more effective in damping vibration in the lower frequency range and 1.15 GPM is more effective in the higher frequency range. Except for one irregular vibration response observed between 75-85 Hz in the *z*-direction (Figure 4.17-b3).
Case 11 **Figure 4.18**		350	Erratic vibration responses are prominent in this higher RPM case (Figure 4.18) than the previous case (Figure 4.17). Shifted and damped vibration peaks plateau at a higher frequency due to flow over a range of frequencies, as seen between 90-100 Hz for 1.15 GPM flow (Figure 4.18-a3&b3)
Case 12 **Figure 4.19**		700	Erratic behavior further increases due to higher RPM but, similar characteristics are more prominent, compared to Case 10 and Case 11.

The first cases from Case 1-3 (Figure 4.8, Figure 4.9 & Figure 4.10) represent cases with the highest axial peak-to-peak excitation. It has been mentioned that the maximum allowable axial excitation was provided up to the limitation of the electromagnetic shaker. As the applied excitation frequency increases more axial force is required for a fixed axial peak-to-peak excitation. Thus, the maximum applied axial excitation frequency for Cases 1-3 was 30 Hz (Figure 4.8, Figure 4.9 & Figure 4.10).

Cases 1-3 (Figure 4.8, Figure 4.9 & Figure 4.10) show that flow rate amplifies vibration amplitude at low frequency and flow dampens vibration in the high frequency range, with low flow rate being more effective in vibration damping (Figure 4.8-a3&b3). The vibration response peaks are larger at the higher RPM range in Case 3 (Figure 4.10-a2&b2), and similarly, fluid flow exhibits higher vibration-damping effectiveness (Figure 4.10-a3&b3). It can also be observed that a higher flow rate shifts the frequency of peak responses further to the lower range.
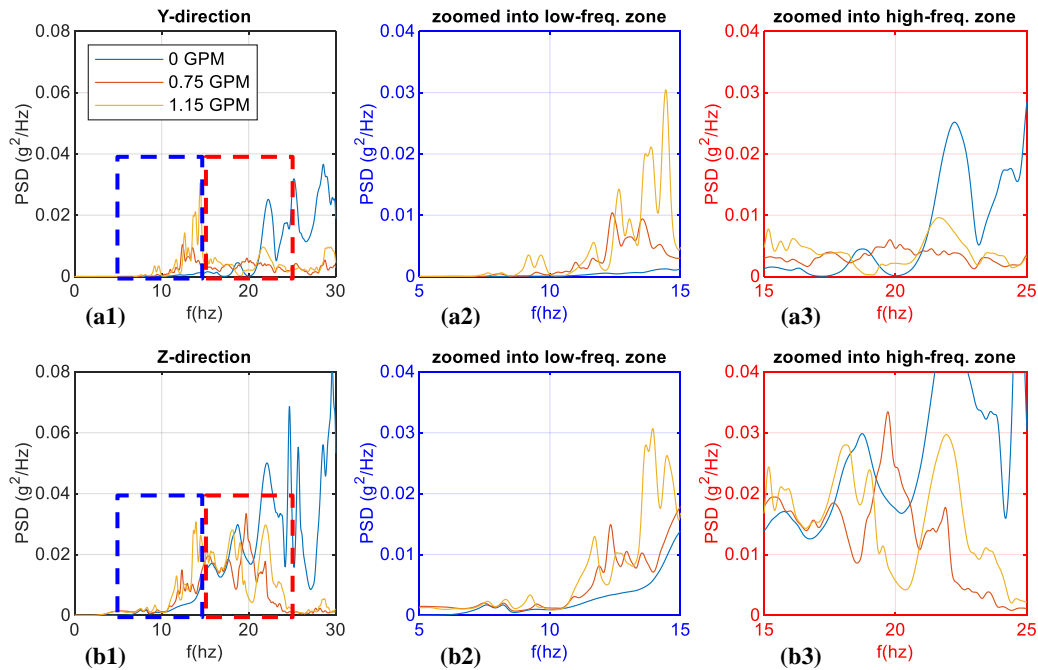
Figure 4.8. Case 1 – Lateral acceleration PSD response for different flow rates in the y & z direction.
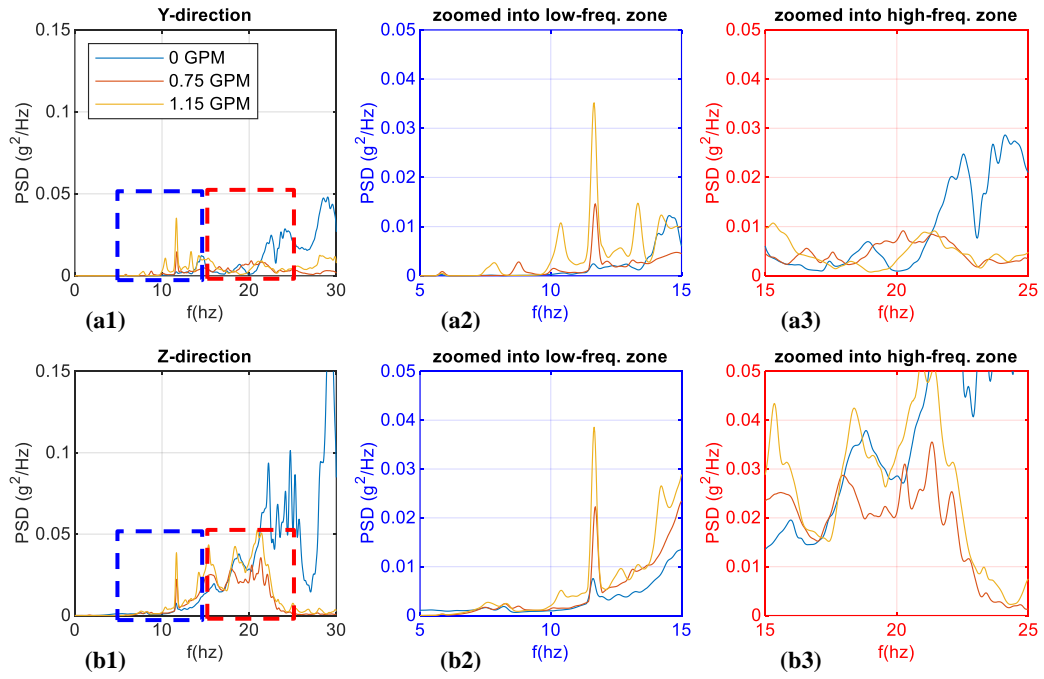
Figure 4.9. Case 2 – Lateral acceleration PSD response for different flow rates in the y & z direction.
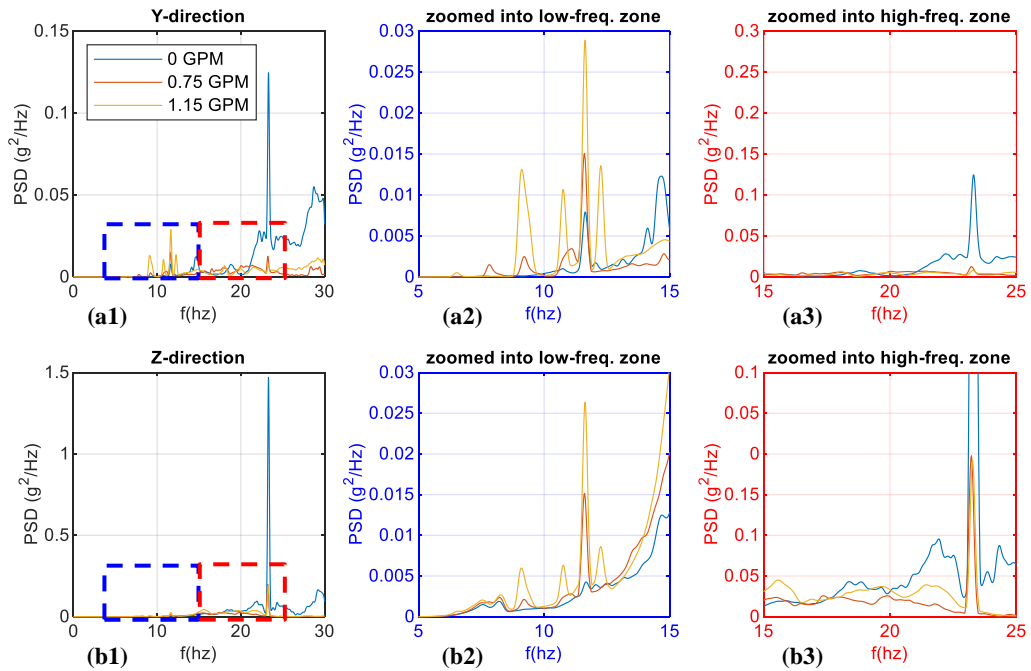

Figure 4.10. Case 3 – Lateral acceleration PSD response for different flow rates in the y & z direction.

It can be said that the circulating fluid does not just dampen the vibratory responses. Fluid presence shifts the harmonic frequency of the system to a lower frequency. It is to be emphasized that a lower value of frequency does indicate a lower level or rank of critical condition. The occurrence only takes place at a different frequency. The critical vibratory response with high magnitude can still be observed, which can be just as detrimental or catastrophic if not avoided.

The effect of a higher flow rate in vibration damping becomes clearer when observed within a broader frequency window of vibration responses, as in Case 4-9 (Figure 4.11 - Figure 4.16). It can be seen that, higher flow rate aid in damping vibration amplitudes in the higher frequency range, especially in the y-direction (Figure 4.11 - Figure 4.16 -a3). Flow seems to have less effect in the z-direction while viewing the narrow windows (Figure 4.11 - Figure 4.16 -b3). But a higher flow rate shows an overall less vibration response while viewing the entire response spectrum (Figure 4.11 - Figure 4.16 -a1&b1).

Comparing Case 4 (Figure 4.11-a3&b3) and Case 7 (Figure 4.14-a3&b3) it is observed that flow is more effective in reducing overall erratic vibration in the lower axial excitation cases. Especially, Case 7 (Figure 4.14-a1&b1) exhibits no large acceleration peaks due to flow at a low frequency range. In Case 4-9 (Figure 4.11 - Figure 4.16) the high vibration response between 55-60 Hz due to flow is expected to be observed due to a shift in the frequency of peak responses or harmonics of the system. Since a high flow rate effectively reduces the value of the first harmonic frequency to a lower frequency, the harmonics become more frequent within a set window of observed frequencies. This also results in the observation of higher vibration peaks for high flow rate conditions at a lower frequency range.
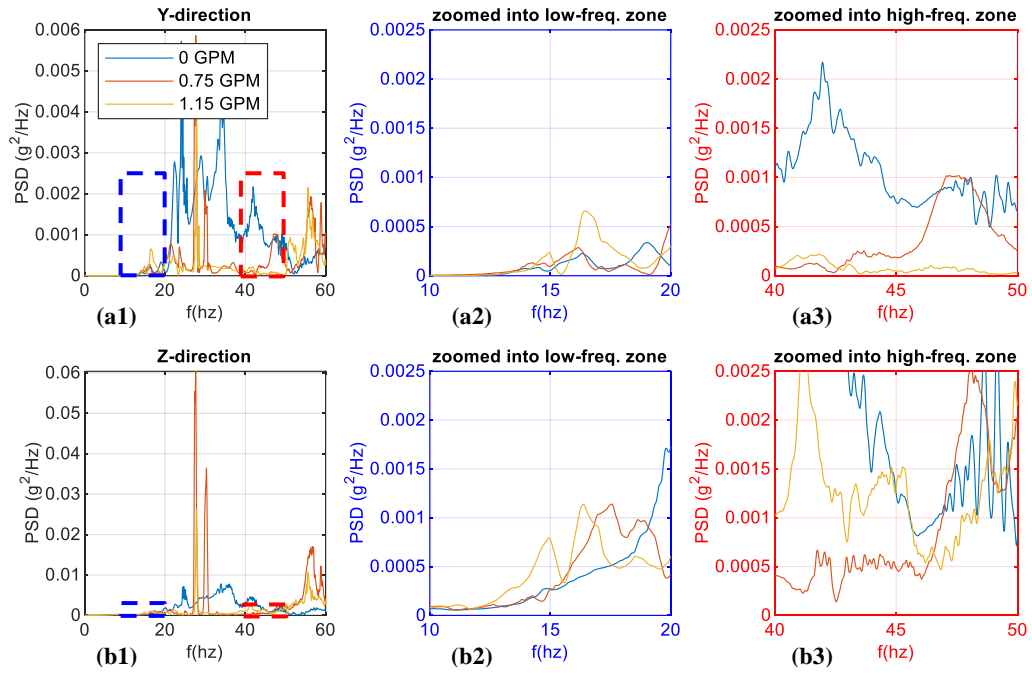
Figure 4.11. Case 4 – Lateral acceleration PSD response for different flow rates in the y & z direction.
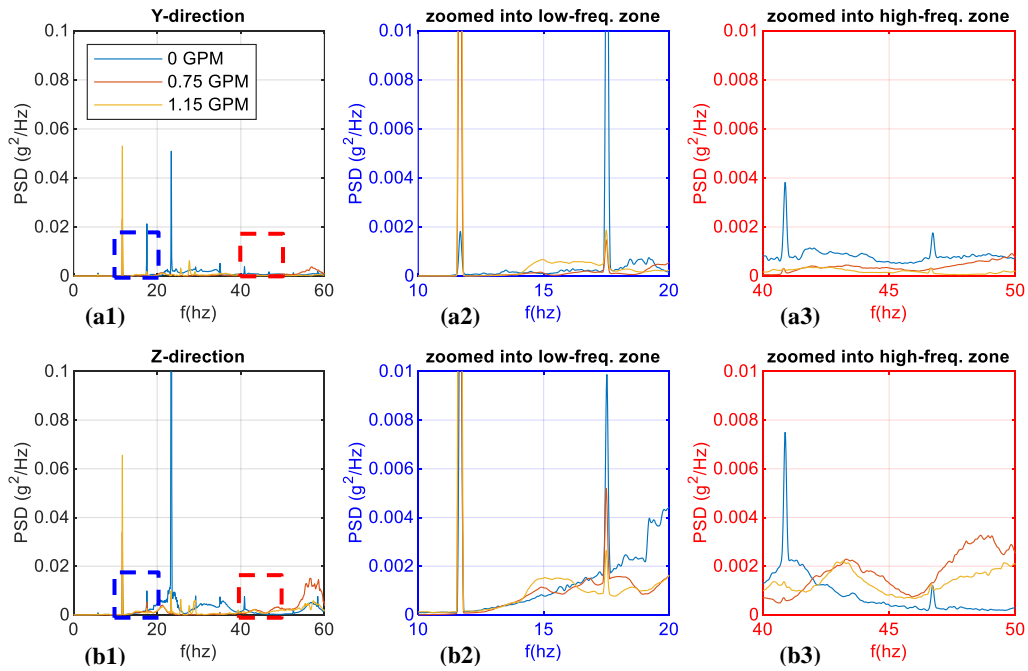

Figure 4.12. Case 5 – Lateral acceleration PSD response for different flow rates in the y & z direction.
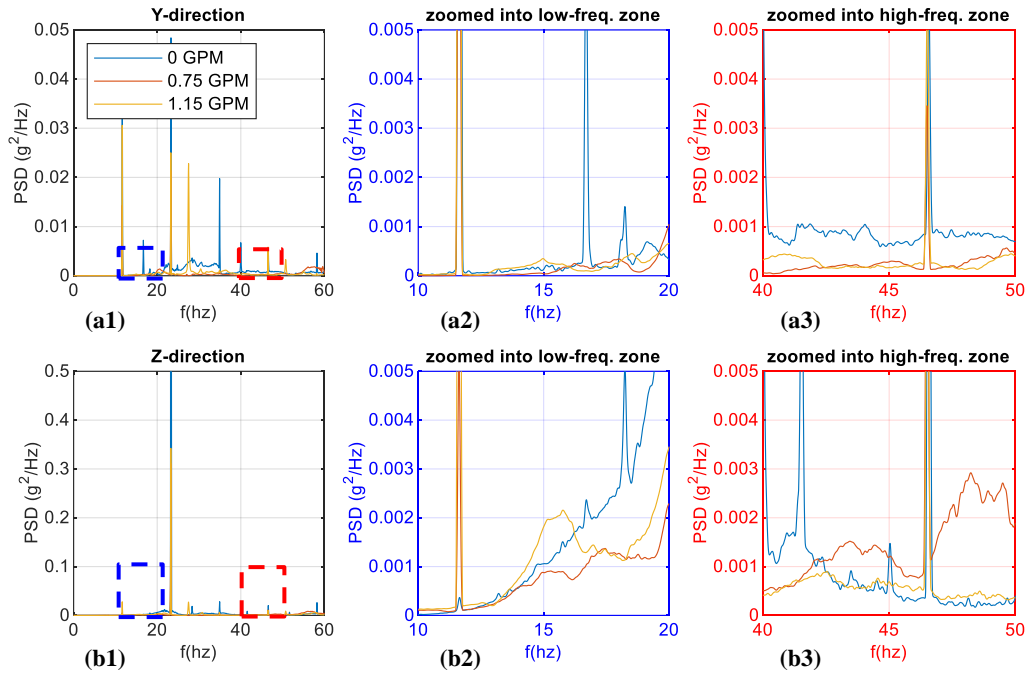
Figure 4.13. Case 6 – Lateral acceleration PSD response for different flow rates in the y & z direction.
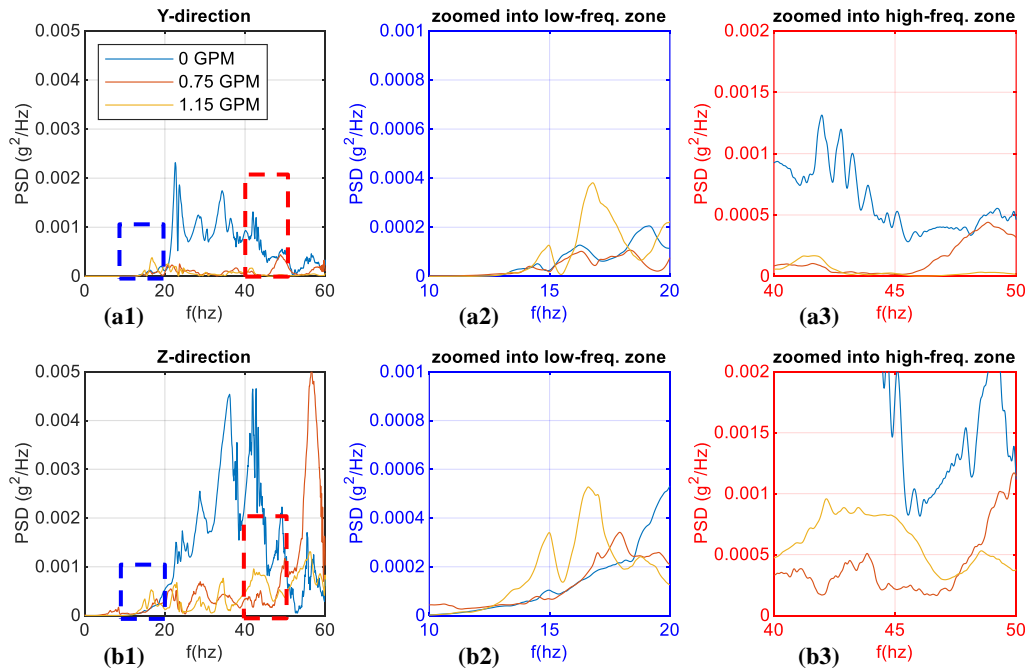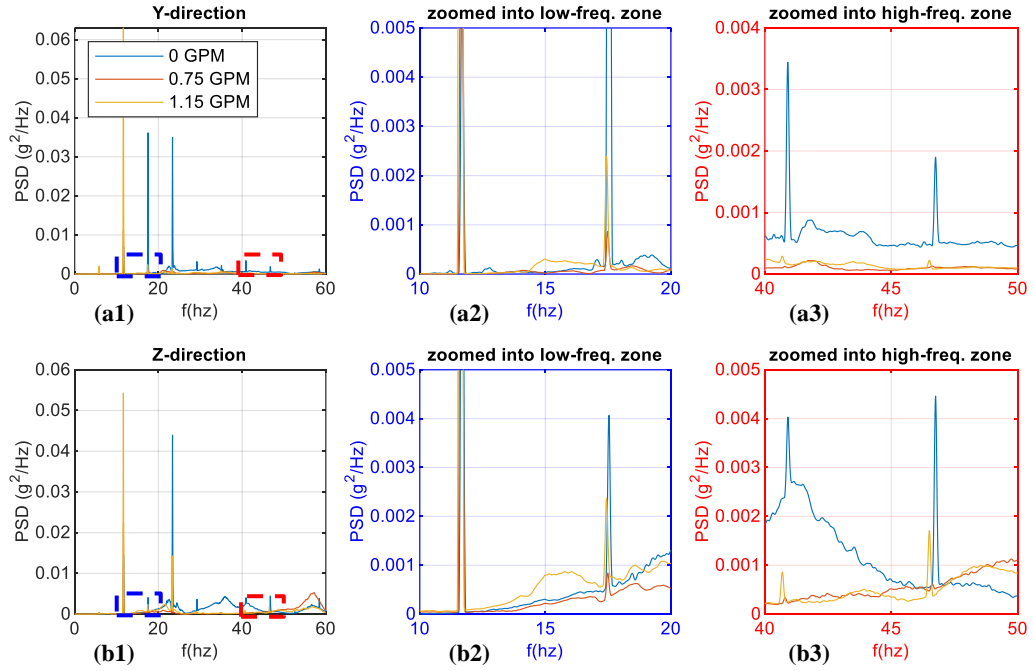

Figure 4.14. Case 7 – Lateral acceleration PSD response for different flow rates in the y & z direction.

Figure 4.15. Case 8 – Lateral acceleration PSD response for different flow rates in the y & z direction.
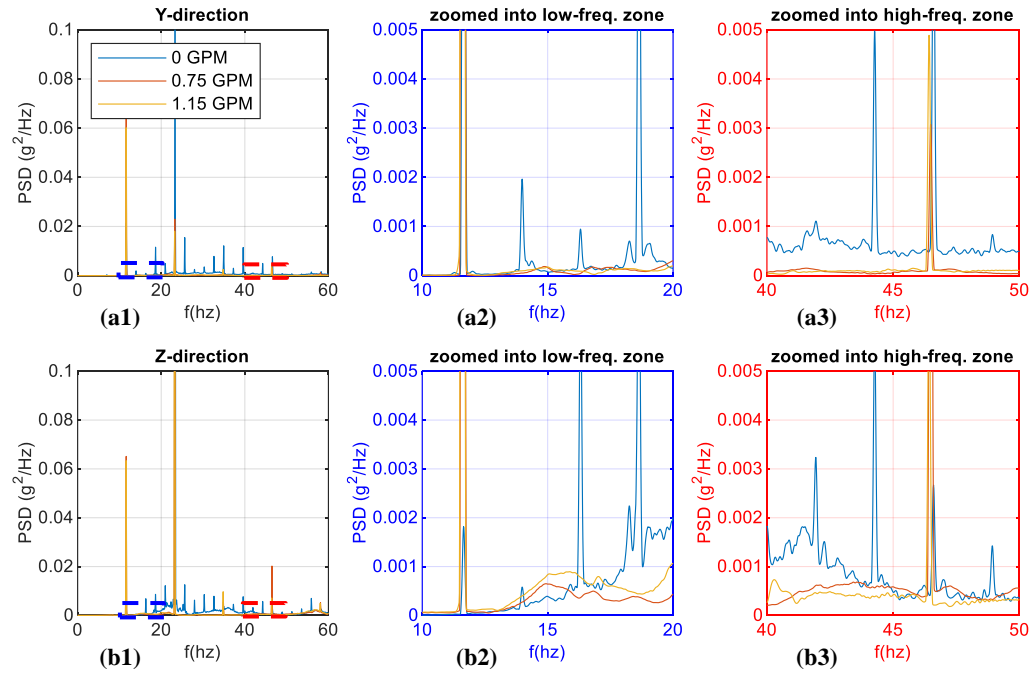

Figure 4.16. Case 9 – Lateral acceleration PSD response for different flow rates in the y & z direction.

The consistent damping efficiency and the nature of shifting frequencies of peak vibration responses are most evident in Case 10-12 (Figure 4.17 - Figure 4.19). The 0.75 GPM flow rate is more effective in damping vibration in the lower frequency range (Figure 4.17 - Figure 4.19 -a3). The 1.15 GPM is more effective in the higher frequency range (Figure 4.17 - Figure 4.19 -b3) except for one irregular vibration response observed between 75-85 Hz in the z-direction of Case 10 (Figure 4.17-b3). Comparing the 0 GPM flow condition to the 1.15 GPM case at high frequency window of 90-100 Hz (Figure 4.10-a3&b3), shifts and damped vibration peaks plateau over a range of frequencies instead of exhibiting large-concentrated peaks at specific frequencies.

A higher flow rate is more consistent in damping vibration, especially for high-frequency vibratory responses. As a result, sudden high vibration peaks are rare in the high frequency range for higher flow rate conditions.
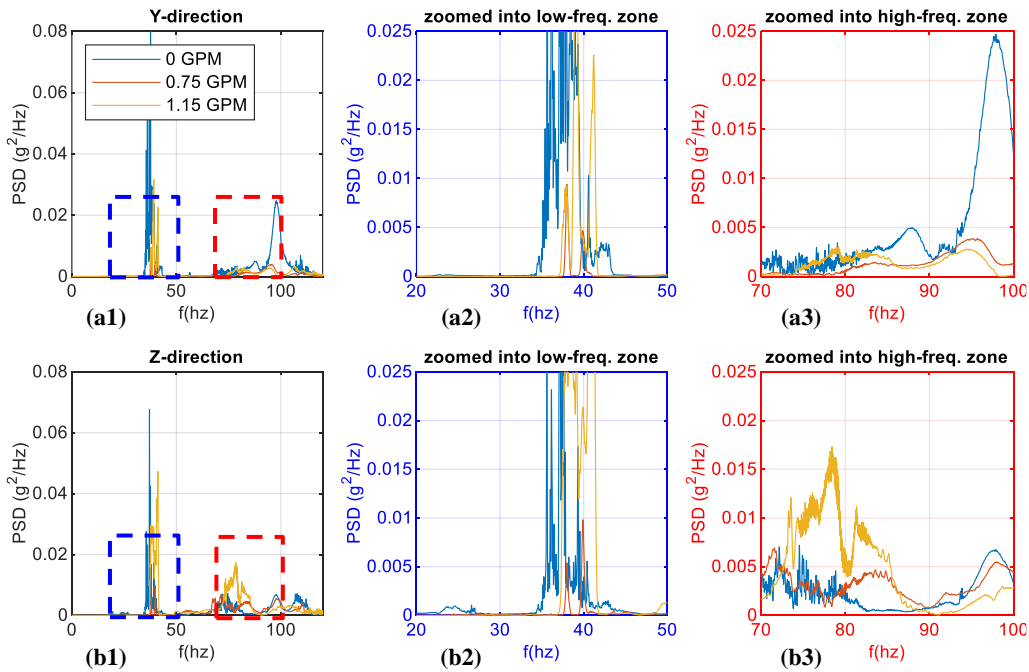

Figure 4.17. Case 10 – Lateral acceleration PSD response for different flow rates in the y & z direction.
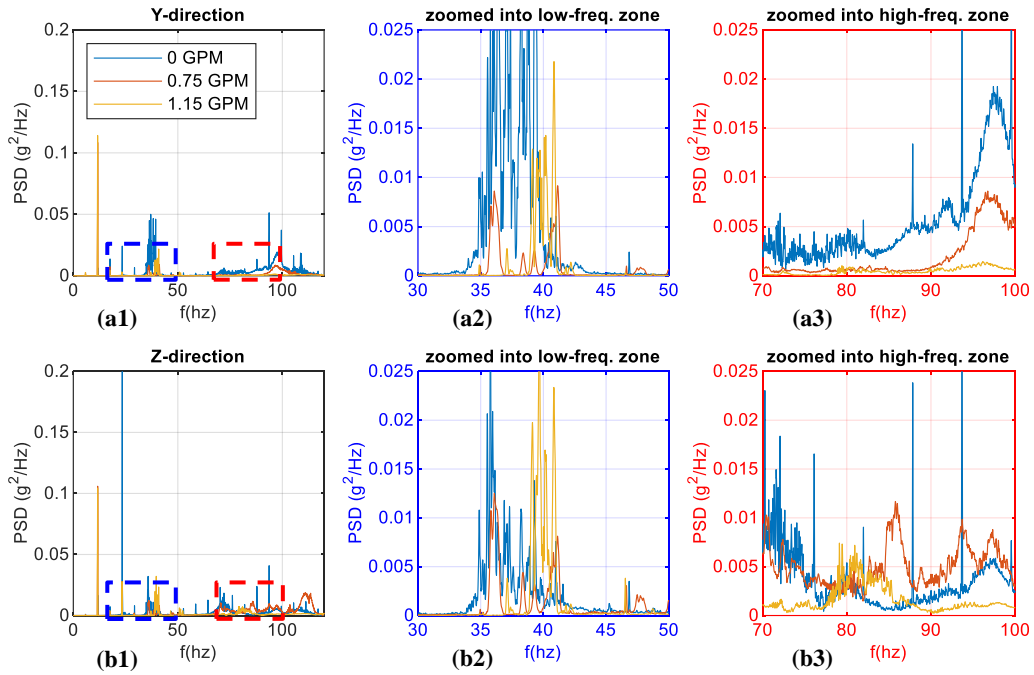
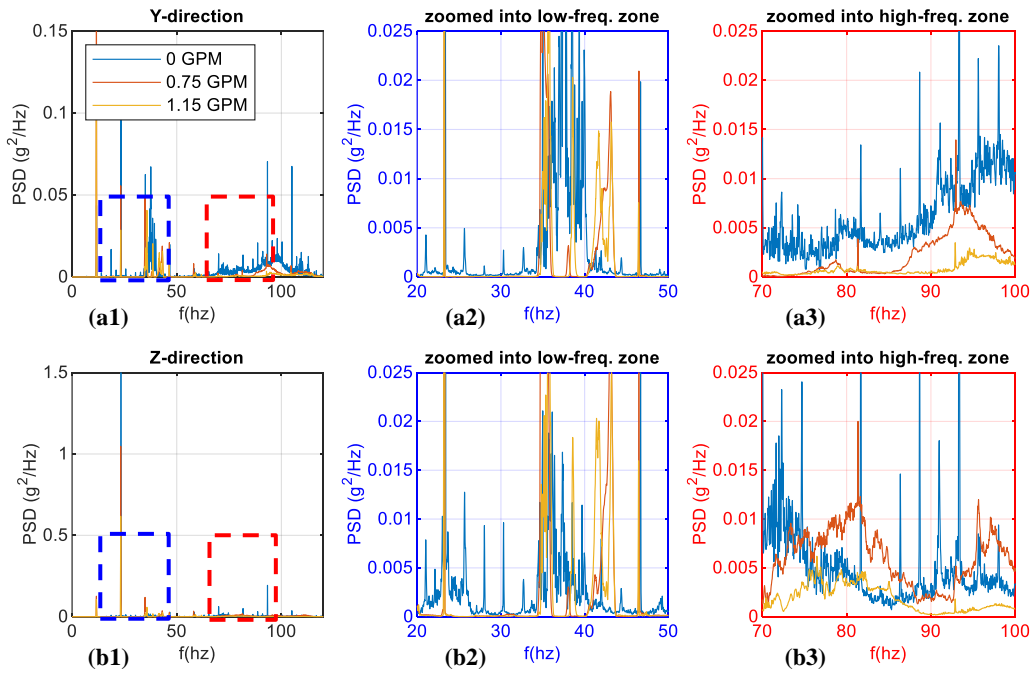*Figure 4.18. Case 11 – Lateral acceleration PSD response for different flow rates in the y & z direction.*

Figure 4.19. Case 12 – Lateral acceleration PSD response for different flow rates in the y & z direction.

CHAPTER V

5   CONCLUSIONS

A mechanically scaled experiment FIDD was designed and fabricated addressing drilling vibration. The high-frequency vibration measurement system and BHA visualization capabilities of FIDD allowed the bridging of drilling dynamics data and BHA trajectory for different lateral vibration conditions. Two investigations were performed using the proposed design. The BHA length varied for the experiments as the design on the surface end was improved after one of the experiments to have better leakage resistance. WOB fluctuation was provided in the form of drill-bit lift-off with sine-sweep motion using a shaker and rotational speed was provided with an electric motor. In one of the experiments, circulated fluid flow was introduced to the system using an electric centrifugal magnetic drive pump. The responses of the BHA were investigated under these induced dynamics.

Investigating the effect of WOB fluctuation on the BHA trajectory, concluded that:

- Harmonic WOB fluctuation causes repeated lateral motion at the low side of the wellbore.

- During severe WOB fluctuation and at high rotational speed, high excitation frequencies are found as double bands in the PSD spectrum, where the difference between the excitation frequencies is the applied rotational speed.

- High WOB fluctuation at high RPM initiates lasting backward whirling even at lower excitation frequencies.

Investigating the effect of fluid flow on the stability of drillstring vibrations concluded that:

- Higher flow rates are more consistent in reducing overall erratic vibration chatter and more effective in damping vibration at a higher frequency.

- As the flow rate increases, a shift in peak frequencies of vibration responses to the lower frequency range is observed. As a result, a higher flow rate increases peak vibration responses in the lower frequency zones.

- Higher flow rate restricts amplitudes of peak vibration responses and plateaus high magnitude responses over a range of frequencies.

The next iteration of this work will explore the total hydrodynamic effect on lateral vibrations with the respective BHA trajectory behavior in the presence of a higher range of flow rates and the effect of wellbore pressure fluctuations along the BHA length. Additionally, different fluids can be used for drilling fluid comparison studies.

REFERENCES

Aarrestad, T.V., Tonnesen, H.A., and A. Kyllingstad. 1986. Drillstring Vibrations: Comparison Between Theory and Experiments on a Full-Scale Research Drilling Rig. *Paper presented at the IADC/SPE Drilling Conference, Dallas, Texas, February.* OnePetro. https://doi.org/10.2118/14760-MS

Al Dushaishi, M. F. 2012. Investigation of drillstring vibration reduction tools. Masters Theses. 5150. Source: https://scholarsmine.mst.edu/masters_theses/5150

Al Dushaishi, M. F., Nygaard, R., and Stutts, D. S. 2016. Effect of drilling fluid hydraulics on drill stem vibrations. *Journal of Natural Gas Science and Engineering, 35,* p. 1059-1069. https://doi.org/10.1016/j.jngse.2016.09.041

Aldred, W. D., and Sheppard, M. C. 1992. Drillstring vibrations: a new generation mechanism and control strategies. Presented at the *SPE Annual technical conference and exhibition, October 4–7, Washington, D.C.* https://doi.org/10.2118/24582-MS

Ambrus, A., Skadsem, H. J., & Mihai, R. G. 2018. Similarity analysis for downscaling a full size drill string to a laboratory scale test drilling rig. In *International Conference on Offshore Mechanics and Arctic Engineering*, *51296,* p. V008T11A005. American Society of Mechanical Engineers. https://doi.org/10.1115/OMAE2018-77202

Antunes, J., Axisa, F., and Hareux, F. 1992. Flexural vibrations of rotors immersed in dense fluids Part II: Experiments. *Journal of Fluids and Structures*, *6*(1), p. 23-38. https://doi.org/10.1016/0889-9746(92)90053-6

Arjun Patil, P., and Teodoriu, C. 2013. Model development of torsional drillstring and investigating parametrically the stick-slips influencing factors. *Journal of Energy Resources Technology*, *135*(1). https://doi.org/10.1115/1.4007915

Asghar Jafari, A., Kazemi, R., and Faraji Mahyari, M. 2012. The effects of drilling mud and weight bit on stability and vibration of a drill string. *Journal of vibration and acoustics*, *134*(1). https://doi.org/10.1115/1.4005033

Axisa, F. and Antunes, J. 1992. Flexural vibrations of rotors immersed in dense fluids: Part 1. Theory. *Journal of Flu& and Structures, 6*(1)*,* p. 3-21. https://doi.org/10.1016/0889-9746(92)90052-5

Bailey, J. J., and Finnie, I. 1960. An Analytical Study of Drill-String Vibration. ASME. *J. Eng. Ind*, *82(2),* p. 122–127. https://doi.org/10.1115/1.3663017

Bailey, J. R., Pastusek, P. E., Junaibi, H. A., Awadhi, M. A., Katheeri, Y. A., Niznik, M. R., ... and Page, C. G. 2016. An integrated workflow to mitigate drilling vibrations and increase daily footage. In *Abu Dhabi International Petroleum Exhibition & Conference*. OnePetro. https://doi.org/10.2118/183550-MS

Bailey, J.R., Biediger, E.A.O., Gupta, V., Ertas, D., Elks, W.C. and Dupriest, F.E. 2008. Drilling vibrations modeling and field validation. *IADC/SPE 112650, IADC/SPE Drilling Conference, Orlando, Florida*. https://doi.org/10.2118/112650-MS

Baird, J. A., and Caskey, B. C. 1984. Analyzing the dynamic behavior of downhole equipment during drilling (No. SAND-84-0758C; CONF-840809-5). Jordan, Apostal, Ritter Associates, Inc., Davisville, RI (USA); Sandia National Labs., Albuquerque, NM (USA). Source: https://www.osti.gov/servlets/purl/6924488

Baird, J. A., Apostal, M. C., and Wormley, D. N. 1985. Analyzing the Dynamic Behavior of Some Typical Rotary Bottom Hole Assemblies During Start Up. *Geothermal Resources Council, Transactions*, *9* (Part 1).

Baker, W. E., Westine, P. S. and Dodge, F. T. 1973. Similarity methods in engineering dynamics: Theory and practice of scale modelling. Hayden Book Company.

Bathe., K.J. 1982. Finite Element Procedures in Engineering Analysis, Prentice-Hall, Englewood Cliffs, NJ.

Baumgart, A. 2000. Stick-slip and bit-bounce of deep-hole drillstrings. *J. Energy Resources Technology, 122(2)*, p. 78-82. https://doi.org/10.1115/1.483168

Bavadiya, V. A., Aljubran, M. J., Kibe, J. M., Christy, S. M., Le, H. N., Ahmed, R., and Florence, F. 2015. Design, construction and operation of an automated drilling rig for the DSATS university competition. In *SPE annual technical conference and exhibition, Houston, Texas, USA, September.* OnePetro. https://doi.org/10.2118/174920-MS

Bavadiya, V. A., Alsaihati, Z., Ahmed, R., and Gustafson, K. 2017. Experimental investigation of the effects of rotational speed and weight on bit on drillstring vibrations, torque and rate of penetration. In *Abu Dhabi International Petroleum Exhibition & Conference*. OnePetro. https://doi.org/10.2118/188427-MS

Berlioz, A., Der Hagopian, J. and Dufour, R. 1996. Dynamic Behavior of a Drill-String: Experimental Investigation of Lateral Instabilities. *J. Vibration & Acoustics,* 118(3), p. 292–298. http://dx.doi.org/10.1115/1.2888180

Blevins, R. D. 1974. Fluid Elastic Whirling of a Tube Row. *J. Pressure Vessel Technol., November, 96(4), p. 263–267.* ASME. https://doi.org/10.1115/1.3454179

Bradbury, R. E. 1962. A lumped parameter approach to longitudinal and torsional vibrations of oil well drill strings. PhD dissertation, Rice University. Source: https://scholarship.rice.edu/handle/1911/89200

Bridgman, P. W. 1992. Dimensional analysis. Yale University Press.

Burgess, T. M., McDaniel, G. L., and Das, P. K. 1987. Improving BHA tool reliability with drillstring vibration models: field experience and limitations. In *SPE/IADC drilling conference*, New Orleans, Louisiana, March. OnePetro. https://doi.org/10.2118/16109-MS

Butterfield, R. 1999. Dimensional analysis for geotechnical engineers. *Geotechnique*, *49*(3), p. 357-366. https://doi.org/10.1680/geot.1999.49.3.357

C. Canudas de Wit, H. Olsson, K. J. Astrom and P. Lischinsky. 1995. A new model for control of systems with friction. In *IEEE Transactions on Automatic Control*, 40(3), p. 419-425, March. https://doi.org/10.1109/9.376053

C. Canudas-de-Wit, F. R. Rubio and M. A. Corchero. 2008. D-OSKIL: A New Mechanism for Controlling Stick-Slip Oscillations in Oil Well Drillstrings. In IEEE Transactions on Control Systems Technology, 16(6), p. 1177-1191, November. https://doi.org/10.1109/TCST.2008.917873

Campbell, R. B. 1980. The Estimation of Natural Frequency and Damping Ratio of Offshore Structures. PhD dissertation, Massachusetts Institute of Technology. Source: https://www.bsee.gov/sites/bsee.gov/files/tap-technical-assessment-program//002ad.pdf

Cayeux, E., Sui, D., Akisanmi, O., and Alani, O. 2017. Challenges in the Automation of a Laboratory-Scale Drilling Rig and Comparison with the Requirements for Full Scale Drilling Automation. In *SPE Bergen One Day Seminar*. OnePetro.

Chen, P., Gao, D., Wang, Z., and Huang, W. 2017. Study on aggressively working casing string in extended-reach well. *Journal of Petroleum Science and Engineering*, *157*, 604-616. https://doi.org/10.1016/j.petrol.2017.07.059

Chen, S. S., Wambsganss, M. T., and Jendrzejczyk, J. A. 1976. Added mass and damping of a vibrating rod in confined viscous fluids. *American Society of Mechanical Engineers*. https://doi.org/10.1115/1.3423833

Christoforou, A. P., and Yigit, A. S. 2003. Fully coupled vibrations of actively controlled drillstrings. *Journal of sound and vibration*, *267*(5), p. 1029-1045. https://doi.org/10.1016/S0022-460X(03)00359-6

Clough, R.W., and Penzien, J. 1993. Dynamics of structures. McGraw-Hill.

Cobern, M., Perry, C., Barbely, J., Burgess, D., and Wassell, M. 2007. Drilling tests of an active vibration damper. Presented at SPE/IADC Drilling Conference 2022 February, Amsterdam, Netherlands. SPE-105400-MS. http://dx.doi.org/10.2118/105400-MS

Dareing, D. W. 1984. Drill collar length is a major factor in vibration control. *Journal of petroleum technology, 36(04)*, 637-644. https://doi.org/10.2118/11228-pa [a]

Dareing, D. W. 1984. Guidelines for Controlling Drill String Vibrations. *J. Energy Resour. Technol, June, 106(2),* p. 272–277. ASME. https://doi.org/10.1115/1.3231051 [b]

Dawson, R. 1984. Drill Pipe Buckling in Inclined Holes. *Journal of Petroleum Technology, 36(10),* p. 1734–1738. SPE-11167-PA. https://doi.org/10.2118/11167-pa

Deily, F. H., Dareing, D. W., Paff, G. H., Ortloff, J. E., and Lynn, R. D. 1968. Downhole Measurements of Drill String Forces and Motions. *J. Eng. Ind. May, 90(2)*, p. 217–225. ASME. https://doi.org/10.1115/1.3604617

Deli, G., Liu, F., and Xu, B. 1998. An analysis of helical buckling of long tubulars in horizontal wells. In *SPE International Oil and Gas Conference and Exhibition in China*. OnePetro. https://doi.org/10.2118/50931-MS

Dimarogonas, A. D., Paipetis, S. A., and Chondros, T. G. 2013. Analytical methods in rotor dynamics. *Springer Science & Business Media.* ISBN : 978-94-007-5904-6

Dong, G., and Chen, P. 2016. A review of the evaluation, control, and application technologies for drill string vibrations and shocks in oil and gas well. *Shock and Vibration*, *2016*. https://doi.org/10.1155/2016/7418635

Dufour, R., Der Hagopian, J., and Lalanne, M. 1985. Influence of an Axial Torque on the Dynamic Behavior of Rotors in Bending. *55th Shock and Vibration Bulletin.* Part 3, p. 27-35.

Duman, O. B., Miska, S., and Kuru, E. 2003. Effect of tool joints on contact force and axial-force transfer in horizontal wellbores. *SPE drilling & completion*, 18(03), p. 267-274. https://doi.org/10.2118/72278-MS

Dykstra, M. W. 1996. Nonlinear Drill String Dynamics. Ph.D. dissertation. University of Tulsa, Tulsa, Oklahoma.

Dykstra, M. W., Chen, D. C-K., Warren, T. M., and J. J. Azar. 1996. Drillstring Component Mass Imbalance: A Major Source of Downhole Vibrations. *SPE Drill & Compl 11*, p. 234–241. https://doi.org/10.2118/29350-PA

Dykstra, M. W., Neubert, M., Hanson, J. M., and M. J. Meiners. 2001. Improving Drilling Performance by Applying Advanced Dynamics Models. *Paper presented at the SPE/IADC Drilling Conference, Amsterdam, Netherlands, February.* https://doi.org/10.2118/67697-MS

Elliott, A. S., and Hutchinson, M. 2015. Fully-Coupled Nonlinear 3-D Time-Domain Simulation of Drilling Dysfunctions Using a Multi-Body Dynamics Approach. *Paper presented at the SPE/IADC Drilling Conference and Exhibition, London, England, UK, March.* OnePetro. https://doi.org/10.2118/173154-MS

Elmgerbi, A. M., Ettinger, C. P., Tekum, P. M., Thonhauser, G., and Nascimento, A. 2021. Application of Machine Learning Techniques for Real Time Rate of Penetration Optimization. *Paper presented at the SPE/IADC Middle East Drilling Technology Conference and Exhibition, Abu Dhabi, UAE, May.* OnePetro. https://doi.org/10.2118/202184-MS

Elmgerbi, A., Chuykov, E., Thonhauser, G., and Nascimento, A. 2022. Machine Learning Techniques Application for Real-Time Drilling Hydraulic Optimization. *Paper presented at*

the International Petroleum Technology Conference, Riyadh, Saudi Arabia, February. OnePetro. https://doi.org/10.2523/IPTC-22662-MS

Eshleman, R. L., and Eubanks, R. A. 1970. Effects of Axial Torque on Rotor Response. An Experimental Investigation. ASME *Paper 70 WA/DE-I4.*

Esmaeili, A., Elahifar, B., Fruhwirth, R. K., and Thonhauser, G. 2013. Formation Prediction Model based on Drill String Vibration Measurements Using Laboratory Scale Rig. In *SPE/IADC Middle East Drilling Technology Conference & Exhibition, October*. OnePetro. https://doi.org/10.2118/166793-MS

Esmaeili, A., Elahifar, B., Fruhwirth, R. K., and Thonhauser, G. 2012. Laboratory scale control of drilling parameters to enhance rate of penetration and reduce drill string vibration. In *SPE Saudi Arabia Section Technical Symposium and Exhibition, April.* OnePetro. https://doi.org/10.2118/160872-MS

Fan, Y., Gao, D., Fang, J. and Xiao, G..2013. Research on the simulation test method for dynamic properties of BHA. *Chin. Petrol. Mach. 41(4)*, p. 6–10. Source: http://en.cnki.com.cn/Article_en/CJFDTOTAL-SYJI201304001.htm

Fear, M. J., Abbassian, F., Parfitt, S. H. L., and McClean, A. 1997. The destruction of PDC bits by severe slip-stick vibration. In *SPE/IADC drilling conference, March*. OnePetro. https://doi.org/10.2118/37639-MS

Finnie, I., and Bailey, J. J. 1960. An Experimental Study of Drill-String Vibration. *J. Eng. Ind. May, 82(2),* p. 129–135. ASME. https://doi.org/10.1115/1.3663020

Forster, I. 2011. Axial excitation as a means of stick slip mitigation-small scale rig testing and full scale field testing. In *SPE/IADC Drilling Conference and Exhibition, Amsterdam, The Netherlands, March*. OnePetro. https://doi.org/10.2118/139830-MS

Forster, I., Macfarlane, A., and Robert, D. 2010. Asymmetric Vibration Damping Tool - Small Scale Rig Testing and Full Scale Field Testing. *Paper presented at the IADC/SPE Drilling Conference and Exhibition, New Orleans, Louisiana, USA, February.* https://doi.org/10.2118/128458-MS

Franca, L. F. P. 2011. Drilling Action of Roller-Cone Bits: Modeling and Experimental Validation. *J. Energy Resour. Technol*, *December, 132(4)*, p. 043101. https://doi.org/10.1115/1.4003168

Fritz, R. J. 1970. The Effects of an Annular Fluid on the Vibrations of a Long Rotor, Part 2—Test. ASME. *J. Basic Eng*. *December, 92(4),* p. 930–937. https://doi.org/10.1115/1.3425166

Fritz, R. J., and Kiss, E. 1966. The vibration response of a cantilevered cylinder surrounded by an annular fluid (No. KAPL-M-6539). Knolls Atomic Power Lab., Schenectady, NY.

Fu, J., Ren, Z., Bai, J., Qin, F., and Li, B. 2018. The friction-reducing principle and application of the drill string with a hydro-oscillator. *Journal of Petroleum Science and Engineering*, *165*, p. 453-461. https://doi.org/10.1016/j.petrol.2018.01.076

Gao, G., and Miska, S. 2009. Effects of boundary conditions and friction on static buckling of pipe in a horizontal well. *SPE Journal*, *14(04),* p. 782-796. https://doi.org/10.2118/111511-pa

Gao, G., and Miska, S. 2010. Dynamic buckling and snaking motion of rotating drilling pipe in a horizontal well. *SPE Journal*, *15(03),* p. 867-877. https://doi.org/10.2118/113883-pa

Ghasemloonia, A., Rideout, D. G., and Butt, S. D. 2015. A review of drillstring vibration modeling and suppression methods. *Journal of Petroleum Science and Engineering*, *131*, p. 150-164. https://doi.org/10.1016/j.petrol.2015.04.030

Grote, K. H. and Feldhusen, J. 2011. Dubbel - Taschenbuch für den Maschinenbau. https://doi.org/10.1007/978-3-642-38891-0

Halsey, G.W., Kyllingstad, A., Aarrestad, T.V., and D. Lysne. 1986. Drillstring Torsional Vibrations: Comparison Between Theory and Experiment on a Full-Scale Research Drilling Rig. *Paper presented at the SPE Annual Technical Conference and Exhibition, New Orleans, Louisiana, October*. https://doi.org/10.2118/15564-MS

Heisig, G., and M. Neubert. 2000. Lateral Drillstring Vibrations in Extended-Reach Wells. *Paper presented at the IADC/SPE Drilling Conference, New Orleans, Louisiana, February.* OnePetro. https://doi.org/10.2118/59235-MS

Henneuse, H. 1992. Surface Detection of Vibrations and Drilling Optimization: Field Experience. *Paper presented at the IADC/SPE Drilling Conference, New Orleans, Louisiana, February*. OnePetro. https://doi.org/10.2118/23888-MS

Hsu, C. S. 1963. On the Parametric Excitation of a Dynamic System Having Multiple Degrees of Freedom. *J. Appl. Mech. September, 30(3)*, p. 367–372. ASME. https://doi.org/10.1115/1.3636563

Iwatsubo, T., Saigo, M., and Sugiyama, Y. 1973. Parametric instability of clamped-clamped and clamped-simply supported columns under periodic axial load. *Journal of sound and vibration, 30(1),* 65-IN2. https://doi.org/10.1016/S0022-460X(73)80050-1

Jansen, J. D. 1993. Nonlinear Dynamics of Oilwell Drillstrings. Ph. D. thesis. Delft University of Technology, Delft, The Netherlands. Source: http://resolver.tudelft.nl/uuid:d205b287-bcdd-4b49-b12a-963d9b906dea

Jansen, J. D., 1991. Nonlinear rotor dynamics as applied to oil well drillstring vibrations. *Journal of Soundand Vibration, 147(1),* p. 115-135. https://doi.org/10.1016/0022-460X(91)90687-F

Kapitaniak, M., Hamaneh, V. V., and Wiercigroch, M. 2016. Torsional vibrations of helically buckled drill-strings: experiments and FE modelling. In *Journal of Physics: Conference Series, 721(1)*, p. 012012. IOP Publishing. https://doi.org/10.1088/1742-6596/721/1/012012

Kapitaniak, M., Hamaneh, V. V., Chávez, J. P., Nandakumar, K., and Wiercigroch, M. 2015. Unveiling complexity of drill–string vibrations: Experiments and modelling. *International Journal of Mechanical Sciences*, *101*, 324-337. https://doi.org/10.1016/j.ijmecsci.2015.07.008

Kapitaniak, M., Vaziri, V., Chávez, J. P., and Wiercigroch, M. 2018. Experimental studies of forward and backward whirls of drill-string. *Mechanical Systems and Signal Processing*, *100*, 454-465. https://doi.org/10.1016/j.ymssp.2017.07.014

Khalil, H. K. 2002. Nonlinear systems (3rd ed.). Prentice hall Upper Saddle River.

Khulief, Y. A., and Al-Sulaiman, F. A. 2009. Laboratory investigation of drillstring vibrations. *Proceedings of the Institution of Mechanical Engineers, Part C: Journal of Mechanical Engineering Science*, *223(10),* p. 2249-2262. https://doi.org/10.1243/09544062JMES15

Khulief, Y. A., Bashmal, S. A., Said, S. A., Al-Otaibi, D. A., and Mansour, K. M. 2014. Prediction of vibration-induced instability due to cross flow in heat exchangers with triangular tube arrays. *Arabian Journal for Science and Engineering, 39(11),* p. 8209-8219. https://doi.org/10.1007/s13369-014-1399-6 [a]

Khulief, Y. A., Mohiuddin, M. A., and El-Gebeily, M. 2014. A new method for field-balancing of high-speed flexible rotors without trial weights. *International Journal of Rotating Machinery*, *2014*. https://doi.org/10.1155/2014/603241 [b]

Leine, R. I., Van Campen, D. H., and Keultjes, W. J. G. 2002. Stick-slip whirl interaction in drillstring dynamics. *ASME Journal of Vibrations and Acoustics, 124,* p. 209–220. https://doi.org/10.1115/1.1452745

Li, W., Huang, G., Jing, Y., Yu, F., and Ni, H. 2019. Modeling and mechanism analyzing of casing running with pick-up and release technique. *Journal of Petroleum Science and Engineering*, *172*, p. 538-546. https://doi.org/10.1016/j.petrol.2018.09.099

Li, W., Huang, G., Ni, H., Yu, F., Huang, B., and Jiang, W. 2020. Experimental study and mechanism analysis of the motion states of bottom hole assembly during rotary drilling. *Journal of Petroleum Science and Engineering*, *195*, 107859. https://doi.org/10.1016/j.petrol.2020.107859

Lian, Z., Zhang, Q., Lin, T., and Wang, F. 2015. Experimental and numerical study of drill string dynamics in gas drilling of horizontal wells. *Journal of Natural Gas Science and Engineering*, *27(3)*, 1412-1420. https://doi.org/10.1016/j.jngse.2015.10.005

Liao, C. M., Balachandran, B., Karkoub, M., and Abdel-Magid, Y. L. 2011. Drill-string dynamics: reduced-order models and experimental studies. *Journal of Vibration and Acoustics*, *133*(4).http://dx.doi.org/10.1115/1.4003406.

Lin, T., Zhang, Q., Lian, Z., Xiao, Z., Wang, T., Li, G., and Ding, J. 2018. Experimental study on vibrational behaviors of horizontal drillstring. Journal of Petroleum Science and Engineering, 164, p. 311-319. https://doi.org/10.1016/j.petrol.2018.01.081

Liu, X., Vlajic, N., Long, X., Meng, G., & Balachandran, B. 2013. Nonlinear motions of a flexible rotor with a drill bit: stick-slip and delay effects. *Nonlinear Dynamics, 72(1),* p. 61-77. https://doi.org/10.1007/s11071-012-0690-x

Lu, H., Dumon, J., and Canudas-de-Wit, C. 2009. Experimental study of the D-OSKIL mechanism for controlling the stick-slip oscillations in a drilling laboratory testbed. In *2009 IEEE Control Applications, (CCA) & Intelligent Control, (ISIC), July,*p. 1551-1556. IEEE. https://doi.org/10.1109/CCA.2009.5280974

Lubinski, A. 1950. A study of the buckling of rotary drilling strings. In *Drilling and Production Practice,* , January. OnePetro.

Mabile, C., Desplans, J.P., and D. Pavone. 1996. A New Way of Using Surface Measurements to Detect Down Hole Vibrations. *Paper presented at the European Petroleum Conference, Milan, Italy, October.* OnePetro. https://doi.org/10.2118/36883-MS

Macpherson, J.D., Mason, J.S., and J.E.E. Kingman. 1993. Surface Measurement and Analysis of Drillstring Vibrations While Drilling. *Paper presented at the SPE/IADC Drilling Conference, Amsterdam, Netherlands, February.* OnePetro. doi: https://doi.org/10.2118/25777-MS

Majeed F. A., Karki, H., Karkoub, M., Abdel-Magid, Y. L. 2013. Experimental Verification of Drill String Vibration Suppression Using an Adaptive Self-Tuning Controller. *International Journal of Acoustics and Vibrations, 18,* p. 20-26. https://doi.org/10.20855/ijav.2013.18.1316

Majeed, F. A., Karki, H., Karkoub, M., and Magid, Y. L. A. 2013. Experimental verification of drill string vibration suppression using an adaptive self-tuning controller. *Int. J. Acoust. Vib*, *18(1),* 20-6. https://doi.org/10.20855/ijav.2013.18.1316

Melakhessou, H., Berlioz, A., and Ferraris, G. 2003. A nonlinear well-drillstring interaction model. *J. Vib. Acoust.*, *125(1),* 46-52. https://doi.org/10.1115/1.1523071

Merlo, M., Maglione, R., and Piatti, C. 1995. An innovative model for drilling fluid hydraulics. *Presented at SPE Asia Pacific Oil and Gas Conference, March, Kuala Lumpur, Malaysia.* SPE-29259-MS. OnePetro. http://dx.doi.org/10.2118/29259-MS

Mihajlovic, N. 2005. *Torsional and lateral vibrations in flexible rotor systems with friction.* Technische Universiteit Eindhoven. https://doi.org/10.6100/IR591879

Mihajlovic, N., van de Wouw, N. H. M. P. M. N. H., Hendriks, M. P. M., and Nijmeijer, H. 2006. Friction-induced limit cycling in flexible rotor systems: an experimental drill-string set-up. *Nonlinear Dynamics*, *46(3),* p. 273-291. https://doi.org/10.1007/s11071-006-9042-z

Mihajlovic, N., Van Veggel, A. A., Van de Wouw, N., and Nijmeijer, H. 2004. Analysis of friction-induced limit cycling in an experimental drill-string system. *J. Dyn. Sys., Meas., Control*, *126(4),* p. 709-720. https://doi.org/10.1115/1.1850535

Mitchell, R. F. 1982. Buckling behavior of well tubing: the packer effect. *Society of Petroleum Engineers Journal*, *22*(05), p. 616-624. https://doi.org/10.2118/9264-PA

Nelson, H.D. 1980. A Finite Rotating Shaft Element Using Timoshenko Beam Theory. *ASME Journal of Mechanical Design, 102,* p. 793-803. http://dx.doi.org/10.1115/1.3254824

Nicholson, J. W. 1994. An Integrated Approach to Drilling Dynamics Planning, Identification, and Control. *Paper presented at the IADC/SPE Drilling Conference, Dallas, Texas, February.* OnePetro. doi: https://doi.org/10.2118/27537-MS

Paidoussis, M. P. 1983. A review of flow-induced vibrations in reactors and reactor components. *Nuclear Engineering and Design, 74(1),* p. 31-60. https://doi.org/10.1016/0029-5493(83)90138-3

Paidoussis, M. P. 1998. Fluid-Structure Interactions. https://doi.org/10.1604/9780125443609.

Paidoussis, M., Luu, T., Prabhakar, S., 2008. Dynamics of a long tubular cantilever conveying fluid downwards, which then flows upwards around the cantilever as a confined annular flow. *J. Fluids Struct., 24 (1)*, p. 111-128. http://dx.doi.org/10.1016/j.jfluidstructs.2007.07.004

Pehlivantürk, C., Chen, D., and van Oort, E. 2017. Torsional drillstring vibration modelling and mitigation with feedback control. *Paper presented at the SPE/IADC Drilling Conference and Exhibition, The Hague, The Netherlands, March.* OnePetro.https://doi.org/10.2118/184697-MS

Popp, T., Stibbe, H., Heinisch, D., Reckmann, H., and Spanos, P. 2018. Backward whirl testing and modeling with realistic borehole contacts for enhanced drilling tool reliability. *Paper presented at the IADC/SPE Drilling Conference and Exhibition, Fort Worth, Texas, USA, March*. OnePetro. https://doi.org/10.2118/189600-MS

Raymond, D. W., Elsayed, M. A., Polsky, Y., and Kuszmaul, S. S. 2008. Laboratory simulation of drill bit dynamics using a model-based servo hydraulic controller. *Proceedings of the ASME 2007 26th International Conference on Offshore Mechanics and Arctic Engineering. Volume 2: Structures, Safety and Reliability; Petroleum Technology Symposium. San Diego, California, USA. June 10–15.* p. 905-914. ASME. https://doi.org/10.1115/OMAE2007-29706

Ren, F., Wang, B., Zhao, L., and Zhu, A. 2017. Experimental investigation and analysis of dynamic buckling of drill string in horizontal well. *Shock and Vibration*, *2017*. https://doi.org/10.1155/2017/1658435

Rezaeepazhand, J., Simitses, G.J., and Starnes, J.H. 1996. Design of scaled down models for predicting shell vibration response*, J. Sound Vibr. 195 (2)* p. 301–311. https://doi.org/10.1006/jsvi.1996.0423

Ritto, T. G., Sampaio, R., and Soize, C. 2009. Drill-string dynamics coupled with the drilling fluid dynamics. *In XIII International Symposium on Dynamic Problems of Mechanics, DINAME, 2009, p. 1-10.* ABCM. Source: https://www.researchgate.net/publication/278805853_Drill-string_dynamics_coupled_with_the_drilling_fluid_dynamics

Saldivar, B., Mondié, S., Niculescu, S. I., Mounier, H., and Boussaada, I. 2016. A control oriented guided tour in oilwell drilling vibration modeling. *Annual reviews in Control*, *42*, 100-113. https://doi.org/10.1016/j.arcontrol.2016.09.002

Samuel, R., Schottle, G. and Gupta, D.B.. 2006. Vibration Analysis, Model Prediction, and avoidance: A case history. *SPE/IADC 102134, SPE/IADC Indian Drilling Technology Conference and Exhibition, Mumbai, India.* https://doi.org/10.2118/102134-MS

Sengupta, A. K. 1994. Numerical simulation of the roller cone drill bit lift-off phenomenon. Rice University.

Shao, D. D. 2013. Analysis of drill string dynamic characteristics in horizontal well hole. *China University of*, *732*.

Shao, D. D., Guan, Z. C., & Wen, X. 2013. Experimental Device of Drilling String Dynamics in Horizontal Well and its Application. *In Advanced Materials Research, 683*, p. 690–693. Trans Tech Publications, Ltd. https://doi.org/10.4028/www.scientific.net/amr.683.690

Shi, Y., Wan, Y., and Wu, C. 2006. Setting up A Simulate device on motion behavior of bottom-hole assembly according to similitude principles. *J. Guangxi Univ. Nat. Sci. Ed. 31,* p. 159–162. Source: http://caod.oriprobe.com/articles/11827080/Setting_up_a_simulate_device_on_motion_behavior_of_bottom_hole_assembl.htm

Shyu, R. J. 1989. Bending Vibration of Rotating Drill Strings. PhD dissertation, MIT, Cambridge, Massachusetts.

Skaugen, E. 1987. The effects of quasi-random drill bit vibrations upon drillstring dynamic behavior. *Paper presented at the SPE Annual Technical Conference and Exhibition, Dallas, Texas, September.* OnePetro. https://doi.org/10.2118/16660-MS

Spanos, P. D., Chevallier, A. M., Politis, N. P., and Payne, M. L. 2003. Oil and gas well drilling: a vibrations perspective. *The Shock and Vibration Digest, 35(*2), p. 85-103. https://doi.org/10.1177/0583102403035002564

Spanos, P.D., Rice U, and Payne, M.L. 1992.Advances in dynamic bottom hole assembly modeling and dynamic response determination. *IADC/SPE 23905, IADCISPE Drilling Conference, New Orleans, Louisiana.*

Srivastava, S., and Teodoriu, C. 2019. An extensive review of laboratory scaled experimental setups for studying drill string vibrations and the way forward. *Journal of petroleum Science and Engineering*, *182*, p. 106272. https://doi.org/10.1016/j.petrol.2019.106272

Stokes, G. G. 1843. On Some Cases of Fluid Motion. *Proceedings of the Cambridge Philosophical Society, 8, May*, p. 105-137.

Stonneger, J. C. 1937. Vibration problems in oil wells. SPE 37-179, American Petroleum Institute.

Stroud, D. R., Lines, L. A., and Minett-Smith, D. J. 2011. Analytical and experimental backward whirl simulations for rotary steerable bottom hole assemblies. *Paper presented at the SPE/IADC Drilling Conference and Exhibition, Amsterdam, The Netherlands, March.* OnePetro. https://doi.org/10.2118/140011-MS

Tang, L., Zhang, S., Zhang, X., Ma, L., and Pu, B. 2021. A review of axial vibration tool development and application for friction-reduction in extended reach wells. *Journal of Petroleum Science and Engineering*, *199*, p. 108348. https://doi.org/10.1016/j.petrol.2021.108348

Tian, J., Hu, S., Li, Y., Yang, Z., Yang, L., Cai, X., ... and Fu, C. 2016. Vibration characteristics analysis and experimental study of new drilling oscillator. *Advances in Mechanical Engineering, 8(6),* p. 1687814016652090. https://doi.org/10.1177/1687814016652090

Ullah, F. K., & Bohn, C. 2018. Dynamic surface control for the reduction of torsional vibrations in a scaled experimental drillstring setup. In *UKACC 12th International Conference on Control (CONTROL)*, p. 199-204, https://doi.org/10.1109/CONTROL.2018.8516736

Unger, A., and Brull, M. A., 1981, Parametric Instabihty of a Rotating Shaft due to Pulsating Torque. *J. Appl. Mech. December, 48(4), p. 948–958. ASME.* https://doi.org/10.1115/1.3157761

Vandiver, K. J., Nicholson, J. W., and Shyu, R. J. 1990. Case studies of the bending vibration and whirling motion of drill collars. *SPE Drilling Engineering, 5(04),* p. 282-290. OnePetro. https://doi.org/10.2118/18652-PA

Vassalos, D. 1999. Physical modelling and similitude of marine structures. *Ocean Eng. 26,*p. 111–123. https://doi.org/10.1016/S0029-8018(97)10004-X

Veeningen, D., Hewlett, R., Salazar, J., Coit, A., and Furniss, E. 2013. Field Tests Quantify Processes Utilizing an Enhanced Downhole Dynamics Measurement Tool for Vibration Mitigation and Performance Optimization. *Paper presented at the SPE/IADC Middle East Drilling Technology Conference & Exhibition, Dubai, UAE, October.* OnePetro. https://doi.org/10.2118/166681-MS .

Wang, H., Guan, Z. C., Shi, Y. C., Chen, W. Q., Liu, Y. W., Zhang, B., ... and Wang, X. H. 2018. Modeling and analyzing the motion state of bottom hole assembly in highly deviated wells. *Journal of Petroleum Science and Engineering*, *170*, p. 763-771. https://doi.org/10.1016/j.petrol.2018.07.005

Wang, P., Yan, T., Bi, X. L., and Sun, S. H. 2012. Fatigue life prediction of buckling string with cracks in horizontal wells of mining engineering. *In Advanced Materials Research,577,* p. 127-131. Trans Tech Publications Ltd. https://doi.org/10.4028/www.scientific.net/AMR.577.127

Warren, T. M., Brett, J. F. and Sinor, L. A. 1990. Development of a Whirl-Resistant Bit.. Presented at SPE Annual Technical conference and exhibition, San Antonio, 8-11 October. SPEDE 5 (4), p. 267-274. Trans., AIME, 289, SPE 19572. https://doi.org/10.2118/19572-PA

Wehrli, C. 1963. Über kritische Drehzahlen unter pulsierender Torsion. *Ing. arch 33,* p. 73–84. https://doi.org/10.1007/BF00531793

Westermann, H., Gorelik, I., Rudat, J., Moritz, C., Neubauer, M., Wallaschek, J., and Höhn, O. 2015. A new test rig for experimental studies of drillstring vibrations. *SPE Drilling & Completion, 30(02),* p. 119-128. https://doi.org/10.2118/176019-pa

Wiercigroch, M. 2010. Modelling and Analysis of BHA and Drill-string Vibrations. *R&D project sponsored by the BG Group*.

Wiktorski, E., Geekiyanage, S., Løken, E., and Sui, D. 2019. Comparative Study of Surface and Downhole Drillstring Vibrations Measurements on a Laboratory-Scale Drilling Rig. *Paper presented at the SPE Norway One Day Seminar, Bergen, Norway, May.* OnePetro. https://doi.org/10.2118/195610-MS

Willems, N., and Holzer, S. M. 1967. Critical Speeds of Rotating Shaft Subjected to Axial Loading and Tangential Torsion. *Journal of Engineering for Industry,* p. 259-264. ASME. https://doi.org/10.1115/1.3610037

Wu, J. J. 2007. Prediction of lateral vibration characteristics of a full-size rotor-bearing system by using those of its scale models. *Finite Elements in Analysis and Design*, *43(10),* p. 803-816. https://doi.org/10.1016/j.finel.2007.05.001

Wu, J. J. 2015. Prediction of the torsional vibration characteristics of a rotor-shaft system using its scale model and scaling laws. *World Academy of Science, Engineering and Technology, International Journal of Mechanical, Aerospace, Industrial, Mechatronic and Manufacturing Engineering, 9(2),* p. 229-34. Source: https://publications.waset.org/10000359/prediction-of-the-torsional-vibration-characteristics-of-a-rotor-shaft-system-using-its-scale-model-and-scaling-laws

Wu, J. J., Cartmell, M. P., and Whittaker, A. R. 2002. Prediction of the vibration characteristics of a full-size structure from those of a scale model. *Computers & structures, 80(18-19),* p. 1461-1472. https://doi.org/10.1016/S0045-7949(02)00095-0

Yigit, A. S., and Christoforou, A. P. 2000. Coupled torsional and bending vibrations of actively controlled drillstrings. *Journal of sound and vibration*, *234(1),* p. 67-83. https://doi.org/10.1006/jsvi.1999.2854

Zhang, H., Guan, Z., Liu, Y., Liang, D., and Xu, Y. 2016. A novel tool to improve the rate of penetration by transferring drilling string vibration energy to hydraulic energy. *Journal of Petroleum Science and Engineering*, *146*, p. 318-325. https://doi.org/10.1016/j.petrol.2016.04.025

Zhu, W.P. and Di, Q.F., 2011. Effect of prebent deflection on lateral vibration of stabilized drill collars. *SPE J. 16 (1),* p. 200–216. https://doi.org/10.2118/120455-PA

Zhu, X., Tang, L., and Yang, Q. 2014. A literature review of approaches for stick-slip vibration suppression in oilwell drillstring. *Advances in Mechanical Engineering*, *6*, p. 967952. https://doi.org/10.1155/2014/96795

Ziegler, H. 1977. Principles of Structural Stability, 2nd edition, Basel, Stuttgart, Birkhatlser.

APPENDIX A. GENERALLY SCALED EXPERIMENTS
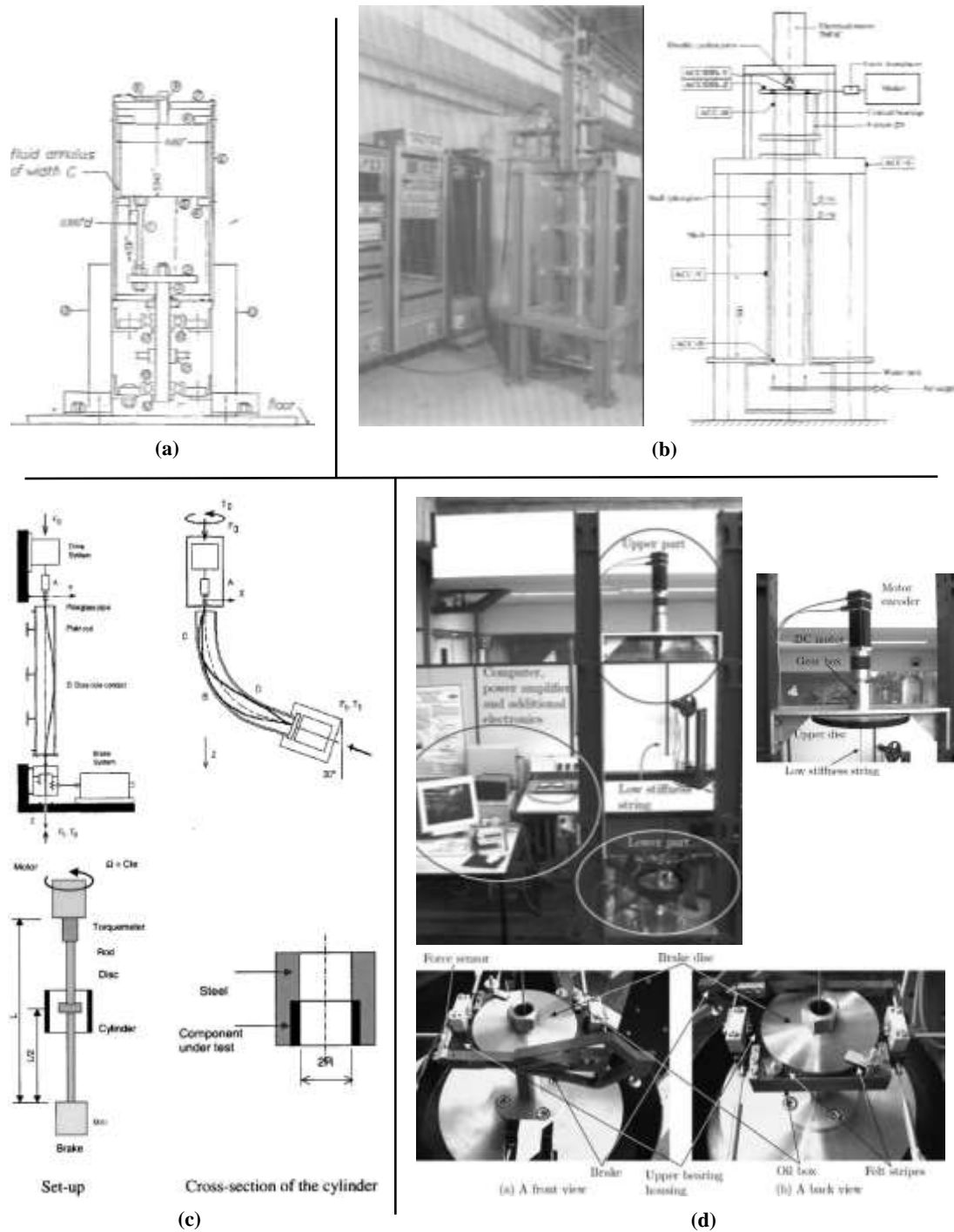
Figure A.1. Sets of experimental setup illustrations from - (a) Fritz (1970), (b) Antunes et al. (1992), (c) Berlioz et. al. (1996) and Melakhessou et. al. (2003), (d) Mihajlovic et al. (2004) and Mihajlovic (2005).
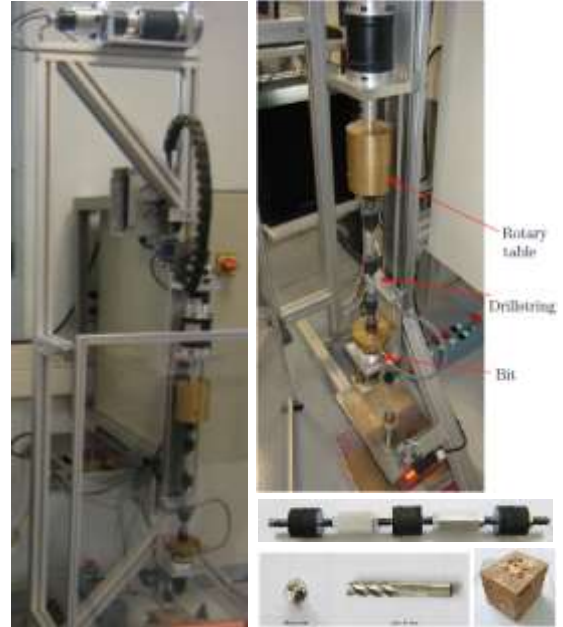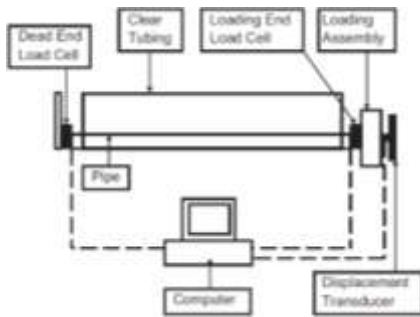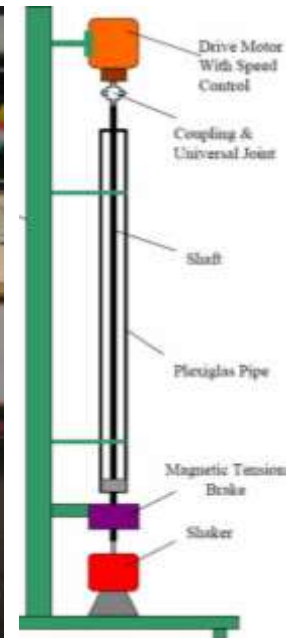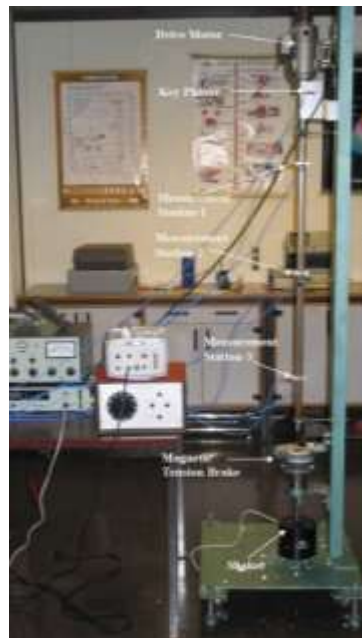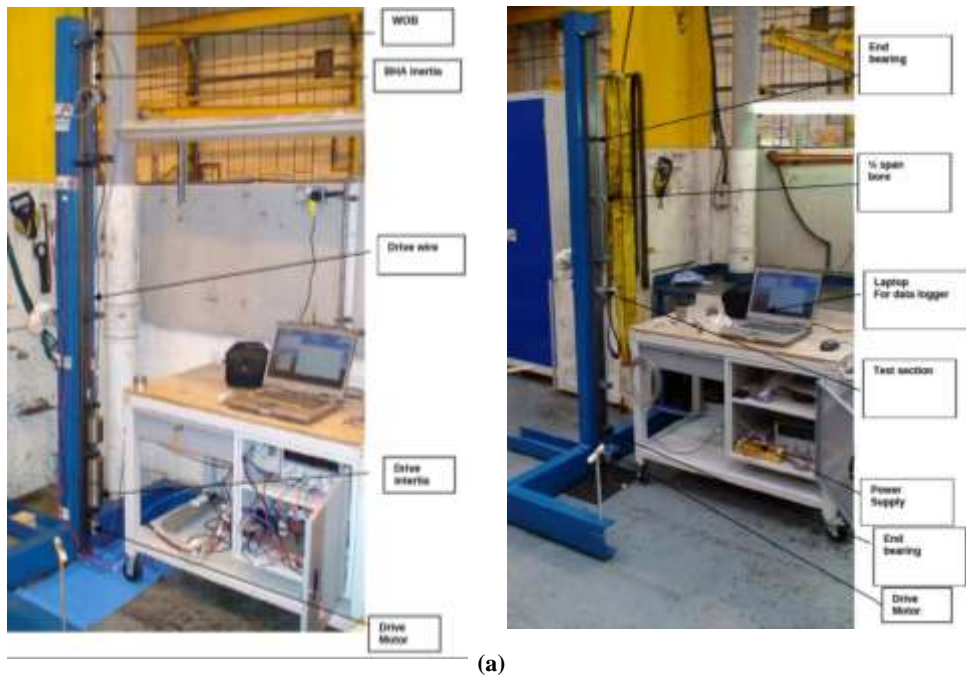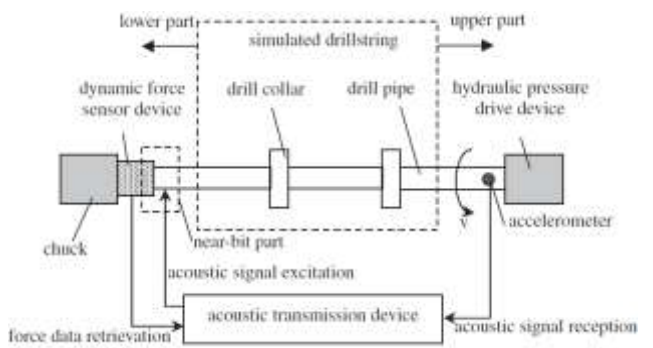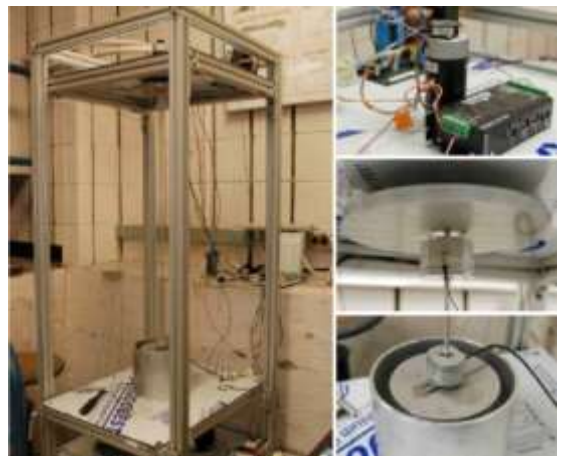
Figure A.2. Sets of experimental setup illustrations from - (a) Raymond et al. (2008), (b) Gao and Miska (2010), (c) Lu et al. (2009), (d) Khulief and Sulaiman (2009).
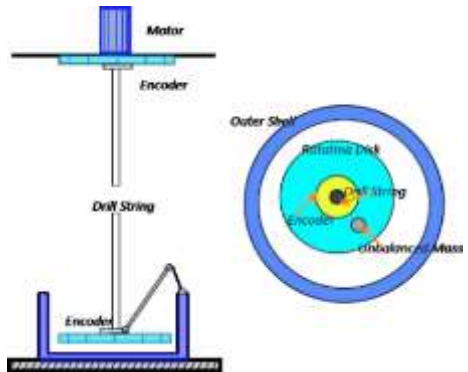
Figure A.3. Sets of experimental setup illustrations from - (a) Forster et al. (2010) and Forster (2011), (b) Franca et. al. (2011), (c) Cheng et al. (2011), (d) Liao et al. (2011).
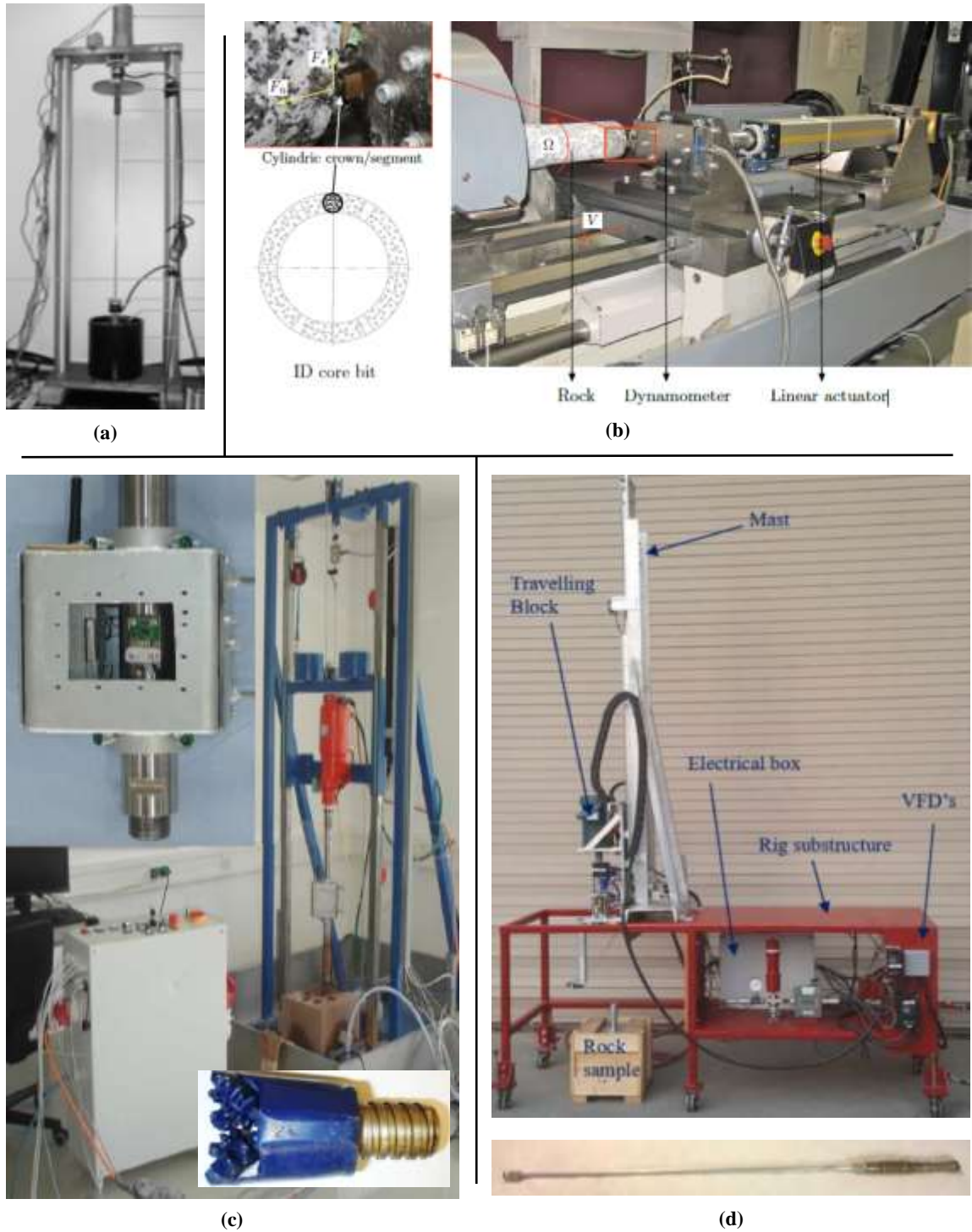
Figure A.4. Sets of experimental setup illustrations from - (a) Mazeed et al. (2013), (b) Mostofi et al. (2013), (c) Esmaeili et al. (2012, 2013) and Elmgerbi et al. (2021, 2022), (d) Bavadiya et. al. (2017).
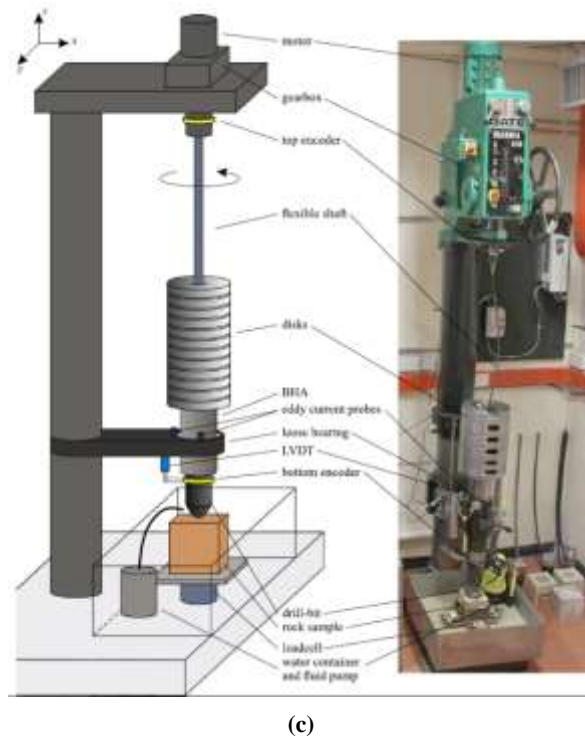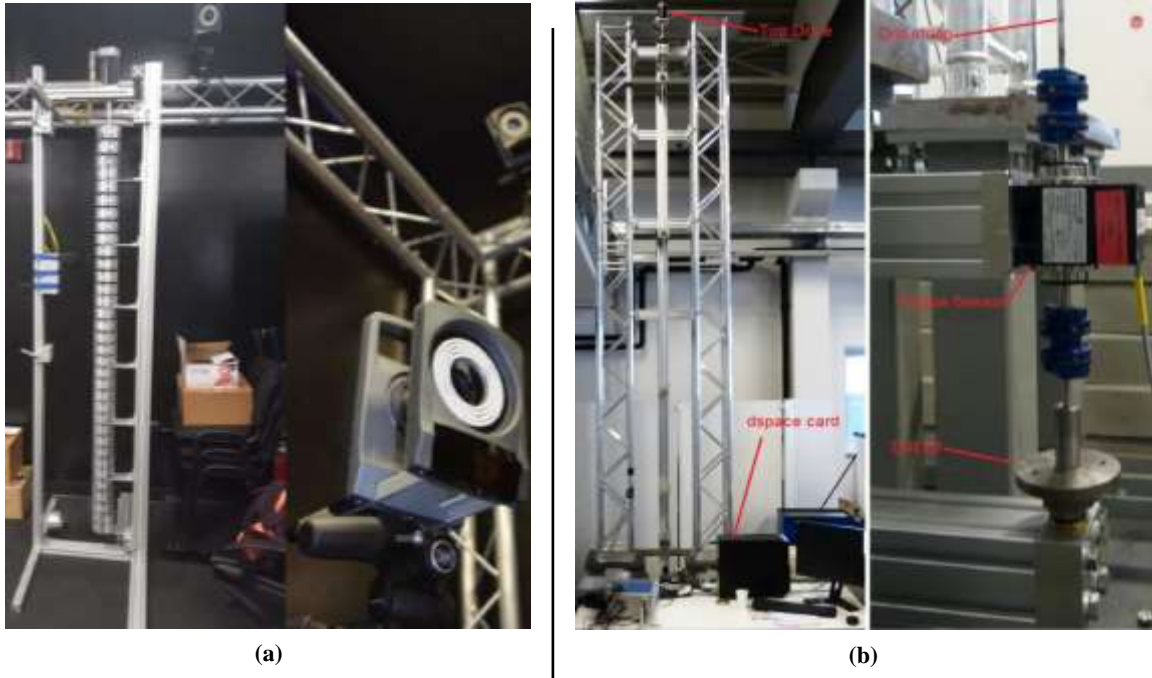
Figure A.5. Sets of experimental setup illustrations from - (a) Pehlivantürk et al. (2017), (b) Ullah (2018), (c) Wiercigroch (2010), Kapitaniak et al. (2015, 2016. 2018) and Wiercigroch et al. (2017).

APPENDIX B. MECHANICALLY SCALED EXPERIMENTS
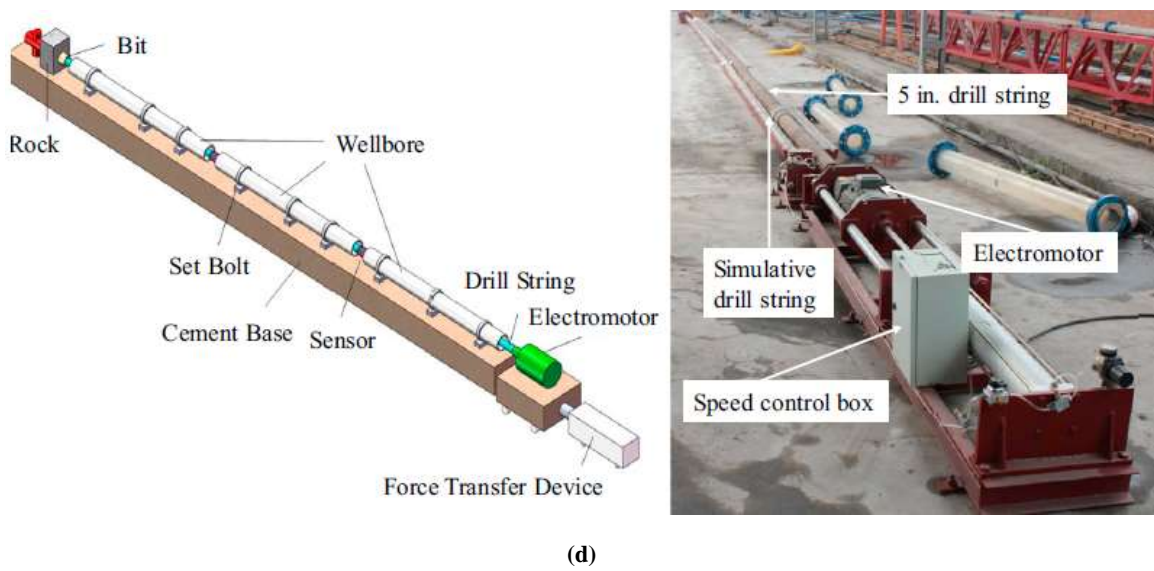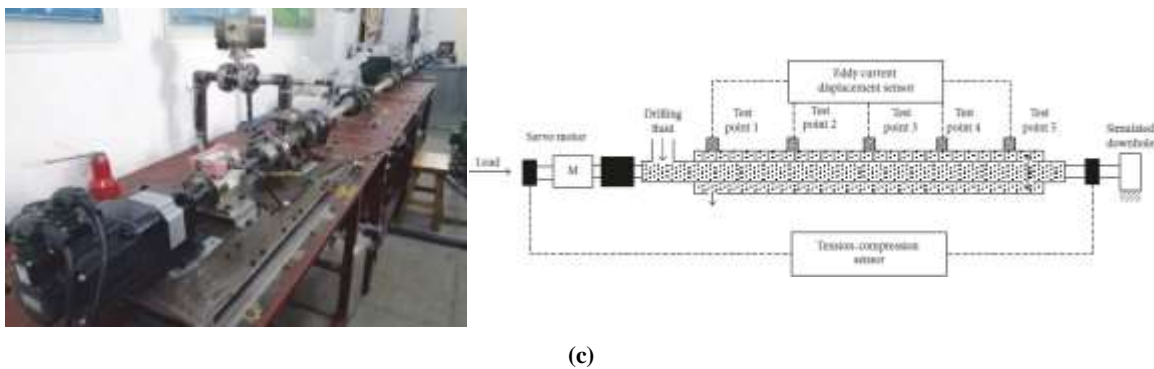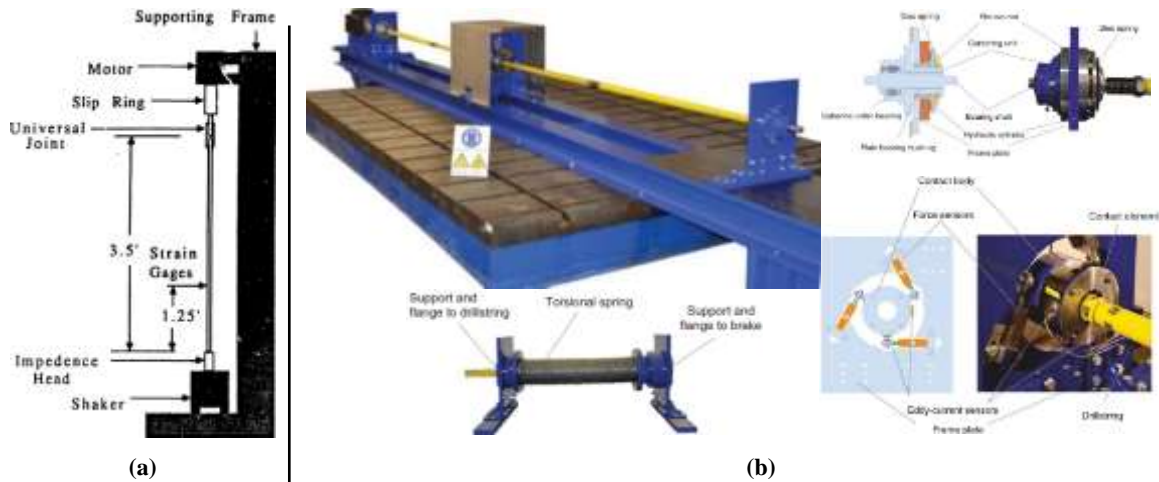
Figure B.1. Sets of experimental setup illustrations from - (a) Shyu (1989), (b) Westermann et al. (2015) and Gorelik and Höhn (2015), (c) Ren et. al. (2017), (d) Lin et el. (2018).

(a)

(b)

(c)
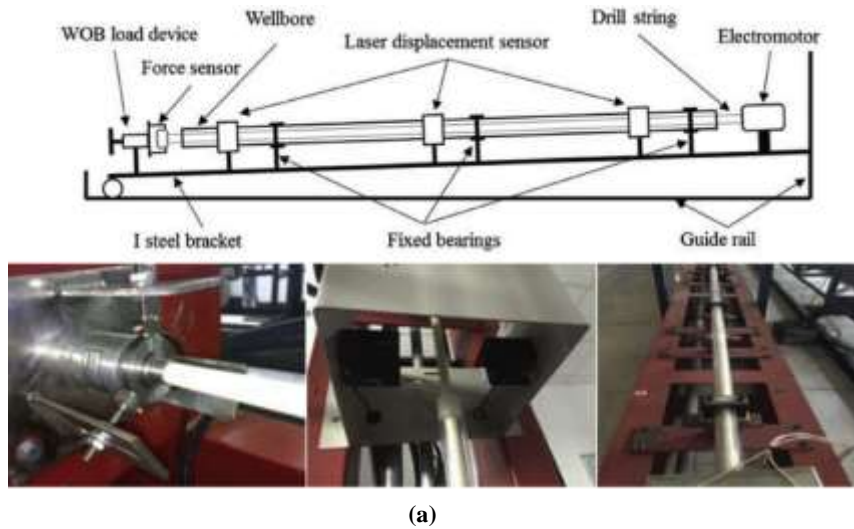
Figure B.2. Sets of experimental setup illustrations from - (a) Wang et al. (2018), (b) Srivastava and Teodoriu (2019), (c) Li et. al. (2020).

APPENDIX C. FABRICATION BLUEPRINT OF THE STRUCTURE

P1. SHAKER ELEVATION PART

HOLE DRILLING
SLIGHTLY LARGER THAN OF MENTIONED DIAMETER
FOR EASY PASSAGE OF BOLTS
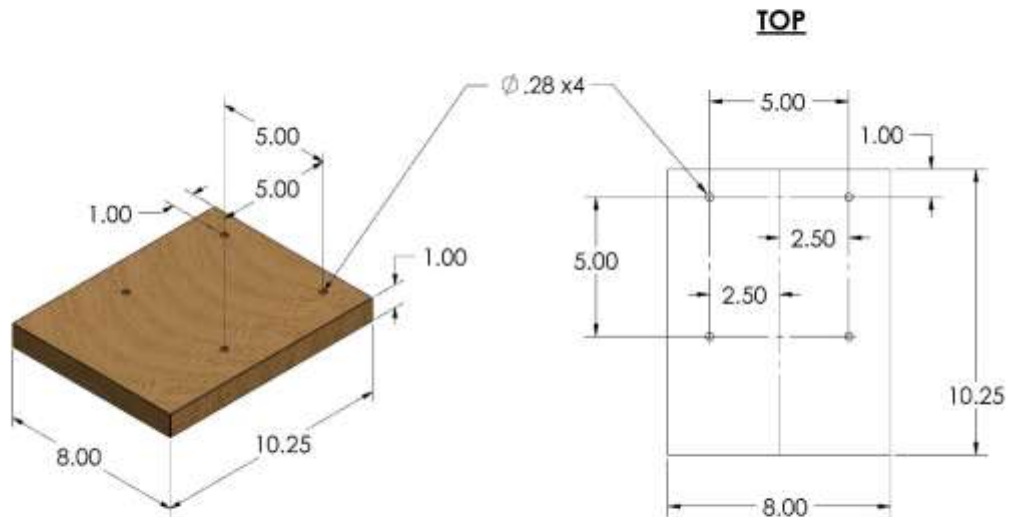
P2. MOTOR ELEVATION PART

HOLE DRILLING
SLIGHTLY LARGER THAN OF MENTIONED DIAMETER
FOR EASY PASSAGE OF BOLTS
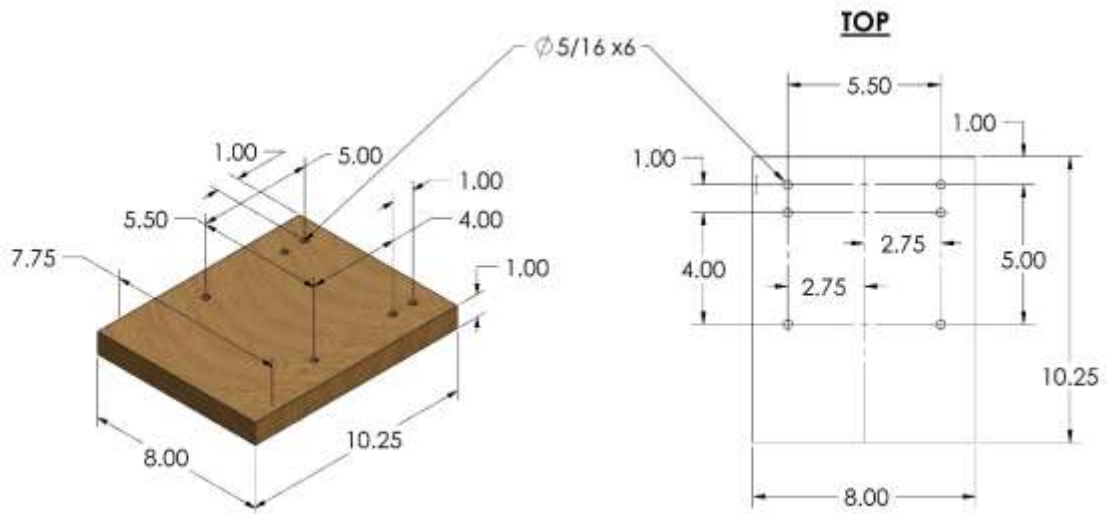
Figure C.1. Parts of vibration damping sandwich for the power system.

RIGHT

24.75
96.00
23.25
Ø.50 x2 @1.50
x5 @12.00
9.25
3.00
1.00
.25
12.00
2.00
12.00
1.50
Ø.50 x4 @2.75
12.00
1.00
1.00
Ø.50 x4 @2.75
2.75

FRONT
.25
3.00
2.00

LEFT

23.25
Ø.50 x2 @1.50
24.75
1.00
x5 @12.00
23.25
2.75
1.50
1.00
Ø.50 x4 @2.75
Ø.50 x4 @2.75
2.75
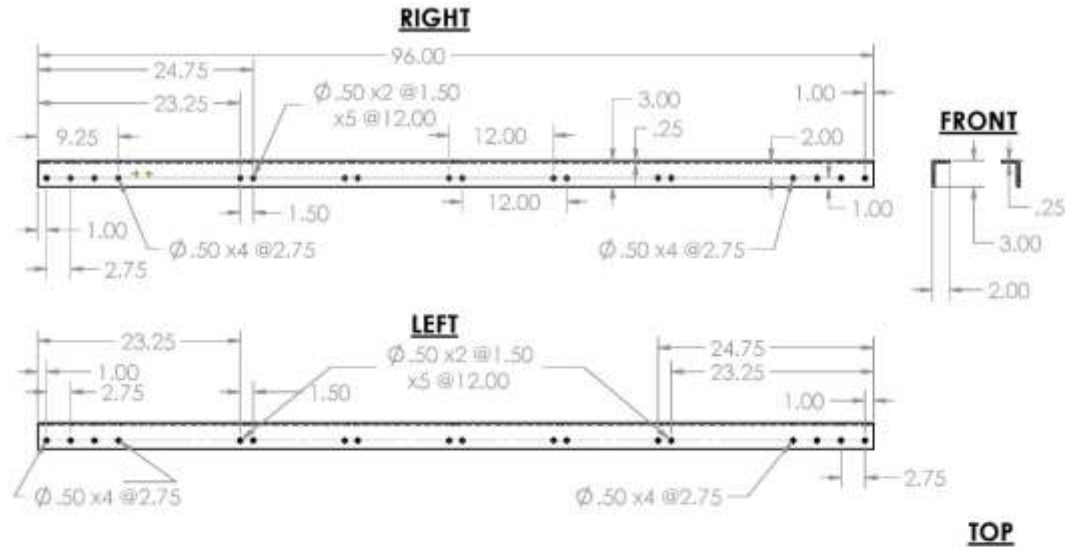
A1. GENERAL ANGLES - SYMMETRIC PAIR
HOLE DRILLING FOR THREADED BOLTS
OF MENTIONED DIAMETER
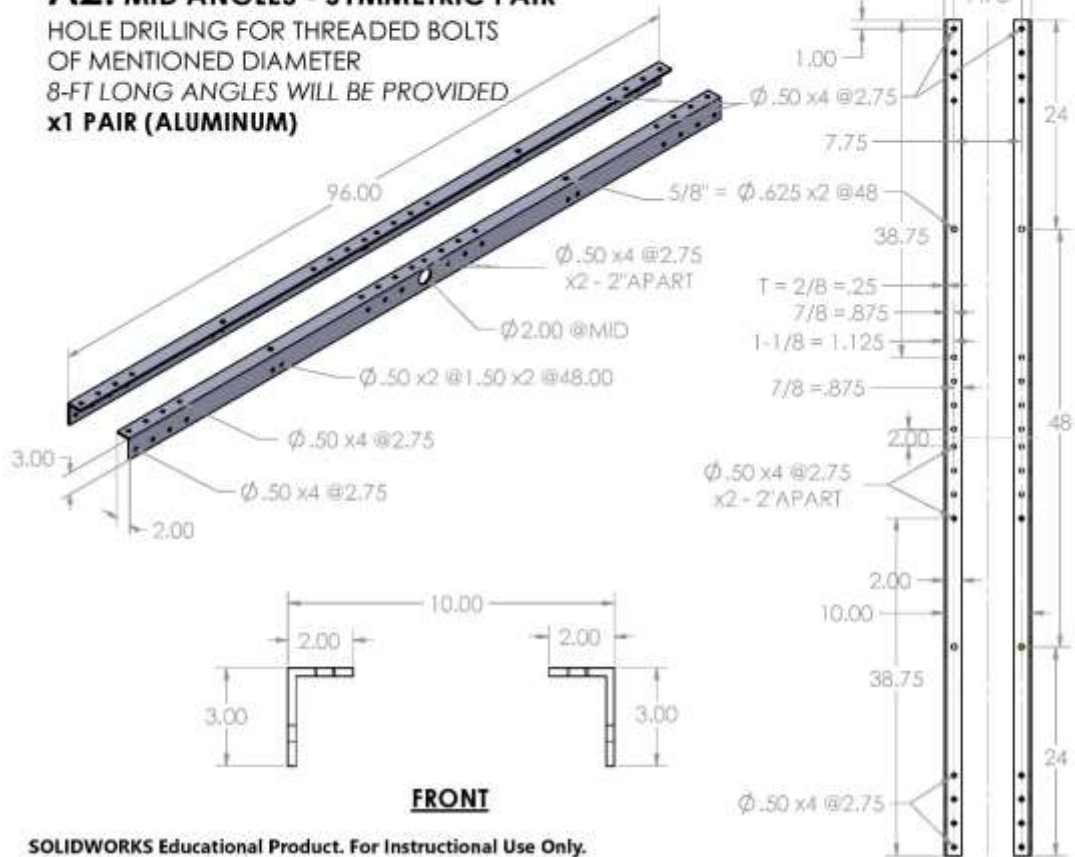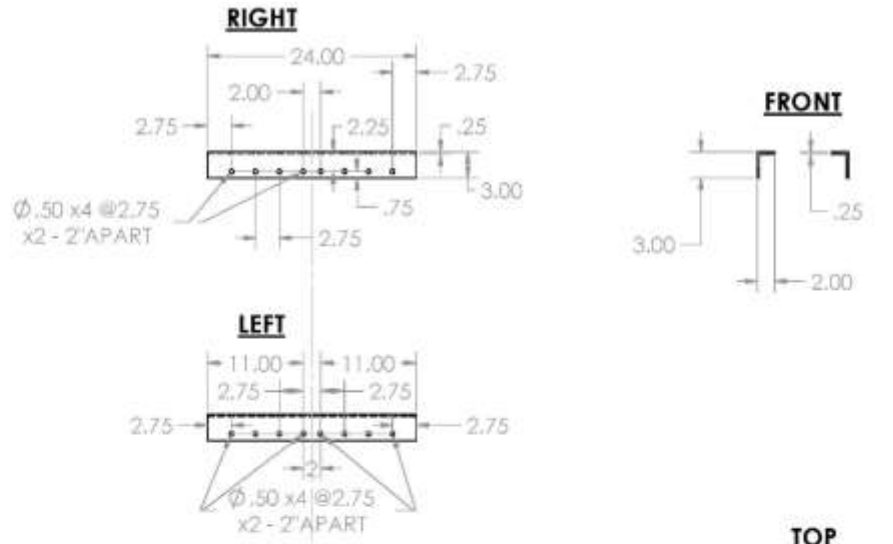8-FT LONG ANGLES WILL BE PROVIDED
x2 PAIRS (ALUMINUM)

TOP
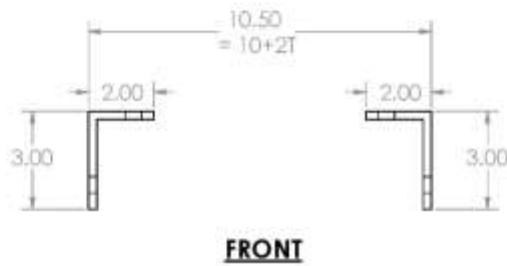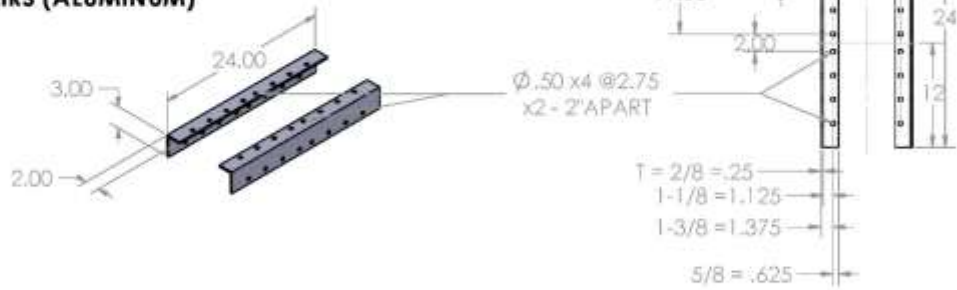10.00
7.75
1.00
Ø.50 x4 @2.75
7.75
96.00
5/8" = Ø.625 x5 @12
12.00
Ø.50 x2 @1.50
x5 @12.00
T = 2/8 =.25
7/8 =.875
1-1/8 = 1.125
5/8 = Ø.625 x5 @12
Ø.50 x4 @2.75
7/8 =.875
3.00
Ø.50 x4 @2.75
2.00
2.00
10.00

10.00
2.00
2.00
3.00
3.00
Ø.50 x4 @2.75

FRONT
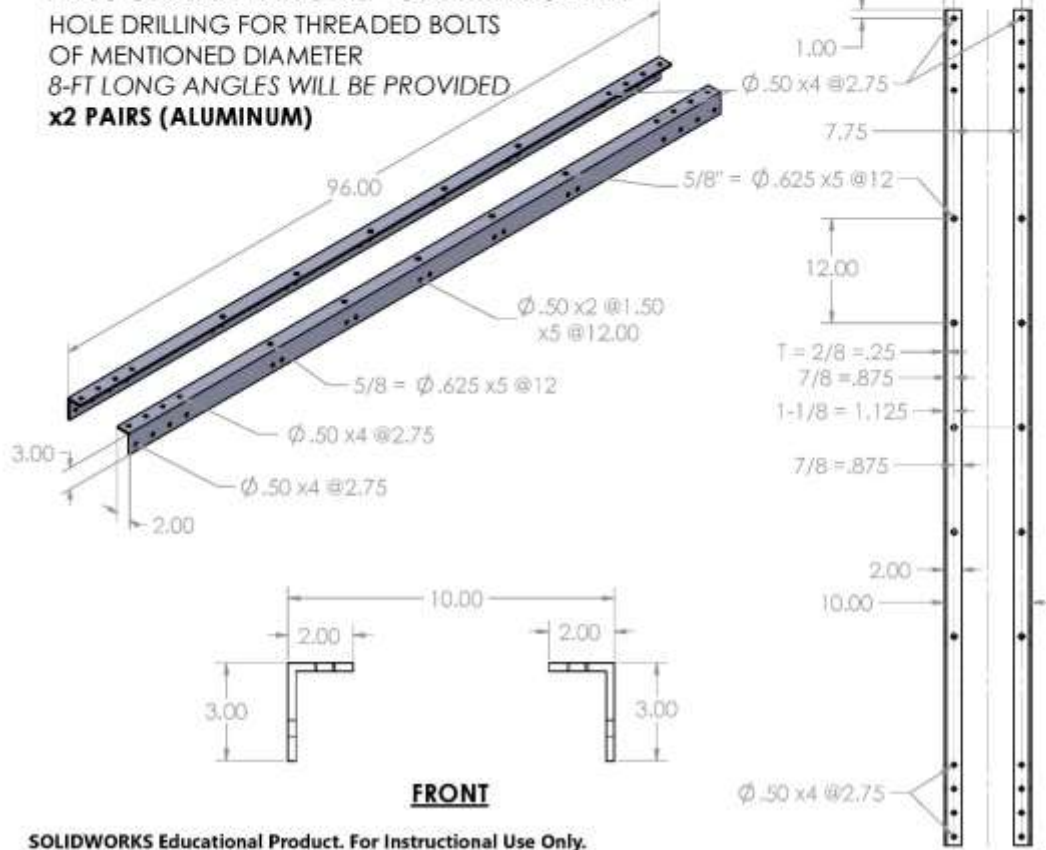
Figure C.2. Skelatal structure end bodies.

116

Figure C.3. Skelatal structure middle bodies.

117

RIGHT

24.00
2.00
2.75
2.25
2.75
.25
3.00
.75
Ø .50 x4 @2.75
x2 - 2'APART
2.75

FRONT

.25
3.00
2.00

LEFT

11.00
11.00
2.75
2.75
2.75
2.75
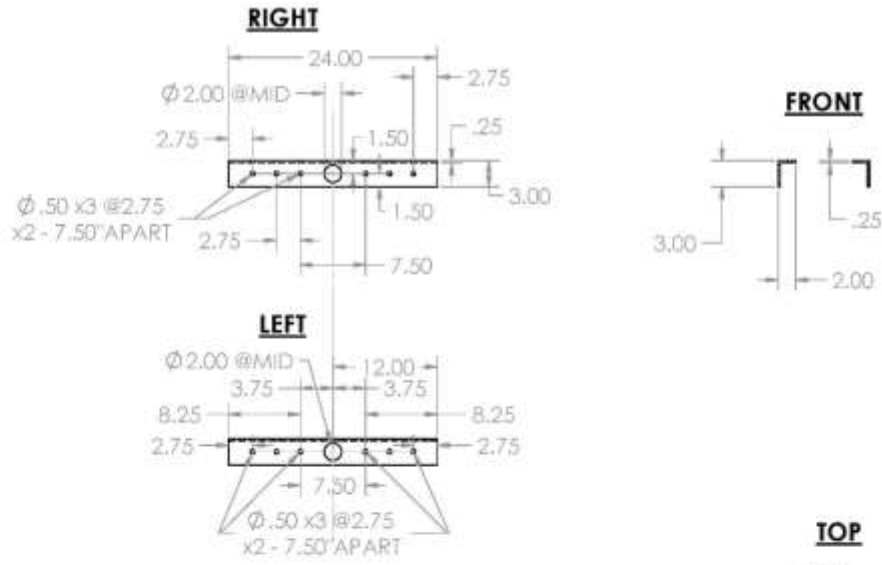2
Ø .50 x4 @2.75
x2 - 2'APART

J1. GENERAL JOINTS - SYMMETRIC PAIR

HOLE DRILLING FOR THREADED BOLTS
OF MENTIONED DIAMETER
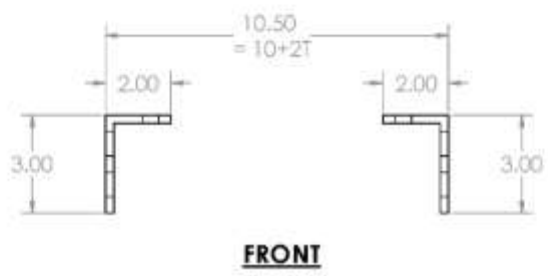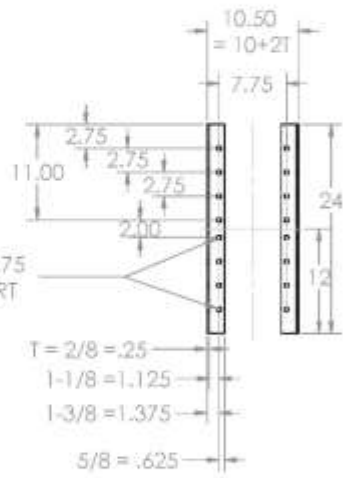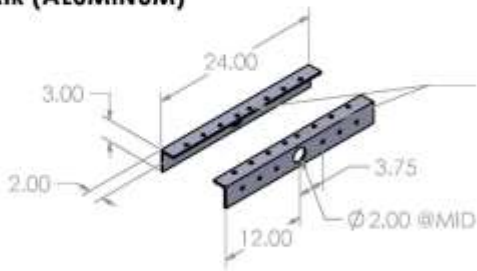2-FT LONG ANGLES WILL BE PROVIDED
x2 PAIRS (ALUMINUM)

24.00
3.00
2.00

Ø .50 x4 @2.75
x2 - 2'APART

TOP

10.50
= 10+2T
7.75
2.75
2.75
11.00
2.00
24
12

T = 2/8 =.25
1-1/8 =1.125
1-3/8 =1.375
5/8 = .625

10.50
= 10+2T
2.00
2.00
3.00
3.00

FRONT

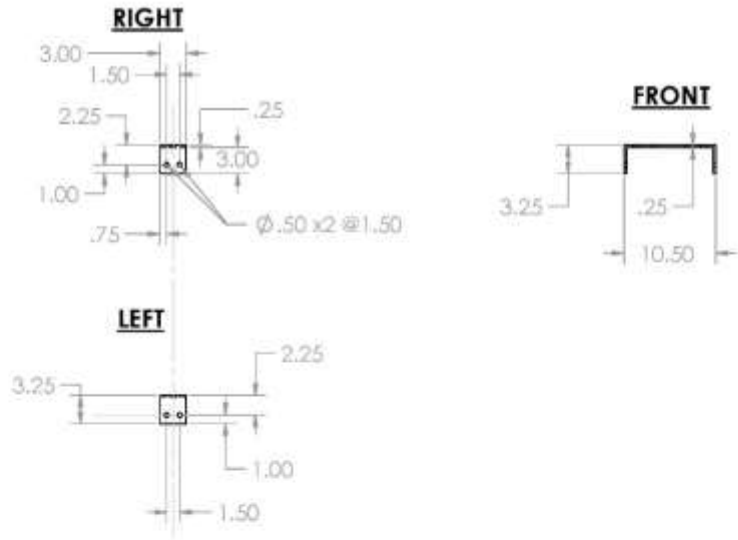*Figure C.4. Skelatal structure lengthwise body joints.*

RIGHT

FRONT

LEFT

J2. MID JOINTS - SYMMETRIC PAIR
HOLE DRILLING FOR THREADED BOLTS
OF MENTIONED DIAMETER
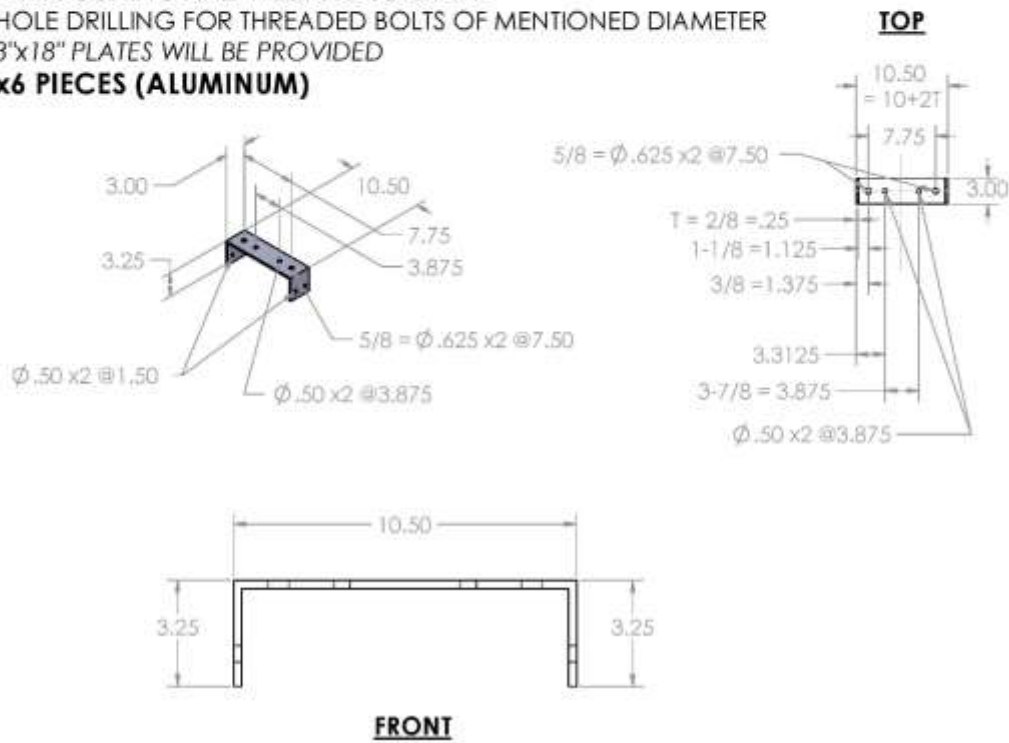2-FT LONG ANGLES WILL BE PROVIDED
x1 PAIR (ALUMINUM)

TOP

FRONT

Figure C.5. Skelatal structure middle lengthwise body joint.

RIGHT

3.00
1.50
.25
2.25
3.00
1.00
.75
Ø.50 x2 @1.50

FRONT

3.25
.25
10.50
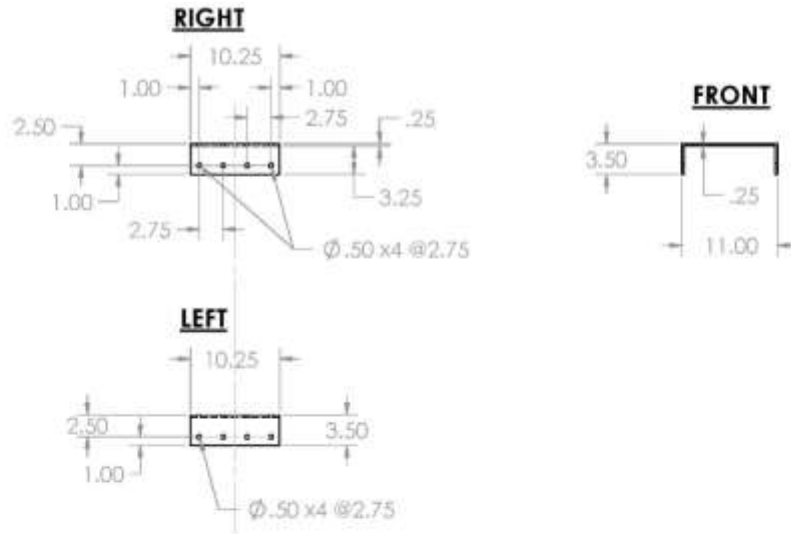
LEFT

2.25
3.25
1.00
1.50

T0. CONNECTING TABLES
PLATE CUTTING AND WELDING TO SHAPE
HOLE DRILLING FOR THREADED BOLTS OF MENTIONED DIAMETER
3"x18" PLATES WILL BE PROVIDED
x6 PIECES (ALUMINUM)

TOP

10.50
= 10+2T
7.75
5/8 = Ø.625 x2 @7.50
3.00
$T = 2/8 = .25$
$1-1/8 = 1.125$
$3/8 = 1.375$
3.3125
$3-7/8 = 3.875$
Ø.50 x2 @3.875

3.00
10.50
7.75
3.25
3.875
5/8 = Ø.625 x2 @7.50
Ø.50 x2 @1.50
Ø.50 x2 @3.875

FRONT

10.50
3.25
3.25

Figure C.6. Skelatal structure accross body joints.

120

RIGHT

10.25

1.00

1.00

2.75

.25

2.50

3.25

1.00

2.75

Ø.50 x4 @2.75

FRONT

3.50

.25

11.00

LEFT

10.25

2.50

3.50

1.00

Ø.50 x4 @2.75

T1 & T2. END TABLES

PLATE CUTTING AND WELDING TO SHAPE
HOLE DRILLING FOR THREADED BOLTS OF MENTIONED DIAMETER
10.25"x18" PLATES WILL BE PROVIDED
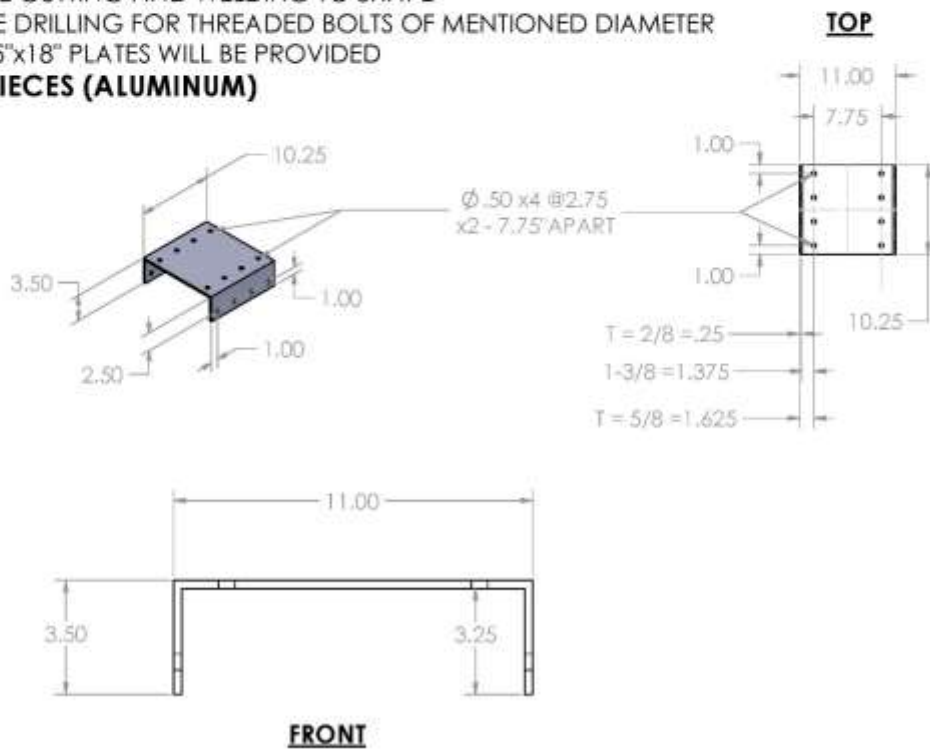
x2 PIECES (ALUMINUM)
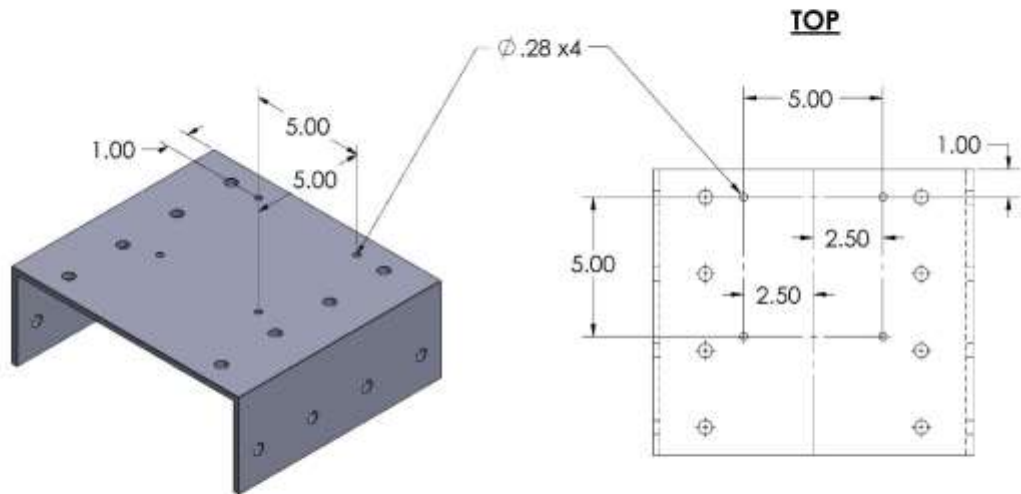
TOP

11.00

7.75

10.25

1.00

Ø.50 x4 @2.75
x2 - 7.75' APART

3.50

1.00

1.00

1.00

2.50

10.25

$T = 2/8 = .25$

$1-3/8 = 1.375$

$T = 5/8 = 1.625$

11.00

3.50

3.25

FRONT

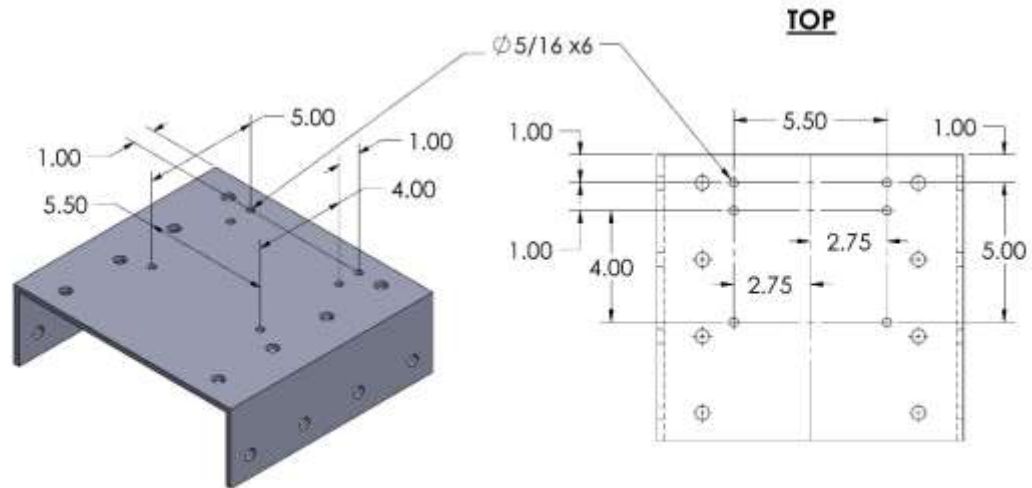*Figure C.7. Support bases for the Power System.*

T1. SHAKER TABLE

HOLE DRILLING
SLIGHTLY LARGER THAN OF MENTIONED DIAMETER
FOR EASY PASSAGE OF BOLTS

T2. MOTOR TABLE

HOLE DRILLING
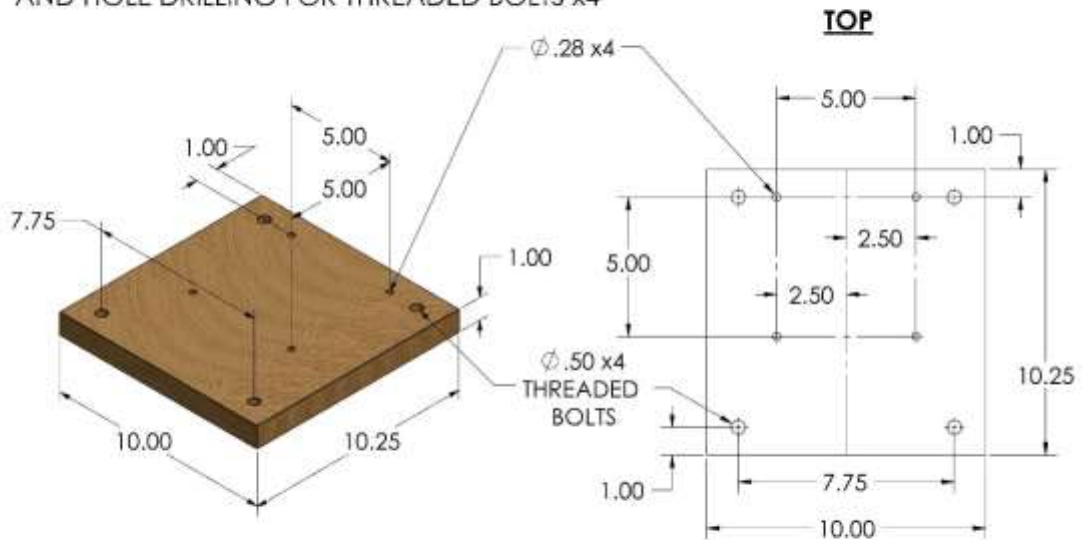SLIGHTLY LARGER THAN OF MENTIONED DIAMETER
FOR EASY PASSAGE OF BOLTS

Figure C.8. Support Bases for the Power System – secondary work for additional perforation for fixation.

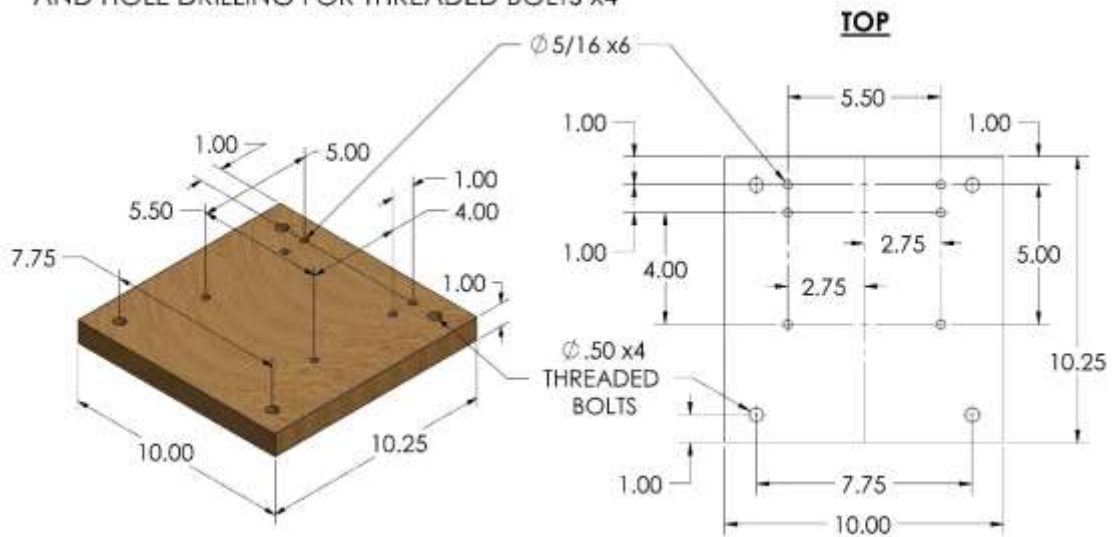# E1. SHAKER BASE ELEVATION

HOLE DRILLING x4
SLIGHTLY LARGER THAN OF MENTIONED DIAMETER
FOR EASY PASSAGE OF BOLTS
AND HOLE DRILLING FOR THREADED BOLTS x4

TOP

E2. MOTOR BASE ELEVATION

HOLE DRILLING x6
SLIGHTLY LARGER THAN OF MENTIONED DIAMETER
FOR EASY PASSAGE OF BOLTS
AND HOLE DRILLING FOR THREADED BOLTS x4

TOP

Figure C.9. Parts of vibration damping sandwich for the power system.

123

S1. SUPPORT BASE

SUPPORTING BASE FOR MOUNTING BEARINGS

HOLE DRILLING FOR BEARING FIXTURES ON THE UPPER BASE PLATE
(ESTIMATED CENTRAL POSITION SHOWN. BEARING WILL BE PROVIDED FOR ACCURACY)
HOLE DRILLING FOR FLOOR FIXTURE ON THE LOWER BASE PLATE
(NOT SHOWN. USE SUITABLE MARKET AVAILABLE FLOOR FIXUTRE MEASUREMENTS)

ARC WELDING FOR FIXING TWO VERTICALLY ALLIGNED RODS WITH BASE PLATES

SUPPORT BASE PLATES TO BE PARALLELLY SECURED TO GROUND
VERTICAL DISTANCE
FROM SHAFT CENTER TO THE GROUND TO BE **49.75-INCHES**

6"x18" PLATES AND Ø2'-48"LONG RODS WILL BE PROVIDED
x2 PIECES (MILD STEEL)
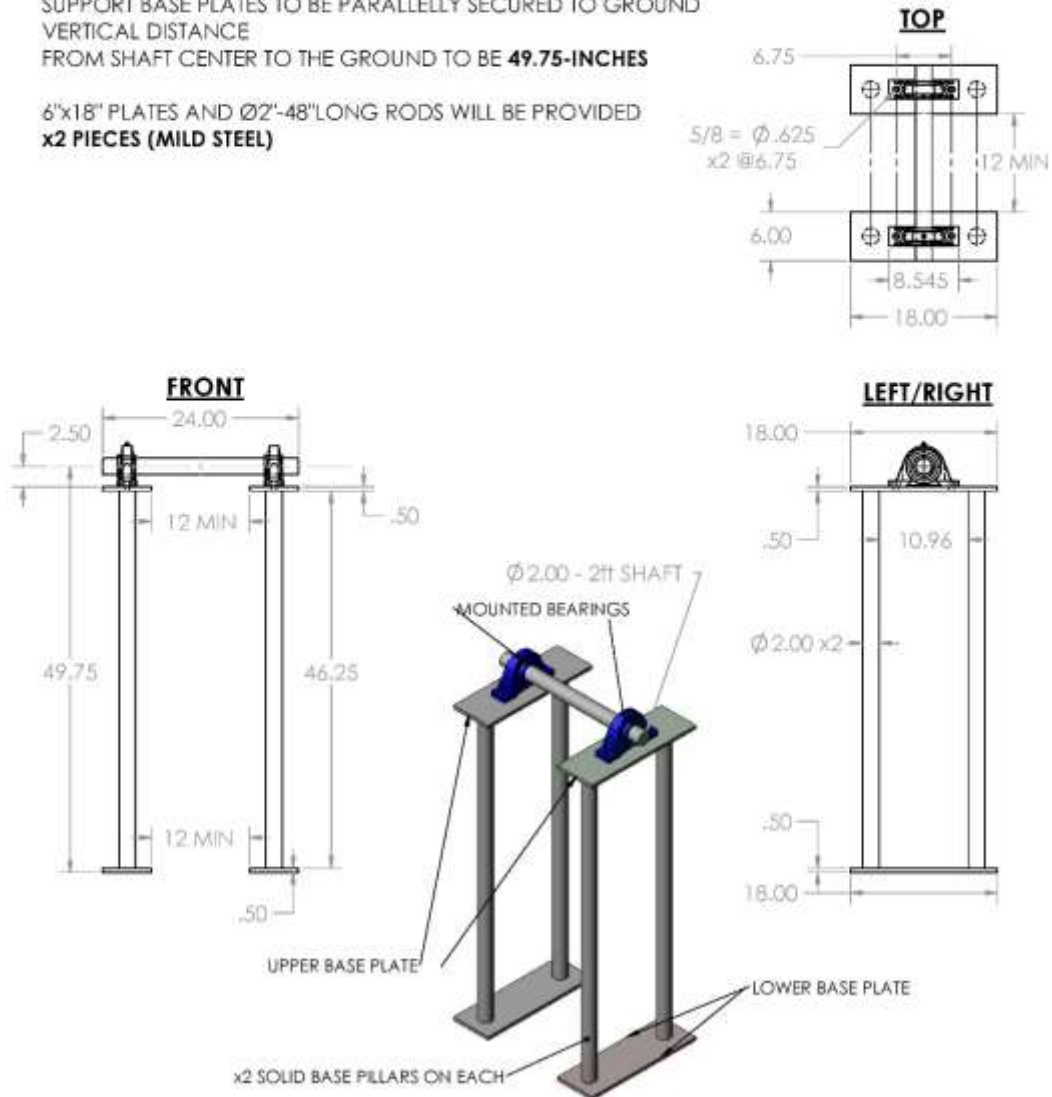
SOLIDWORKS Educational Product. For Instructional Use Only.

Figure C.10. Middle support base for the Skelatal Structure.

124

FRONT

LEFT/RIGHT

S2. SUPPORT STAND

FLAT PERFORATED PLATE
WELDED TOGETHER TO INCREASE THICKNESS AND
CUT TO MAINTAIN CERTAIN HEIGHT LEVEL & ALIGNMENT,
FROM GROUND TO A SINGLE HOLE CENTER
DRILLING HOLES ON ANGLES &
WELDING ONTO THE PLATE
AS SHOES FOR FLOOR FIXTURE

VERTICAL DISTANCE
FROM ONE HOLE CENTER TO GROUND
TO BE **48 INCHES**

24"x120"x0.25" PERFORATED PLATE
AND EIGHT 4"x4"x2" ANGLES WILL BE PROVIDED

x4 PIECES (MILD STEEL)

102.00

.50

2.00

Ø 1.00 @1.25

1.25

1.25

FROM THE FLOOR TO
CENTER OF A HOLE
STAYS PARALLEL TO THE GROUND
AT 4FT

48.00

S3. SUPPORT BAR

A ROD SANDED TO EASILY PASS THROUGH
THE PERFORATED HOLES OF THE STAND
AND EXACTLY CUT IN HALF ALONG THE LENGTH

A Ø1"-24"LONG ROD WILL BE PROVIDED
x2 PIECES (MILD STEEL)

24.00 IN LENGTH

4.00

.50

Ø1.00 SHAFT

4.00

2.00

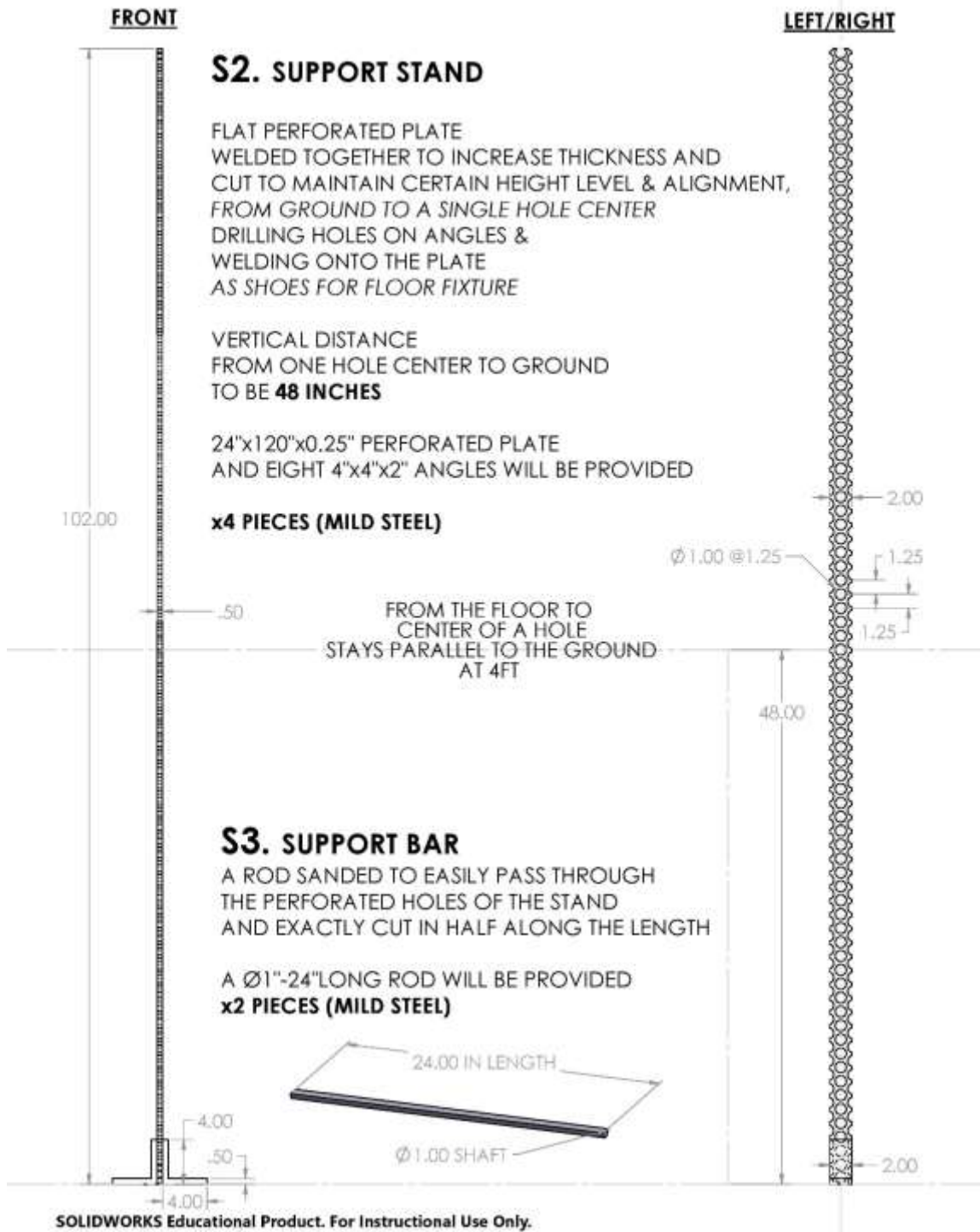SOLIDWORKS Educational Product. For Instructional Use Only.

Figure C. 11. End supports for the Skelatal Structure.

125

VITA

Eshan Kumer Maitra

Candidate for the Degree of

Master of Science

Thesis: FLUID INDUCED DRILLING DYNAMICS – A MECHANICALLY SCALED EXPERIMENTAL INVESTIGATION

Major Field: Petroleum Engineering

Biographical:

Education:

Completed the requirements for the Master of Science in Petroleum Engineering at Oklahoma State University, Stillwater, Oklahoma in May 2023.

Completed the requirements for the Bachelor of Science in Mechanical Engineering at Ahsanullah University of Science and Technology, Dhaka, Bangladesh in 2019.

Experience: 2 years Graduate Research Assistant at the Oklahoma State University

Professional Memberships: Society of Petroleum Engineers